GROWTH OF EPITAXIAL SILICON LAYERS
BY ION BEAM SPUTTERING

Thesis submitted for the degree of

Doctor of Philosophy

by

Keith Pearmain

August, 1971

Department of Metallurgy,
Imperial College of
Science and Technology,
University of London.

ABSTRACT

An ion beam sputtering technique has been developed which made possible the production of homo-epitaxial Si layers by sputtering for the first time. The A^+ ion beam source was considerably modified from the initial design of Hill and Nelson (1965) to give the purity needed for the production of semiconductor layers without mass analysis of the ion beam. Typically, a 12keV 4mA beam of A^+ ions struck a Si target at 60° incidence and ejected sputtered atoms were deposited at a rate of 200 Å/min on a heated Si(111) substrate placed just above the target. Epitaxial layers were grown at temperatures above about 700°C and the structural quality of these layers was evaluated by transmission electron microscopy. Layers grown at temperatures in excess of 900°C contained only dislocation defects normally to a density of about $8x10^9$ cm^{-2}, whereas epitaxial layers grown at lower temperatures also exhibited stacking faults and microtwinning. The existence of defects in epitaxial layers has been correlated with the severity of bombardment of the substrate during deposition by secondary ions from the target. In all cases, the bombardment conditions were severe enough to continually transform a thin 100 Å thick surface region of the newly-deposited sputtered layer to a disordered state. The subsequent reordering characteristics of this disordered surface controlled not only the prominence of individual defects in any epitaxial layer but also whether a layer was single crystal. Electrical properties of epitaxial layers were also strongly dependent on bombardment conditions allowing only high resistivity N-type layers to be grown independent of target conductivity-type and resistivity.

The ion beam sputtering properties of Si and GaAs have also been investigated. The similarity in results for single crystal targets to those for polycrystalline targets was again attributed to ion-bombardment-induced surface disorder. Stoichiometric layers of GaAs could only be obtained from polycrystaline targets.

C O N T E N T S

CONTENTS

		PAGE NO.
ABSTRACT		2
CHAPTER 1	INTRODUCTION	9
CHAPTER 2	REVIEW OF THE EFFECTS CAUSED BY ION BOMBARDMENT OF SEMICONDUCTORS	13
2.1.	SPUTTERED ATOMS	13
2.1.1.	The process of sputtering	13
2.1.2.	The energy of sputtered atoms	14
2.1.3.	Sputtering yield	14
2.1.4.	Influence of the target material on the sputtering yield	17
2.1.5.	Influence of the type of bombarding ion on the sputtering yield	17
2.1.6.	Influence of the bombarding ion energy on the sputtering yield	20
2.1.6.1.	General trends	20
2.1.6.2.	Semiconductor targets	22
2.1.7.	Influence of the ion angle of incidence on the sputtering yield	27
2.1.8.	Angular distribution of sputtered particles from polycrystalline samples	30
2.1.9.	Preferential ejection of sputtered atoms from single crystals	32
2.1.9.1.	Mechanisms of preferential ejection	32
2.1.9.2.	Ejection directions for semiconductors	33
2.1.9.3.	Composition of sputtered deposits from compound semiconductors	36
2.1.10.	Pressure-dependent sputtering	38
2.1.11.	Nature of the neutral sputtered particles	39
2.2.	OTHER PARTICLES EMITTED	40
2.2.1.	Electrons	40
2.2.2.	Secondary positive ions	42
2.2.2.1.	General trends	42
2.2.2.2.	Semiconductor targets	44
2.2.3.	Secondary negative ions	47

		PAGE NO.
2.3.	TARGET EFFECTS	49
2.3.1.	Ion bombardment damage	49
2.3.1.1.	Formation of damage	49
2.3.1.2.	Critical ion doses for damage in Si and Ge	50
2.3.1.3.	Extent of surface disorder	50
2.3.1.4.	Annealing behaviour of bombarded crystals and the structural defects remaining	53
2.3.1.5.	Defects remaining in crystals bombarded at elevated temperatures	56
2.3.1.6.	The critical annealing temperature, T_a	58
2.3.1.6.(a)	Determination of T_a from atom ejection patterns	58
2.3.1.6.(b)	Determination of T_a from the angular regularities of the secondary electron emission coefficient	59
2.3.1.6.(c)	Determination of T_a from the energy distribution of scattered ions	61
2.3.1.6.(d)	Determination of T_a from sputtering yields	61
2.3.1.6.(e)	Determination of T_A, the amorphisation temperature	62
2.3.2.	Ion implantation	64
2.3.2.1.	Ion penetration	64
2.3.2.2.	Ion sorption	64
2.3.2.3.	P-N junction devices	65
2.3.3.	Surface topography of target after ion bombardment	66
CHAPTER 3	EQUIPMENT AND EXPERIMENTAL TECHNIQUES	69
3.1.	GENERAL ARRANGEMENT	69
3.2.	THE VACUUM SYSTEM	72
3.3.	ION BEAM SOURCE	76
3.3.1.	Choice of type of source	76
3.3.2.	Operation of source	78
3.3.3.	Construction of source	79
3.3.4.	Equipment used with the ion source	81
3.3.4.1.	Power supplies	81

		PAGE NO.
3.3.4.2.	Water cooling	82
3.3.4.3.	Inert gas supply	83
3.3.5.	Performance of ion source	83
3.3.6.	Minimisation of metal contamination from the source	85
3.4.	TARGETS AND TARGET HOLDERS	89
3.4.1.	Si targets used	89
3.4.2.	GaAs targets used	89
3.4.3.	Target holders	89
3.5.	SHUTTER BETWEEN TARGET AND SUBSTRATE	92
3.6.	SILICON SUBSTRATES; METHODS OF SUPPORT AND HEATING	93
3.6.1.	Substrates used	93
3.6.2.	Substrate holder and measurement of layer thickness	93
3.6.3.	Experimental considerations for substrate heating	93
3.6.4.	Methods of heating	94
3.6.5.	The substrate heater used	97
3.6.6.	Measurement of substrate temperatures	97
3.7.	PROCEDURE FOR A TYPICAL RUN FOR PRODUCING EPITAXIAL SILICON LAYERS	99
3.8.	ASSESSMENT OF QUALITY OF SILICON LAYERS	103
3.8.1.	Structural assessment by transmission electron diffraction (TED) and microscopy (TEM)	103
3.8.1.1.	Preparation of specimens for the electron microscope	103
3.8.1.2.	Electron microscopy of Si layers	105
3.8.2.	Structural assessment by reflection high-energy electron diffraction (RHEED)	105
3.8.3.	Electrical measurements	106
3.9.	Si AND GaAs SPUTTERING EXPERIMENTS	107
3.9.1.	Measurement of sputtering yield	107
3.9.2.	Topography of target surface after bombardment	107
3.9.3.	The angular distribution of sputtered atoms	107

PAGE NO.

3.9.4.	Chemical composition of sputtered deposits from GaAs targets	108
3.9.5.	Procedure for a typical run when determining the sputtering properties of Si and GaAs	108
CHAPTER 4	EXPERIMENTAL RESULTS AND DISCUSSION OF RESULTS	110
4.1.	ANALYSIS OF HOMO-EPITAXIAL SPUTTERED SILICON LAYERS	110
4.1.1.	Conditions of growth	110
4.1.2.	Analysis of diffraction patterns	110
4.1.2.1.	TED patterns and the epitaxial temperature	113
4.1.2.2.	RHEED patterns	113
4.1.2.3.	TED patterns of very thin regions and an estimate of the thickness of surface disorder	115
4.1.3.	Defects in epitaxial layers	117
4.1.3.1.	Substrates at ion source potential	117
4.1.3.2.	Substrates at earth potential	120
4.1.3.3.	Substrates at earth potential with no shutter between the target and substrate	122
4.1.4.	Growth model	124
4.1.4.1.	Influence of oxygen	124
4.1.4.2.	Ion bombardment model	125
4.1.4.3.	Nucleation and initial stages of growth	126
4.1.5.	Electrical measurements	127
4.2.	SPUTTERING YIELD AND TOPOGRAPHY OF TARGET SURFACES AFTER BOMBARDMENT	131
4.2.1.	Sputtering yield	131
4.2.2.	Macrotopography of targets after bombardment	134
4.2.3.	Microtopography of targets after bombardment	136
4.3.	THE ANGULAR DISTRIBUTION OF SPUTTERED ATOMS	141

		PAGE NO.
4.3.1.	Polar distributions of sputtered Si	141
4.3.2.	Contour map distributions of sputtered Si	145
4.3.3.	Deposition rate of sputtered Si onto self substrates	145
4.3.4.	Effect of rate of ion dose and total dose on contour map distributions	147
4.3.5.	Effect of temperature on contour map distributions	149
4.3.6.	Contour map distribution of sputtered GaAs	149
4.3.7.	Chemical composition of sputtered deposits from GaAs targets	151
CHAPTER 5	CONCLUSIONS AND RECOMMENDATIONS FOR FURTHER WORK	153
5.1.	CONCLUSIONS	153
5.2.	RECOMMENDATIONS FOR FURTHER WORK	156
APPENDIX		160
A.1.	BRAZING TO UHV STANDARDS	161
A.2.	ESTIMATE OF RATE OF ION DOSE TO SUBSTRATE DURING DEPOSITION	164
A.3.	PROPOSED SPUTTERING METHOD TO PREVENT ENTIRELY BOMBARDMENT OF THE SUBSTRATE WITH CHARGED PARTICLES	166
REFERENCES		170
ACKNOWLEDGEMENTS		176

CHAPTER 1

INTRODUCTION

Single crystals of Ge, Si and GaAs of extremely high purity and perfection are the basic materials for most semiconductor devices. Si and GaAs are useful for devices operating at higher temperatures than is possible with Ge. During the past fifteen years considerable effort has been devoted to perfecting the techniques of growing epitaxial semiconductor layers with a view to fabricating new and improved solid state electrical devices. The term "epitaxial" describes the situation where there is a simple orientation relationship between the crystal lattices of the layer and its substrate. "Homo-epitaxial" specifies the situation where the crystal lattices of the layer and substrate are identical.

The methods most commonly used in industry for the growth of homo-epitaxial semiconductor layers are chemical; either the reduction of a halide by hydrogen or the pyrolitic decomposition of a hydride onto a single crystal substrate of the same material. Under normal conditions, homo-epitaxial layers of Si cannot be grown at temperatures less than 1200°C for growth rates from 0.1 to 0.5µ/min. The main crystallographic defects in these chemical layers are stacking faults, often up to a density of $10^3 cm^{-2}$. The disadvantage of high epitaxial temperature is the possibility of appreciable diffusion of impurities leading to junctions which are not very sharp.

Alternative methods of growth are vacuum evaporation and sublimation which are more versatile and are particularly suitable to the production of complicated device geometries not readily available by chemical methods. Unvala (1962) first reported the homo-epitaxial deposition of Si layers in ordinary high vacuum using an electron bombardment evaporation technique which was capable of producing layers deposited at rates of growth and with properties comparable to those by chemical methods. In later papers (Unvala 1963(a) and (b),

Booker and Unvala 1963 and 1965, and Unvala and Booker 1964), it was shown that the minimum epitaxial temperature of 1100°C at a growth rate of 0.1μ/min and the presence of stacking faults in layers were direct results of oxygen contamination from the vacuum environment. The level of oxygen contamination necessary to have a marked effect on the nucleation process was obviously much less than that necessary in the LEED studies of Lander and Morrison (1962) where an oxidised Si surface was produced at 1100°C if the pressure of oxygen exceeded about 5×10^{-3} torr. Recently Censlive (1971) has repeated Unvala's experiments in the ultra high vacuum pressure range where very low values of the partial pressure of oxygen were maintained and found that the epitaxial temperature could be reduced to 400°C at a growth rate of 0.1μ/min with layers containing only stacking fault defects to a density of $10^{2} cm^{-2}$. Similar results were found in studies where sublimation from the solid rather than evaporation from the melt was used and possible chemical activity between molten source Si and residual oxygen was eliminated (Thomas and Francombe 1967(a) and (b), Weisberg 1967).

The least developed technique for growing epitaxial semiconductor layers is sputtering which has the main advantage of eliminating the need for heating the source material to high temperature. Possible chemical activity of the source with vacuum environment is therefore eliminated and, in the case of compound semiconductors, possible decomposition of the source is prevented. Furthermore, the sputtering technique is particularly suitable for compound semiconductors because stoichiometric layers of GaAs have been produced directly from polycrystalline sources (Moulton 1962, Pearmain and Unvala 1971) without the need of compensating for the less volatile element as is the case with conventional evaporation methods. Si layers showing preferred orientation have been grown at 200°C by triode sputtering (Clark and Alibozek 1968) but there is no published account of good quality epitaxial Si layers grown by any sputtering method. Only limited information is available on the growth of epitaxial layers of Ge (Krikorian 1964, Haq 1965,

Wolsky et al 1965, Krikorian and Sneed 1966, Layton and Cross 1967, and Luby 1969) and GaAs (Molnar et al 1964). With diode-sputtered Ge layers, the homo-epitaxial temperature was greater than the corresponding vacuum evaporation value (Krikorian and Sneed 1966) unless deliberate ion bombardment of the growing surface was employed (Haq 1965, Luby 1969). The increase in the equivalent epitaxial temperature for diode-sputtered layers was interpreted by Krikorian and Sneed (1966) as being due to the effect of gas atom collisions at the substrate surface lowering the effective temperature of surface atoms. Molnar et al (1964) found that different discharge and heating conditions at the substrate affected the growth of diode-sputtered GaAs layers. With triode sputtering, reduced epitaxial temperatures for Ge were observed (Wolsky et al 1965, Layton and Cross 1967) because the nucleation process was now influenced by the "extra" energy of sputtered atoms and also by gas discharge conditions (Bovey 1969). Only in a few cases was an assessment of the quality of sputtered Ge and GaAs layers made (Krikorian 1964, Haq 1965, Wolsky et al 1965, and Molnar et al 1964). The twinning and high fault density present in these layers could be due to inherent limitations in the diode and triode sputtering techniques used. These limitations are high operating pressures and, therefore, greater background impurities, low deposition rates and limited control of unwanted primary and secondary ions incident on the substrate surface. Recently Unvala and Pearmain (1970) and Pearmain and Unvala (1971) have developed an ion beam sputtering technique capable of producing the purity and quality needed for epitaxial semiconductor layers and reported for the first time the production of good quality epitaxial Si layers by any sputtering technique. This thesis is mainly concerned with the detailed construction and operation of the ion beam sputtering equipment developed together with an assessment of the quality of homo-epitaxial Si layers grown by the sputtering technique. Finally information of the sputtering properties of Si and GaAs with intense beams of high energy ions is presented.

The reason for developing a sputtering technique suitable for semiconductor applications was the need for an alternative method of producing homo-epitaxial Si and GaAs layers. Si was chosen as the initial semiconductor material because of its known sensitivity to contamination and also because there was no published account of good quality epitaxial Si layers by any sputtering method. An ion beam sputtering technique was developed because it offered low operating and background pressures and rates approaching those by chemical and evaporation methods together with the best method of controlling bombardment of substrate surfaces with unwanted ions. Finally the production of Ge, Si or GaAs epitaxial layers by ion beam sputtering has not been previously reported.

The work is presented in four parts. Chapter 2 which follows is a survey of the most relevant literature applied to the effects of ion bombardment of semiconductor surfaces. Chapter 3 deals with the equipment and experimental techniques used. The results obtained and a discussion of these results are combined in Chapter 4. Finally general conclusions and recommendations for further work are outlined in Chapter 5.

CHAPTER 2

REVIEW OF THE EFFECTS CAUSED BY ION BOMBARDMENT OF SEMICONDUCTORS

The effects caused by ion bombardment of solid surfaces are quite numerous and usually rather involved; see for example the review articles by Kaminsky (1965) and Carter and Colligon (1968) which are mainly concerned with bombardment effects of metal surfaces.

In each of the sections that follow, whenever there is a lack of published data for semiconductor surfaces, a general introduction to the particular subject more applicable to all types of surfaces is given followed by a review of the results, if any, for semiconductor surfaces.

2.1. SPUTTERED ATOMS

2.1.1. The process of sputtering

Basically the process, a physical one, occurs when energetic particles (eg. ions) bombard a surface causing the erosion of the outer layers. The uncharged (ie. neutral) eroded material can be deposited onto a suitably placed substrate. There is no real significance in using ions because the same effects are produced by neutral atom bombardment. However, it is experimentally more convenient to use ions.

The mechanism of energy transfer from the bombarding ion to the resulting sputtered atom is now established to be by momentum reversal. The incident ion is slowed down by a succession of energetic collisions with the lattice atoms in its path. Some of these atoms recoil with sufficient energy to initiate a chain-reaction cascade of collisions. If this collision cascade intersects the surface, atoms which receive energy greater than the surface binding energy - usually of the order of several eV - will be ejected and escape.

From the mechanism of sputtering it is clear than an advantage of using a sputtering technique rather than one of evaporation is that no direct heating of the source is

required in order to obtain ejection of neutral atoms from the surface.

2.1.2. The energy of sputtered atoms

Perhaps the biggest difference between sputtered and evaporated atoms is the fact that sputtered atoms have energies that can be as great as two orders of magnitude greater than that of the evaporated atom. The energy distribution curve for sputtered atoms exhibits a Maxwellian form with a high-energy tail. The majority of sputtered atoms have energies from 1eV to 10eV whereas the energy distribution for evaporated atoms peaks at about 0.1eV. A typical energy distribution of sputtered Si atoms for a particular set of conditions is shown in FIG. 2.1.

FIG. 2.2. and FIG. 2.3. show the manner in which the most probable and average ejection energies vary with the atomic number of the target. Both curves, obtained for a fixed set of experimental conditions, show periodicity, in that, within each period, these energies tend to increase with decreased filling of the "d"-shell. Comparison with FIG. 2.4. shows that the values of most probable and average ejection energies are largest for those target materials which have the smallest sputtering yields. The other parameters which can dramatically affect sputtered atom energy are type of bombarding ion, ion energy, angle of incidence of ions, and type of crystal.

2.1.3. Sputtering yield

This parameter is defined as the total number of ejected atoms per incident ion. It is normally determined by the weight loss of the target and integrated current measurements using the relation, sputtering yield = $\frac{1596dM}{AIt}$ atoms/ion, where dM = weight loss of the target in mgms,

I = current in mA,

t = bombardment time in minutes,

and A = mass number of the target atom.

The effect of the weight of implanted ions is negligible when large values of bombardment current and time are used.

It is usual to give the value of the sputtering

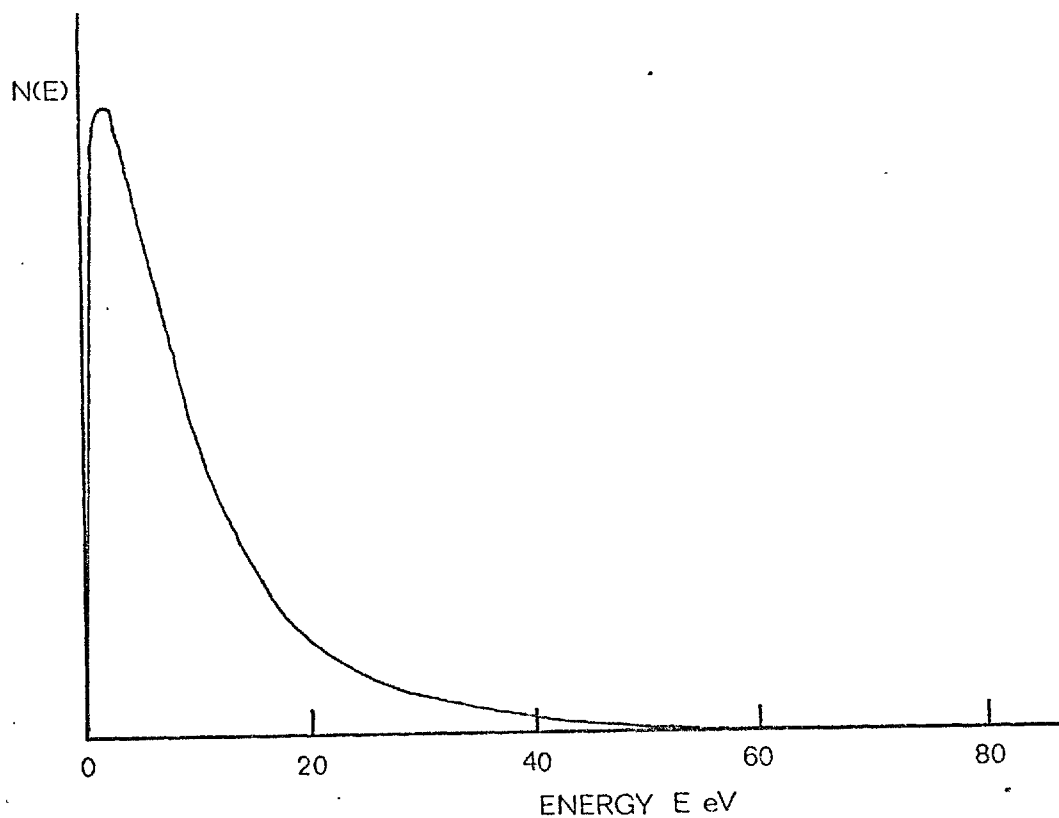

FIG. 2.1. ENERGY DISTRIBUTION OF ATOMS EJECTED IN THE NORMAL DIRECTION FROM A POLY-CRYSTALLINE Si TARGET UNDER BOMBARDMENT BY NORMALLY INCIDENT Kr^+ IONS AT 1.2keV.

AFTER STUART AND WHENER (1965)

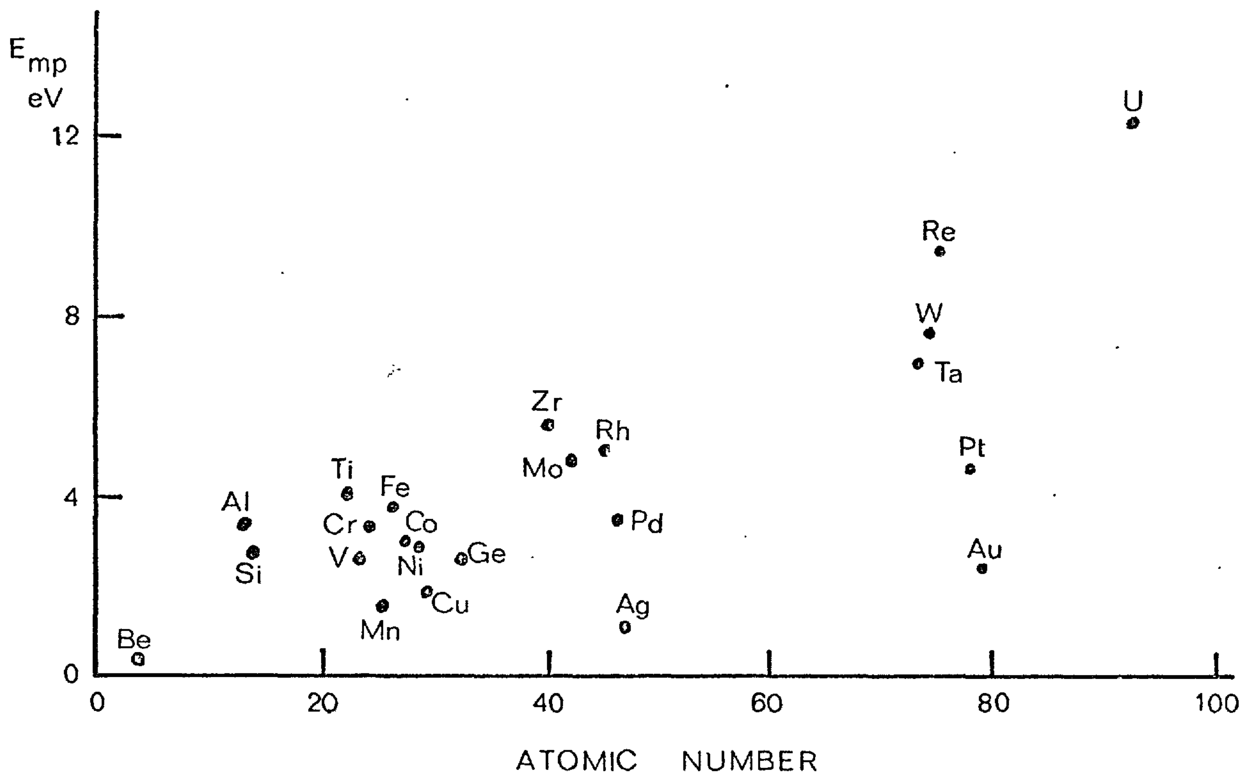

FIG. 2.2. MOST PROBABLE EJECTION ENERGIES E_{mp} FOR ATOMS EJECTED IN THE NORMAL DIRECTION FROM POLYCRYSTALLINE TARGETS UNDER BOMBARDMENT BY NORMALLY INCIDENT Kr^+ IONS AT 1200eV. AFTER STUART AND WEHNER (1965).

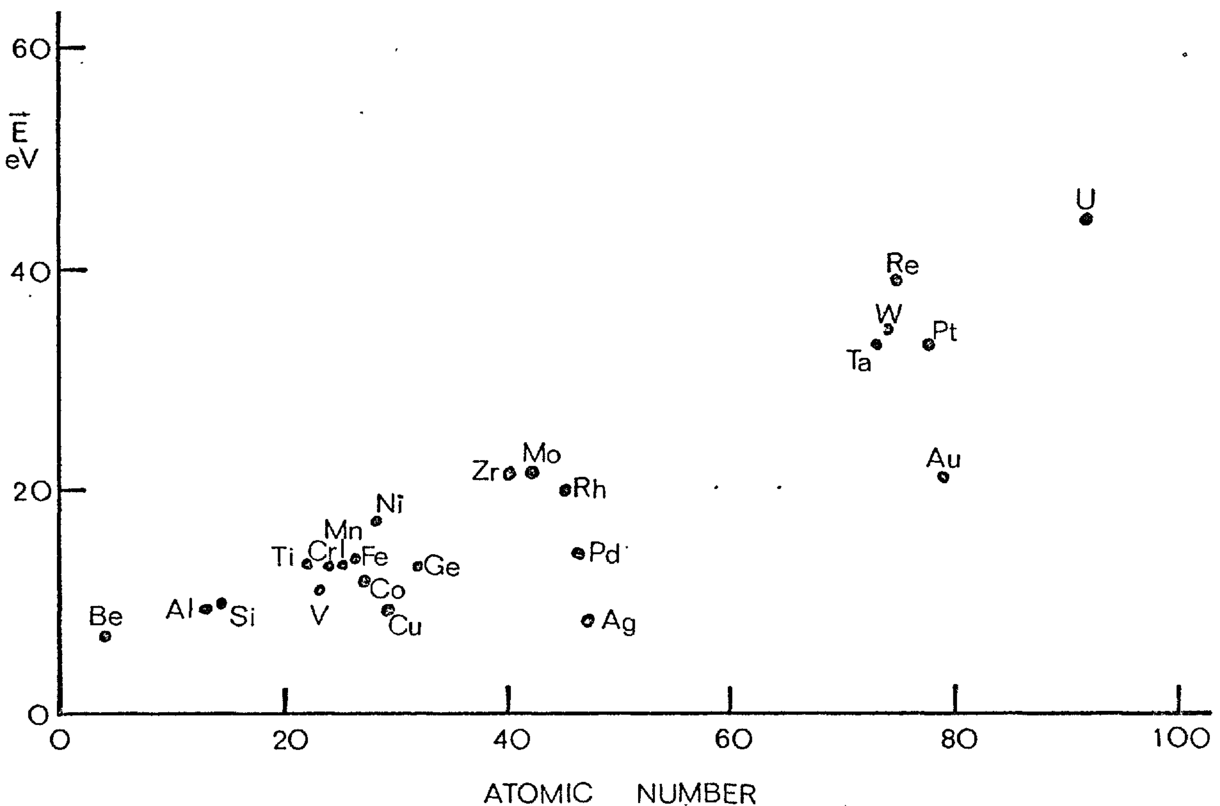

FIG. 2.3. AVERAGE EJECTION ENERGIES ($\bar{E}$) FOR ATOMS EJECTED IN THE NORMAL DIRECTION FROM POLYCRYSTALLINE TARGETS UNDER BOMBARDMENT BY NORMALLY INCIDENT Kr^+ IONS AT 1200eV. AFTER STUART AND WEHNER (1965).

yield derived from the target current measurements. This value is called the apparent sputtering yield (S*) because the target current is the sum of the ion current to the target and the secondary electron current from the target.

For singly-charged bombarding ions, $S^* = \frac{S}{1+\gamma}$,

where S = true sputtering yield,
and γ = secondary electron emission coefficient for singly-charged ions.

For the production of films by sputtering, the sputtering yield directly determines the deposition rate of sputtered atoms. For higher values of sputtering yield, higher deposition rates are obtained and vice versa. With a fixed value of sputtering yield the deposition rate can be further increased by increasing the number of ions which bombard the source.

2.1.4. Influence of the target material on the sputtering yield

FIG. 2.4. shows the variation of the sputtering yield for normally incident 0.4keV and 45keV Kr^+ions as a function of the target atomic number. This periodic dependence of the sputtering yield is again closely related to the state of the electron concentrations in the "d"-shells. For targets with the more open electronic structure (eg. Si), ions penetrate to such depths that the transmission of energy back to the surface where sputtering occurs becomes less efficient. When the "d"-shells are filled, ion ranges are relatively small and energy is more readily projected back towards the surface resulting in more efficient sputtering.

2.1.5. Influence of the type of bombarding ion on the sputtering yield

FIG. 2.5. shows the variation of the sputtering yield for 45keV bombardment of Ag, Cu and Ta targets as a function of ion atomic number. Periodicity is clearly evident with various maxima occurring corresponding to the rare gas ions and with repeatability of the general shape of the curve for each maxima. One of the most interesting features of the result is that for bombardment by particular ions

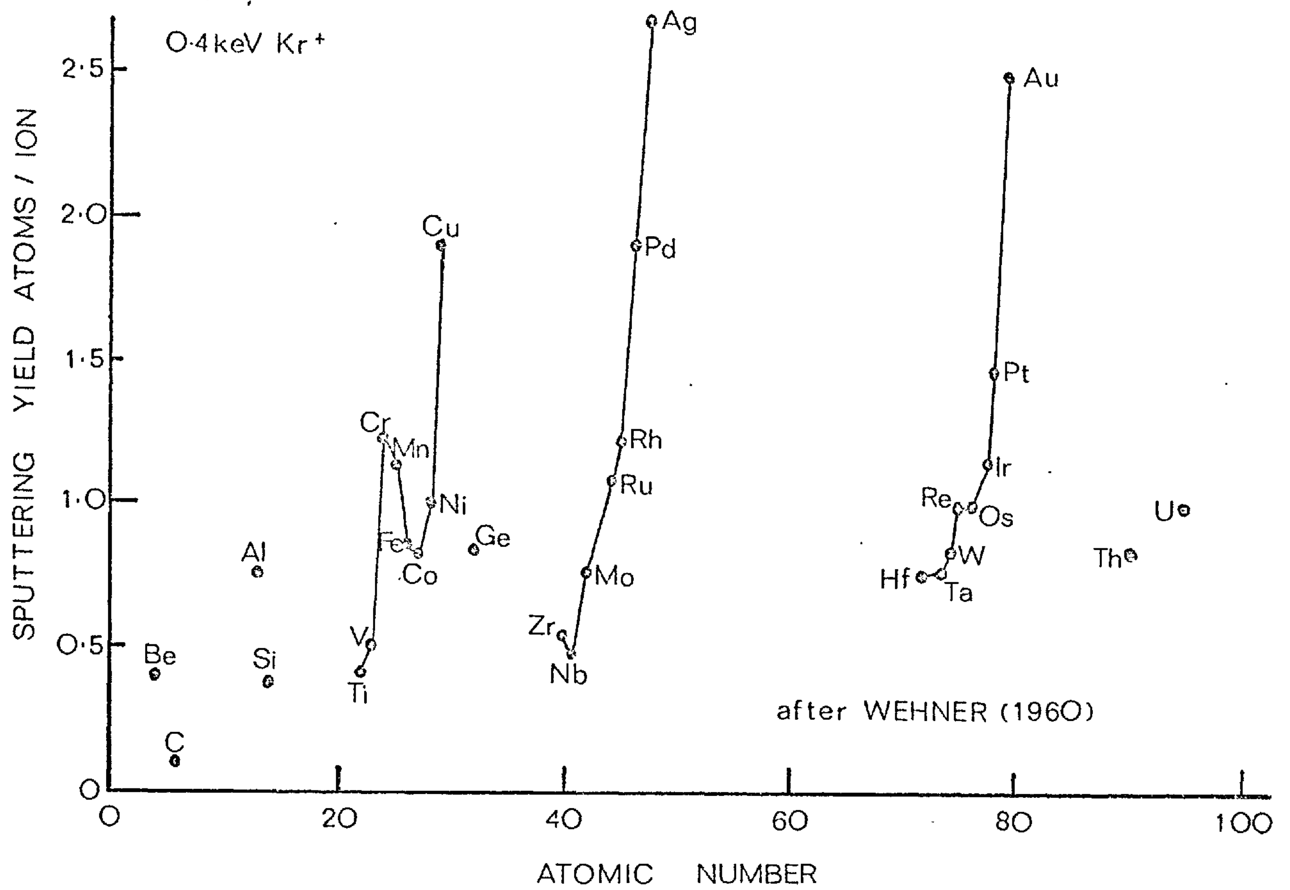

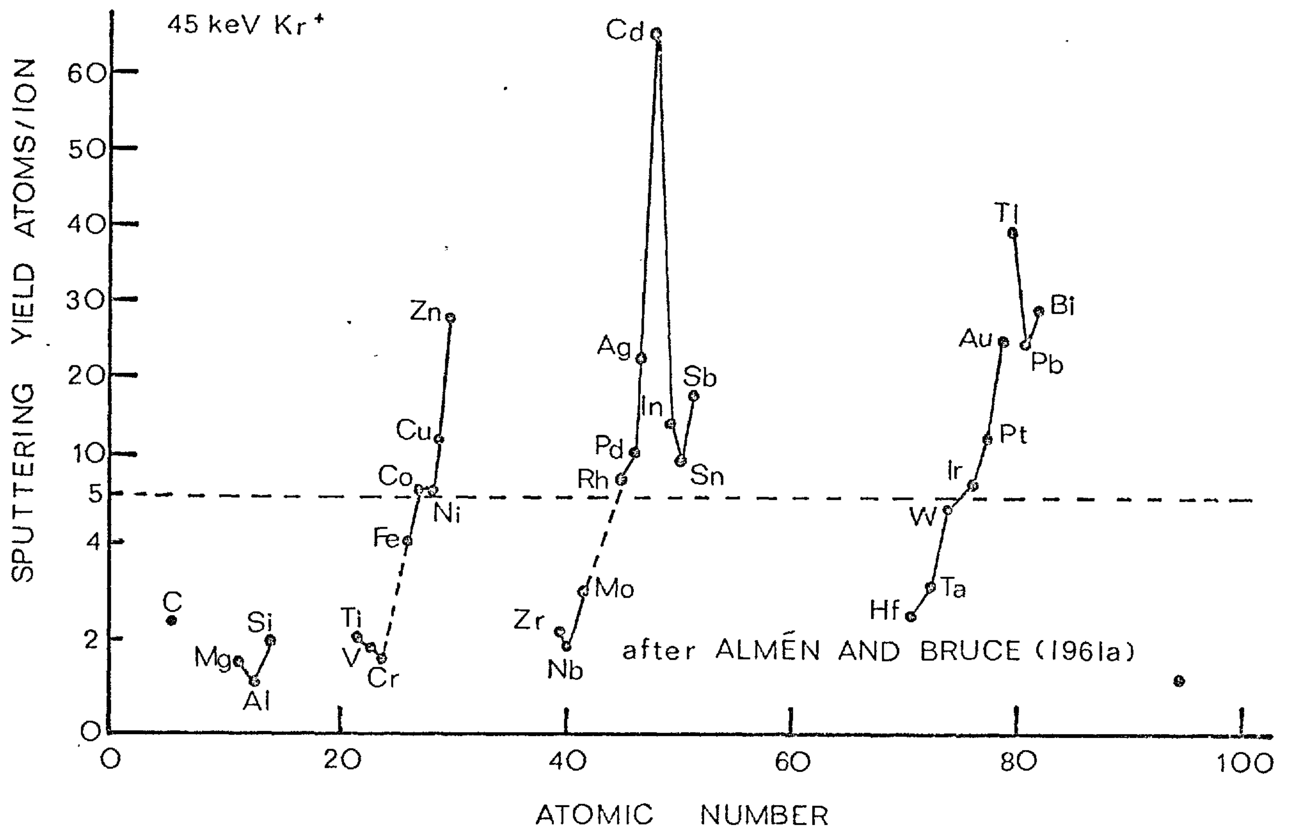

FIG. 2.4. VARIATION OF SPUTTERING YIELD WITH ATOMIC NUMBER OF TARGET FOR BOMBARDMENT WITH NORMALLY INCIDENT 0.4 and 45keV Kr^+ IONS

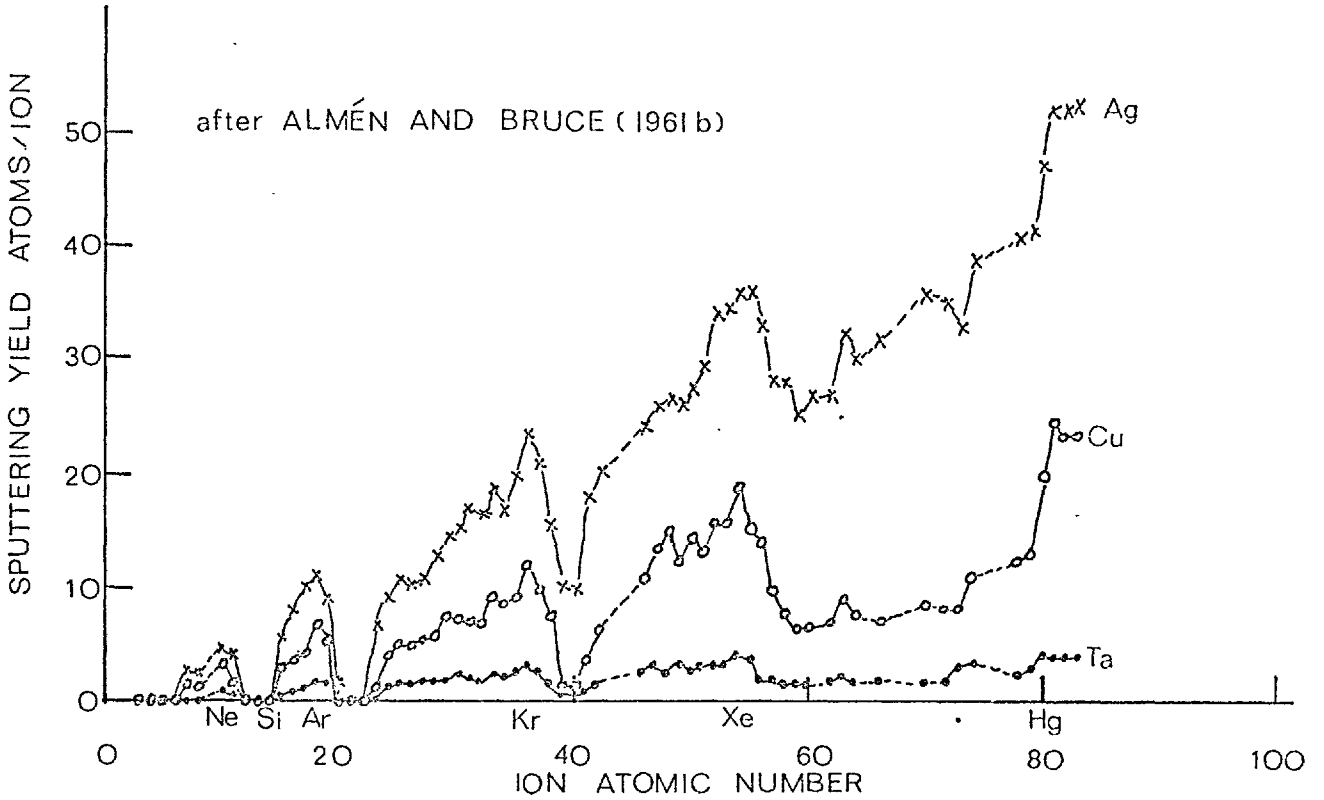

FIG. 2.5. VARIATION OF SPUTTERING YIELD WITH ATOMIC NUMBER OF THE BOMBARDING ION FOR 45keV BOMBARDMENT OF Ag, Cu AND Ta.

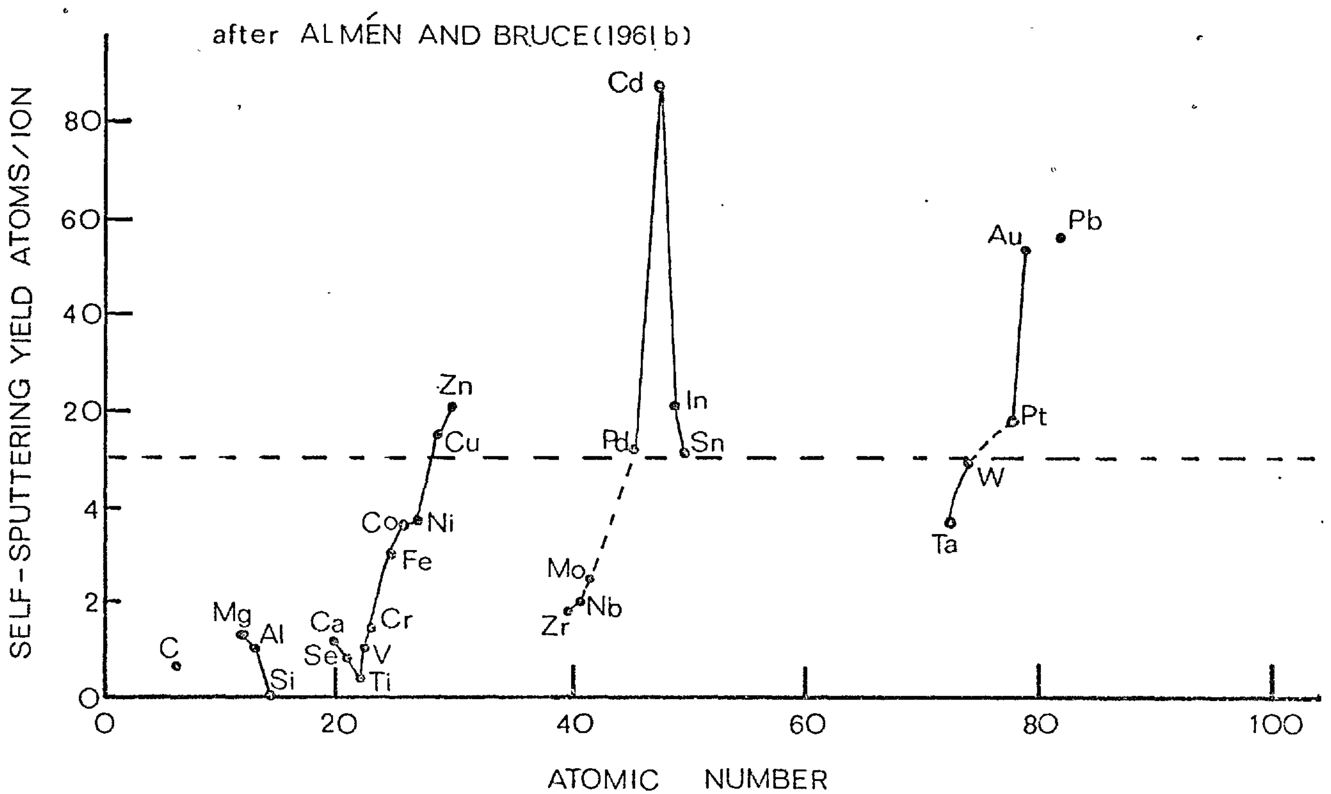

FIG. 2.6. THE SELF-SPUTTERING YIELD FOR 45keV IONS AS A FUNCTION OF THE ATOMIC NUMBER OF THE SPUTTERING SYSTEM ($Z_{target} = Z_{ion}$).

(eg. Si^+) "zero-sputtering" occurs. This implys that ions gradually build up in a layer on the surface and protect the underlying material.

A periodic dependence observed for self-sputtering yields (see FIG. 2.6.) is related to the state of electron concentrations in the "d" and "s" shells. When the shells are filled, more efficient self-sputtering occurs. For 45keV Si^+ions, the Si self-sputtering yield appears to be zero and a layer of Si builds up on the target surface.

2.1.6. Influence of the bombarding ion energy on the sputtering yield

2.1.6.1. General trends

The manner in which the sputtering yield varies with the ion energy is now well established. Typical curves for polycrystalline Cu are shown in FIG. 2.7. No sputtering occurs until the energy of the ions reaches some threshold value E_T, usually between 15 and 30eV. The value of E_T is close to the threshold for the displacement of lattice atoms. The sputtering yield then increases quite quickly until a maximum is reached. At even higher energies yields decrease again. This decrease of the sputtering yield at high energies is attributed to the fact that ions are now penetrating further into the target lattice and dissipating their energy in collisions too deep to transmit a disturbance back to the surface.

Typically, for rare gas ions, the heavier the bombarding ion the larger the peak value of the sputtering yield and the higher the energy value required before the sputtering yield decreases. Both these observations are explained by the fact that the heavier ions do not penetrate the target lattice so far and energy transfer from the ion to the surface via the collision cascade is therefore easier. In the low-energy region, up to several hundred eV, the heavier rare gas ions do not necessarily give the larger values of sputtering yield. The influence of trapped gas is thought to be the controlling factor at low energies where sputtering yields for all materials are small.

When single crystals are used as targets the process

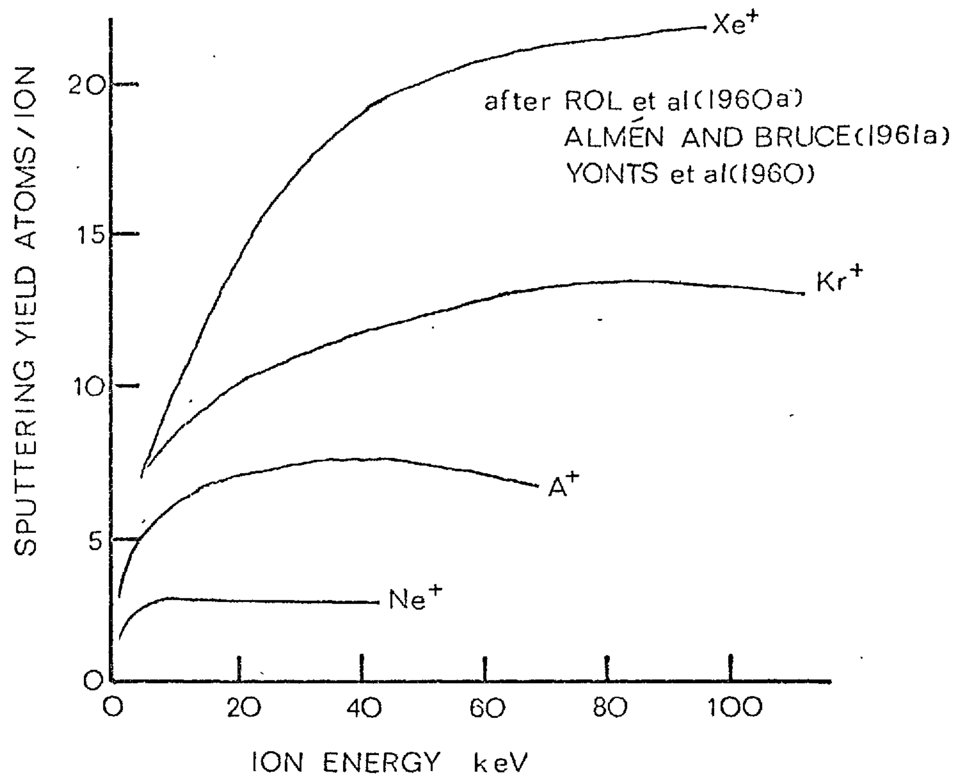

FIG. 2.7. THE MANNER IN WHICH THE SPUTTERING YIELD OF POLYCRYSTALLINE Cu VARIES WITH ION ENERGY FOR DIFFERENT NOBLE GAS IONS.

SPUTTERING YIELD ATOMS/ION
0
2
4
6
8
(111)
(100)
(110)
after SOUTHERN et al (1963)
MAGNUSON AND CARLSTON (1963)
ZDANUK AND WOLSKY (1965)
100eV
1keV
10keV
100keV
ION ENERGY

FIG. 2.8. SPUTTERING YIELD OF Cu SINGLE CRYSTALS AS A FUNCTION OF A^+ ION ENERGY.

of ion channelling must be considered (see SECTION 2.3.2. on ion implantation). Since the atoms of a crystalline solid are arranged in a regular lattice, those special ion trajectories which happen to pass exactly between the rows and planes of atoms without having major collisions will clearly experience an anomalously low rate of energy loss. This implies that the ions can penetrate into certain single crystals to a depth far beyond their statistical range. This phenomenon is known as channelling.
Typical sputtering yield-ion energy curves for the three low-index orientations of Cu single crystals bombarded by A^+ions are shown in FIG. 2.8. By making a comparison between FIGS. 2.7. and 2.8., it is clear that, for the same bombarding ion, the peak value of sputtering yield occurs at a lower value of energy for the single crystal targets than for a polycrystalline target. The peak values of sputtering yield are also less for the three low-index orientations. These two points illustrate that with channelling and enhanced ion penetration it is more difficult to achieve energy transfer from the ion to the surface via the collision cascade. Further examination of FIG. 2.8. shows that at high energies an orientation effect is found which can be related to the transparency of the lattice to the bombarding ion. The most closely packed lattice ((111) in FIG. 2.8.) allows the least transparency to bombarding ions andconsequently has the highest sputtering yield. At low energies the transparency model does not apply and it is thought that the binding energy of the surface atom dominates.

2.1.6.2. Semiconductor targets

The determination of the threshold energy for sputtering has presented many difficulties. In the energy region of the threshold, the amount of sputtered material is very small and, therefore, determination of the threshold depends on the sensitivity of measurement of sputtering yield. Different authors, depending on the sensitivity with which they were able to detect sputtered atoms, have arrived at different apparent threshold values. Wehner (1956) used Hg^+ions of energy up to 300eV and

measured sputtering yields by the weight loss of the target technique. He extrapolated the sputtering yield data to the condition of zero sputtering and found a threshold value of between 60 and 70eV for Si. Wolsky and Zdanuk (1961) used a sensitive microbalance to determine the change in target weight during sputtering and found that the probable threshold was between 15 and 20eV for the A^+-Si system. This value was close to the displacement energy threshold of 13eV for Si atoms (Loferski and Rappaport 1959).

A summary of all the published sputtering yield versus ion energy data for Si is shown in FIG. 2.9.

At low bombarding ion energies considerable information has been obtained by Wehner and co-workers, and Wolsky and Zdanuk (1961). Wolsky used (111) Si targets, whereas the majority of Wehner's experiments were performed with polycrystalline Si targets. A large discrepancy was obtained between the two sets of results which was probably not due to the difference in crystallinity of the target. Wehner used relatively high current densities (up to 15 $mAcm^{-2}$) and maintained target temperatures above 300°C, whereas Wolsky used low current densities (up to 20μAcm^{-2}) with the target at or near room temperature. Wolsky did not remove the oxide layer on the Si surface prior to sputtering and this, combined with a low ratio of bombarding ions to bombarding background-gas particles, probably meant that the clean surface condition was not met (see SECTION 2.1.10.). The much higher current densities used by Wehner almost certainly guaranteed that clean Si surfaces were maintained. Wehner has also shown that at low energies the heavier bombarding ions did not necessarily result in the larger values of sputtering yield. In this energy region, where more than one bombarding ion was necessary for the ejection of a neutral sputtered atom, the dominant factor was thought to be the influence of trapped gas.

At higher energies, the sputtering yield of Si has been investigated by Southern et al (1963). They bombarded Si (111) crystals with normally incident 1 to 5keV A^+ ions and found that a peak value of sputtering

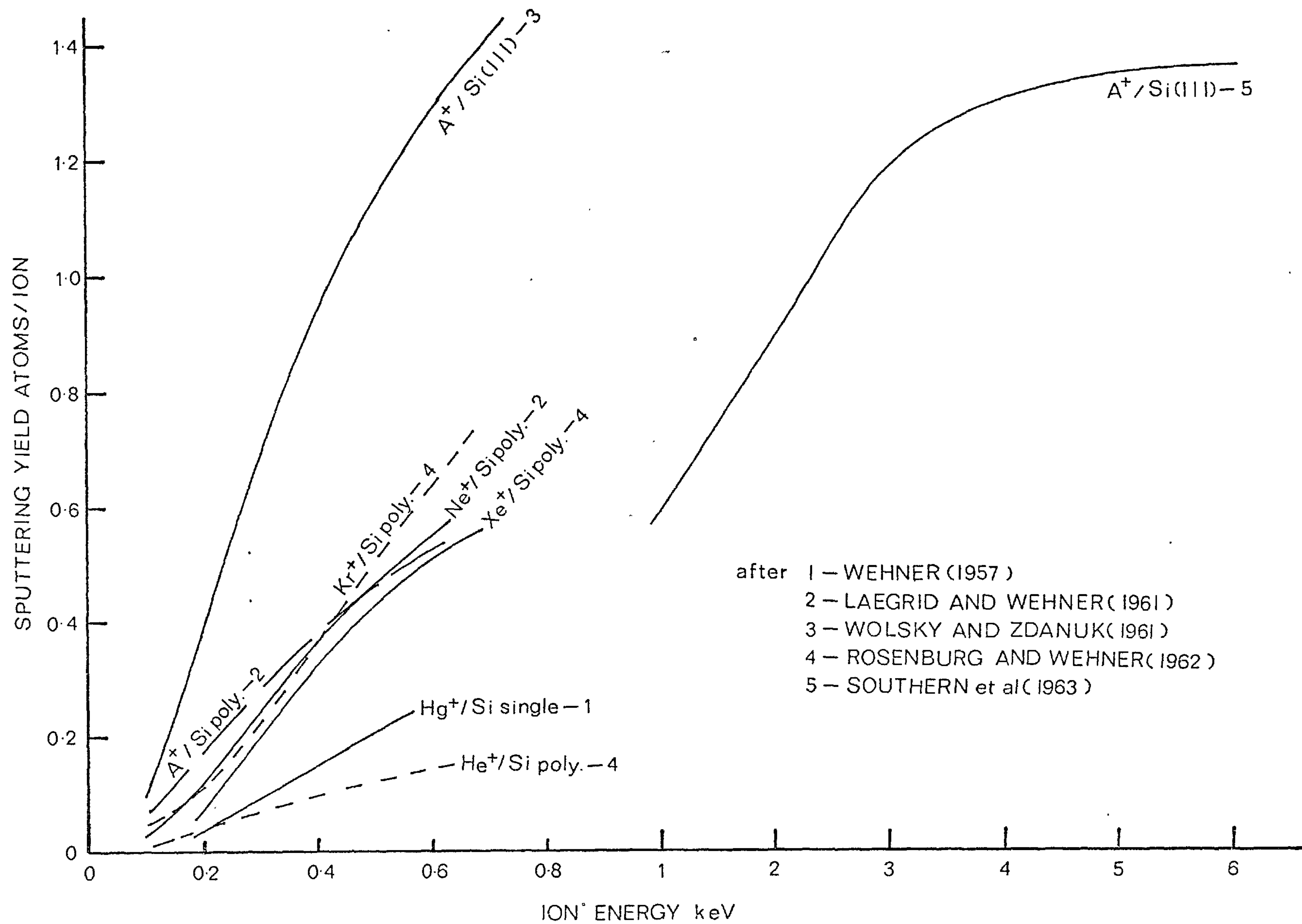

FIG. 2.9. VARIATION OF SPUTTERING YIELD WITH ION ENERGY FOR Si TARGETS BOMBARDED AT NORMAL INCIDENCE.

yield was reached at about 5keV. Only continuous sputtered deposits were observed and the absence of atom ejection along preferred crystallographic directions (SECTION 2.1.9.2.) indicated that an amorphous surface layer had been created (SECTION 2.3.1.6.).

Only low-energy yield data has been reported in the literature for GaAs. Comas and Cooper (1966) bombarded GaAs(110) single crystals with normally incident 75 to 600eV A^+ ions and the yield varied in the manner shown in FIG. 2.10. The results shown represented the case where an amorphous surface layer was present again because ejection of sputtered atoms along preferred crystallographic directions was not observed.

The effect of crystal orientation on the sputtering yield at various ion energies has been investigated by various workers.

Anderson (1966a) studied the temperature dependence of the sputtering yield from the three low-index faces of Ge under low-energy (up to 500eV) A^+ ion bombardment. He has shown that for target temperatures above a critical value, called T_a (for his experiments T_a=280°C), the sputtering yields were quite different with

$$S^*(100) > S^*(111) \sim S^*(110),$$

whereas below T_a the sputtering yields for the "(100)" and "(110)" surfaces were nearly identical but less than the high-temperature yield for the (100) surface and higher than the high-temperature yield for the (110) surface. The significance of T_a was that for target temperatures above T_a the damage produced by bombarding ions annealed out more rapidly than it was being produced, whereas below T_a the damage remained frozen-in and an amorphous surface phase resulted. The difference in sputtering yield for temperatures above and below T_a has been used to measure T_a (see SECTION 2.3.1.6.(d).

The order of the yields was also determined by Southern et al (1963), who studied Ge(100), (110) and (111) yields for bombardment by 1 to 5keV A^+ ions. Southern did not find any significant differences in yields at low energies but at the higher energies yields

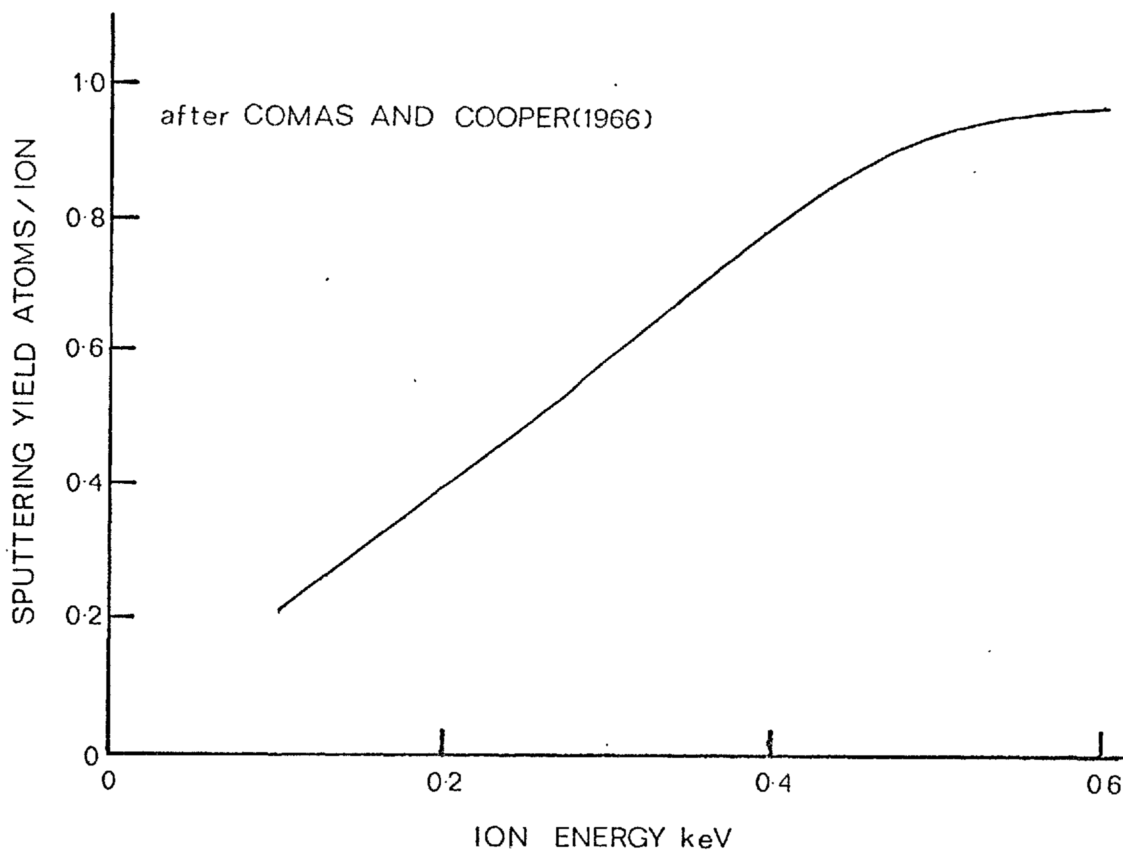

FIG. 2.10. VARIATION OF SPUTTERING YIELD WITH ION ENERGY FOR A GaAs(110) TARGET BOMBARDED WITH NORMAL INCIDENCE A^+ IONS.

seemed to decrease in the same order as found by Anderson. Target temperatures were not specified but were probably below T_a as substantiated by the fact that no preferential atom ejection directions were observed. Possibly the slight differences they observed at higher energies were caused by the increased heating of the target by the bombarding beam.

Davies et al (1964) have studied the range of high-energy (≥20keV) Xe^+ ions in Si. They found that the penetration decreased in the order $[\bar{1}10] \gg [\bar{1}11] > [\bar{1}00]$. Accordingly, using the transparency model, one would anticipate that the sputtering yield decreased in the order (100) > (111) ≫ (110). However, the work of Anderson and Southern suggested that the yield of the (111) surface was nearest the (110). Furthermore, if transparency was the most significant factor one would expect that the highly damaged surface ($T < T_a$) should have the highest yield since it must have the lowest transparency. This was not the case, as Anderson found that the yield of this surface was actually less than for the (100) surface. The binding energy of the surface atoms and the atom positions were thought to be the controlling mechanisms in the energy range up to several keV. On the other hand, Comas and Cooper (1967) sputtered GaAs single crystals with 140eV A^+ ions and found that the sputtering yields varied in the manner $(111) \sim (\bar{1}\bar{1}\bar{1}) > (110)$ suggesting perhaps that the transparency model could not be entirely dismissed at low ion energies.

2.1.7. Influence of the ion angle of incidence on the sputtering yield

As the angle of incidence from the target normal is increased the sputtering yield also increases. This increase in sputtering yield is due to the fact that the efficiency of momentum reversal is improved at angles of attack away from the target normal. Typical curves for the A^+-polycrystalline Cu system are shown in FIG. 2.11., which also shows that the rate of increase of sputtering yield with angle of incidence depends on the energy of the bombarding ion. At the larger values of incidence,

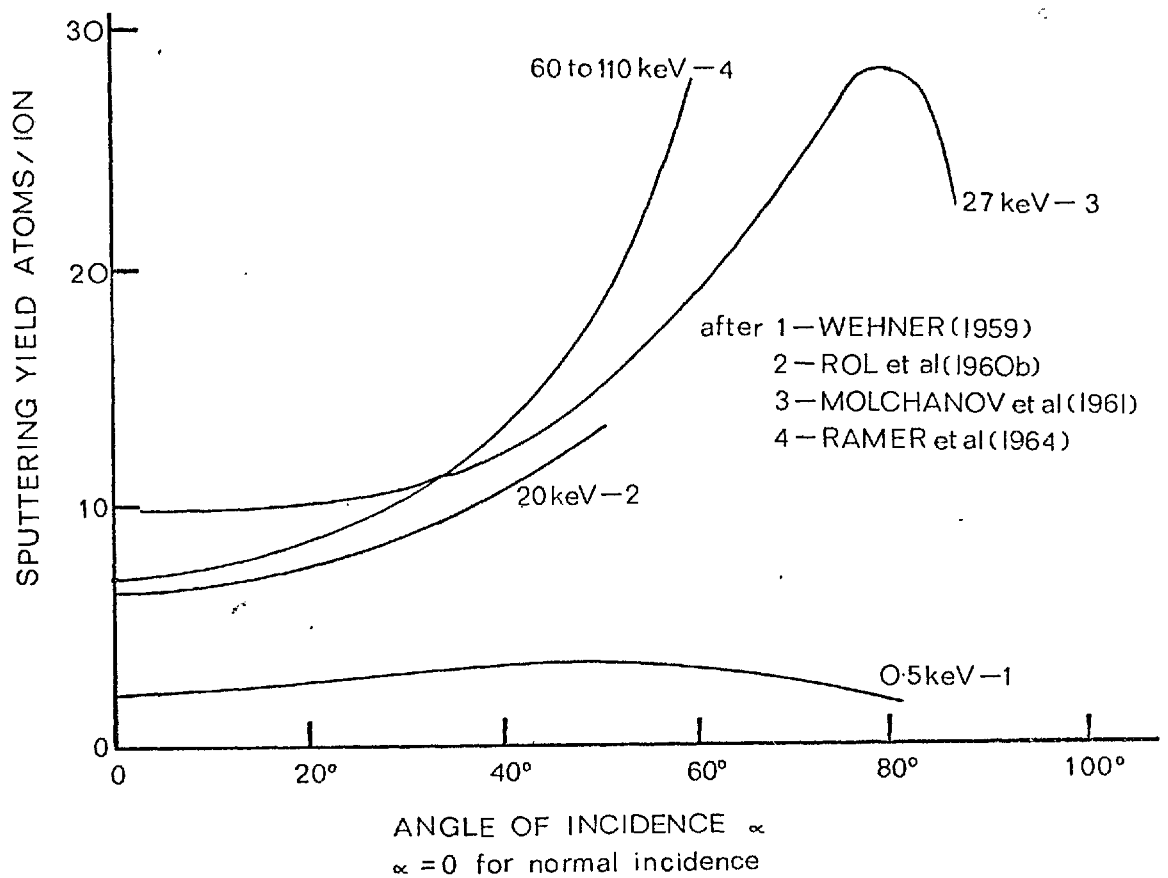

FIG. 2.11. VARIATION OF THE SPUTTERING YIELD OF POLY-CRYSTALLINE Cu WITH ION ANGLE OF INCIDENCE FOR DIFFERENT A^+ ION ENERGIES.

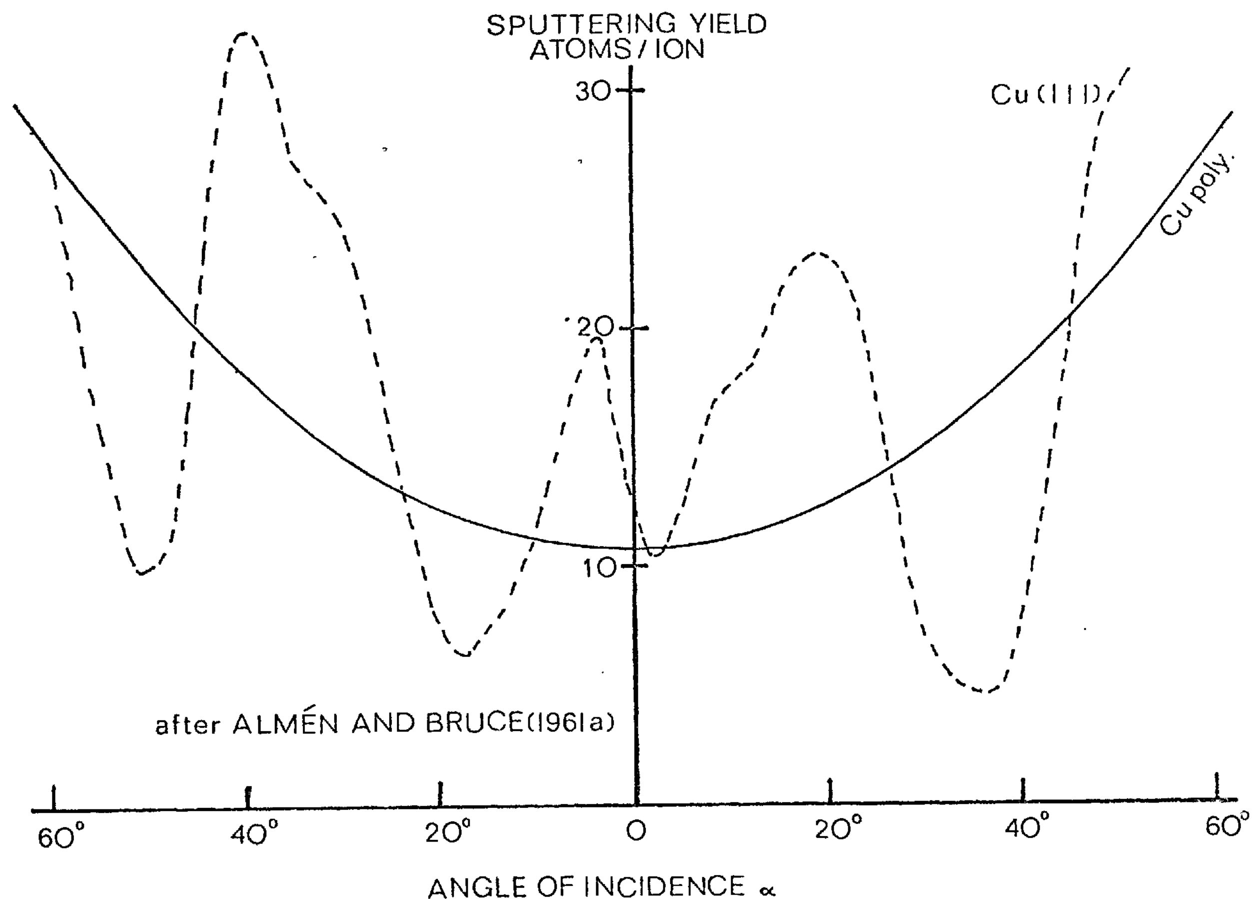

FIG. 2.12. SPUTTERING YIELD OF Cu CRYSTALS AS A FUNCTION OF ANGLE OF INCIDENCE OF 45keV Kr^+ IONS. THE (111) Cu SINGLE CRYSTAL IS TURNED AROUND A (110) AXIS IN THE (111) PLANE. THE (111) DIRECTION IS 3° FROM 0.

the sputtering yield goes through a maximum. This behaviour may be caused in part by the marked increase in the reflection of the primary ion beam at large angles of incidence (see SECTION 2.2.2.1.). Lindhard (1965) shows that the critical angle $\hat{\alpha}$, for such reflection is given by

$$\hat{\alpha} = \frac{\pi}{2} - \sqrt{\frac{5\pi a_o^2 \, n^{2/3} \, Z_1 \, Z_2 \, E_R}{(Z_1^{2/3} + Z_2^{2/3}) \, E_1}}$$

where a_o is the Bohr radius 0.53°A,
n is the density of atoms per unit volume,
Z_1 and Z_2 are the atomic numbers of ion and atom,
E_R is the Rydberg energy 13.6eV
and E_1 is the primary ion energy.

The equation correctly predicts that $\hat{\alpha}$ increases with ion energy and the effect of increasing either Z_1 or Z_2 is to decrease $\hat{\alpha}$. A small shift in the optimum sputtering angle can be caused by the degree of surface roughness of the target. Crystallites of different orientation in a polycrystalline target are sputtered at different rates so the surface roughness increases during sputtering. A decrease in yield occurs because many of the sputtered atoms are now unable to clear the surface and become trapped on surface protrusions.

For single crystal targets, the sputtering yield depends strongly and in a complicated way on the angle of incidence. Instead of increasing monotonically with increasing angle of incidence, the sputtering yield shows pronounced maxima and minima. A typical result for a Cu(111) surface is shown in FIG. 2.12. along with the corresponding result for a polycrystalline Cu sample. The origin of the strong anisotropy of the curve for the single crystal is associated with the concept of channelling, with the maxima corresponding to opaque directions of the lattice and the minima to transparent directions. The curve for the polycrystalline target in fact represents the average of a multitude of curves for differently oriented single crystals bombarded in different planes and at different angles.

No information regarding the influence of the ion

angle of incidence on the sputtering yield for semiconductor targets has been reported in the literature.

However, Stewart and Thompson (1969) bombarded a Si surface with a 5 to 8keV A^+ion beam and observed the formation of conical protrusions (see SECTION 2.3.3.) on the surface with the aid of the scanning electron microscope. The resulting cones, with their axes along the direction of ion incidence (45° to surface normal), were shown to have a half-angle corresponding to the peak in the graph of sputtering yield versus angle of ion incidence for a polycrystalline target.

2.1.8. Angular distribution of sputtered particles from polycrystalline samples

The distribution of evaporated atoms from a heated source, whether single or polycrystalline, shows a cosine-type distribution. For normally-incident ions, the ion energy determines the distribution of sputtered material from polycrystalline samples. At low energies (up to 1keV), the distribution is "under-cosine" ie. relative to a cosine distribution more particles are ejected in directions parallel to the surface and fewer in the direction of the normal. As the ion energy is increased a cosine distribution is reached at about 10keV, but by 20keV an "over-cosine" distribution results.

There is also a dependence of the distribution on the ion angle of incidence. In general, particles are preferentially sputtered in the direction in which the ion beam would be directed if it was specularly reflected from the target surface.

The only published data for polycrystalline semiconductor targets is that of Wehner and Rosenburg (1960). They bombarded a polycrystalline Ge target with normally-incident Hg^+ ions of energy up to 1keV and found that an "under-cosine" distribution resulted. (see FIG.2.13)

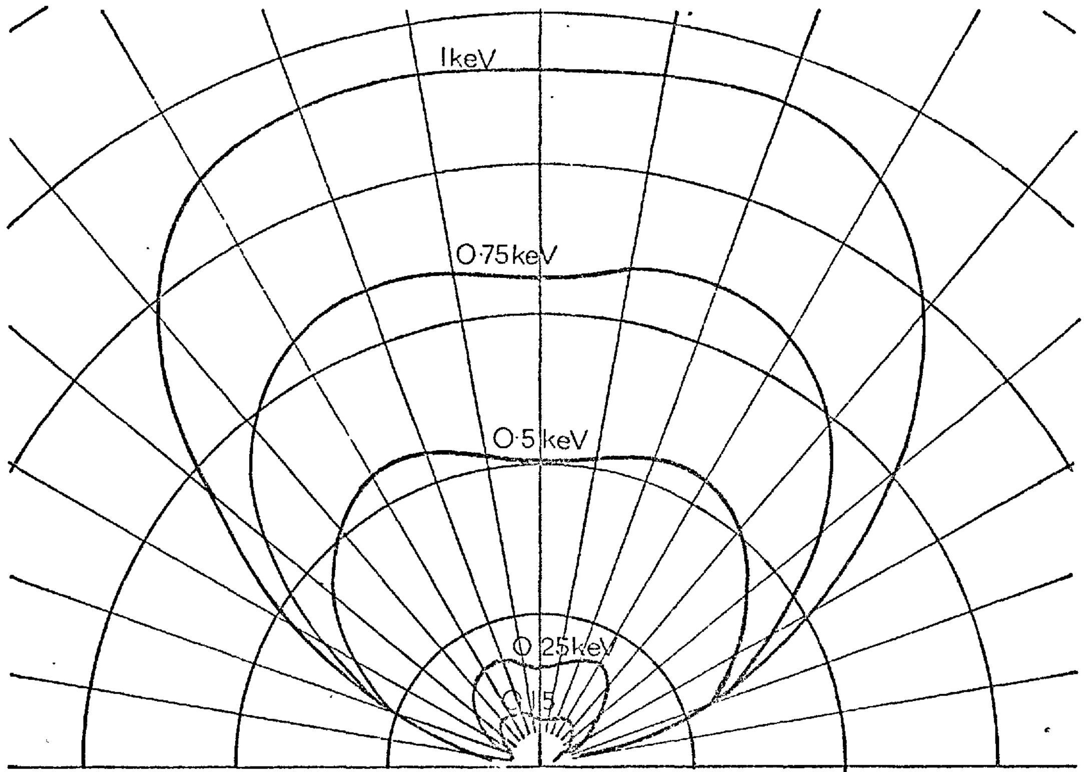

FIG. 2.13. POLAR DIAGRAM OF MATERIAL SPUTTERED FROM POLYCRYSTALLINE Ge BY NORMALLY INCIDENT Hg^{+} IONS OF 0.15 TO 1keV ENERGY.

2.1.9. Preferential ejection of sputtered atoms from single crystals

The discovery that atoms were sputtered from single crystals primarily in certain preferred crystallographic directions was made by Wehner (1955). This was the first experimental evidence for collisions related to crystal directions.

2.1.9.1. Mechanisms of preferential ejection

Silsbee (1957), in a theoretical study, derived that sputtering maxima, along low-index directions of the crystal, could be caused by atomic collision sequences, focused along these directions. Silsbee has shown for a row of hard spheres with radius R and a distance apart D that a collision sequence will travel along the row if $D<4R$ and if the angle the primary recoil atom makes with the row is small. The condition $D<4R$ also implied that, after each collision, each atom was closer to its original equilibrium position than to that of its neighbour. Consequently, no re-displacement occurred and successive collisions simply transmitted energy along the line in a packet which was subject to attenuation. On reaching the surface with an energy greater than the binding energy, atoms were ejected in the same directions. Silsbee focusing (ie. $D<4R$) along straight closely-packed rows of atoms (ie. nearest-neighbour directions) is only possible along $\langle 110 \rangle$ directions for the fcc structure, and along $\langle 111 \rangle$ and $\langle 100 \rangle$ directions for the bcc structure. In the diamond structure there are no straight close-packed rows of atoms as a consequence of covalent bonding.

However, Vineyard et al (1960) have calculated that focusing was also possible, although with less efficiency, in directions which are not close-packed if neighbouring atoms were taken into account (ie. along next-nearest-neighbour directions). This form of focusing behaves with striking similarity to the converging lens in optics. The lens-focusing action of the surrounding atoms explains $\langle 111 \rangle$ and $\langle 100 \rangle$ ejection for the fcc structure, and $\langle 110 \rangle$ ejection for the bcc structure.

Usually the main ejection sequences for both fcc and bcc structures are accompanied by several less-intense

streaks. The presence of these streaks becomes more important at very high energies where the prominence of Silsbee and lens focusing declines because ions now penetrate into the target so far and recoil chain collision processes are inefficient. The streaks were interpreted by Ogilvie and Ridge (1959) on the basis of a channelling mechanism which makes it possible to transport atoms over long ranges. The preferential ejection is now along inter-planar spaces which offer less resistance to the passage of the recoils. The channelling mechanism is probably more important for the semiconductor materials because along certain directions in the diamond-cubic lattice there are wide open channels and the absence of close-packing of atoms suggests that Silsbee focusing cannot occur. From the transparency data of Si, determined by Davies et al (1964), one would expect that at very high energies the effectiveness of ejection directions should decrease in the order $\langle 110 \rangle \gg \langle 112 \rangle > \langle 111 \rangle \sim \langle 100 \rangle$ for the diamond structure materials.

The mechanisms of preferential ejection discussed up till now are strictly high-energy mechanisms (for energies greater than several keV). At low energies, where path lengths are small, Harrison et al (1966) have shown that crystal dependences of ejection can be explained solely by glancing near-surface collisions. From consideration of efficiency of energy transfer, ejection occurs most favourably in directions corresponding to collisions with least energy loss.

2.1.9.2. Ejection directions for semiconductors

A table summarising a wide variety of observed ejection directions for Si and Ge single crystals is shown in TABLE 2.A. TABLE 2.B. shows the results for the III-V compound semiconductors.

The failure of some observers to see preferred atom ejection directions is explained on the basis that target temperatures were not sufficiently high to anneal out damage produced by the bombarding ions and prevent the formation of an amorphous surface layer (see SECTION 2.3.1.6.). The temperature determing the transition from an isotropic deposit to a deposit showing spots due

REFERENCE	Bombarding ion	Energy	mA cm^{-2} (or ion sec^{-1} cm^{-2})	Target temperature	Single crystal target	Ejection directions
WEHNER (1956)	Hg^+	up to 300eV		300°C	Ge	$\langle 111 \rangle$
ANDERSON and WEHNER (1960)	Hg^+	up to 800eV	5mA cm^{-2} ($3x10^{16}$)	300°C	Ge	$\langle 111 \rangle$ and $\langle 100 \rangle$
ANDERSON (1962)	Hg^+ Ne^+ A^+	up to 800eV		300°C	Ge and Si	$\langle 111 \rangle$ and $\langle 100 \rangle$
YURASOVA and SIROTENKO (1962)	Kr^+	1-10keV	5 to 15mA cm^{-2} ($3x10^{16}$ to $1x10^{17}$)	?	Ge	$\langle 110 \rangle$ and $\langle 100 \rangle$
SOUTHERN et al (1963)	A^+	1-5keV	50 to 200μA cm^{-2} ($3x10^{14}$ to $1x10^{15}$)	at or near room temperature	Ge(100), (111) and (110) AND Si(111)	ONLY CONTINUOUS DEPOSIT OBTAINED
HASIGUTI et al (1963)	A^+	6keV	100 to 300μA cm^{-2} ($6x10^{14}$ to $2x10^{15}$)	?	Ge(111), (110) And (100)	CIRCULAR DEPOSITS WHICH MEANT ATOM EJECTIONS WERE ISOTROPIC
COLOMBIE et al (1966)	A^+	80keV	4mA cm^{-2} ($2\frac{1}{2}x10^{16}$)	?	Ge(100)	ISOTROPIC DEPOSIT
					Ge(111)	ION DOSE $\sim 1x10^{19}$ ions cm^{-2} GAVE $\langle 110 \rangle$ and $\langle 112 \rangle$ DIRECTIONS. ION DOSE $\sim 2x10^{19}$ ions cm^{-2} GAVE NEARLY ISOTROPIC DEPOSIT

TABLE 2.A. OBSERVED EJECTION DIRECTIONS FROM Si and Ge single crystals

REFERENCE	BOMBARDING ION	ENERGY	mA cm^{-2} (or ion sec^{-1} cm^{-2})	TARGET TEMPERATURE	SINGLE CRYSTAL TARGET	EJECTION DIRECTIONS AND CHEMICAL COMPOSITION OF SPUTTERED DEPOSIT
WOLSKY et al (1964)	A^+	up to 1keV	8 to 100μA cm^{-2} ($5x10^{13}$ to $6x10^{14}$)	?	GaSb(111)	$\langle 111 \rangle$ and $\langle 100 \rangle$ EXCESS OF Ga
ANDERSON AND WEHNER (1964)	Ne^+ A^+ Kr^+ Xe^+	up to 800eV	1mA cm^{-2} ($6x10^{15}$)	$T > T_a$	InSb(110) and InAs(110)	$\langle 111 \rangle$ and $\langle 100 \rangle$ SUSPECTED COMPOSITION OF 2$\langle 111 \rangle$ SPOTS NOT IDENTICAL
COMAS AND COOPER (1966)	A^+	up to 600eV	3mA cm^{-2} ($2x10^{16}$)	$< 100°C$	GaAs(110)	ONLY CONTINUOUS DEPOSIT OBTAINED. NO INFORMATION ON CHEMICAL COMPOSITION.
ANDERSON (1966b)	Ne^+ A^+	500eV	1mA cm^{-2} ($6x10^{15}$)	$T > T_a$	GaAs(110) and InAs(110)	$\langle 111 \rangle$ AND $\langle \bar{1}\bar{1}\bar{1} \rangle$. $\langle \bar{1}\bar{1}\bar{1} \rangle$ spot, Ga-55: As-45. $\langle 111 \rangle$ spot, Ga-45: As-55. NO CHANGE FOR InAS.
COMAS AND COOPER (1968)	A^+	up to 600eV	1 to 6mA cm^{-2} ($6x10^{15}$ to $4x10^{16}$)	$T > T_a$	GaAs and GaP (111)	$\langle 110 \rangle$ AND $\langle 114 \rangle$.
					($\bar{1}\bar{1}\bar{1}$)	NO PREFERENTIAL EJECTION
					(100)	$\langle 110 \rangle$
					(110)	$\langle 110 \rangle$; EQUAL AMOUNTS OF Ga AND As.

TABLE 2.B. OBSERVED EJECTION DIRECTIONS AND CHEMICAL COMPOSITION OF SPUTTERED DEPOSITS FROM COMPOUND SEMICONDUCTORS

REFERENCE	BOMBARD-ING ION	ENERGY	mA cm^{-2} (or ion sec^{-1} cm^{-2})	TARGET TEMPERATURE	SINGLE CRYSTAL TARGET	EJECTION DIRECTIONS AND CHEMICAL COMPOSITION OF SPUTTERED DEPOSIT
YURASOVA AND SIROTENKO (1962)	Kr^+	1 to 10keV	5 to 15mA cm^{-2} ($3x10^{16}$ to $1x10^{17}$)	?	InSb	⟨110⟩ AND ⟨100⟩ NO INFORMATION ON CHEMICAL COMPOSITION
SOUTHERN et al (1963)	A^+	1 to 1.7keV	50 to 200μA cm^{-2} ($3x10^{14}$ to $1x10^{15}$)	AT OR NEAR ROOM TEMPERATURE	InSb(111)	3 ⟨110⟩ spots ON CONTINUOUS BACKGROUND. NO INFORMATION ON CHEMICAL COMPOSITION.
YURASOVA et al (1964)	Kr^+	1keV	1mA cm^{-2} ($6x10^{15}$)	?	InSb and GaAs	⟨110⟩, ⟨111⟩, ⟨100⟩ and ⟨114⟩ EXCESS OF In FOR InSb AND EXCESS OF Ga FOR GaAs

TABLE 2.B. Continued

to preferential ejection along certain crystallographic directions is called the critical annealing temperature, T_a, and ejection patterns have been used to measure T_a (see SECTION 2.3.1.6.(a)).

Wehner and Anderson have consistently shown $\langle 111 \rangle$ and usually $\langle 100 \rangle$ ejection to predominate in their low-energy studies (up to 800eV). The $\langle 111 \rangle$ direction is the direction of the line of centres of nearest neighbours in the diamond-cubic lattice. Although "lens focusing" can operate in $\langle 111 \rangle$ directions, it seems unlikely in this energy range where path lengths of ions and collision processes are small. The $\langle 111 \rangle$ and $\langle 100 \rangle$ ejection directions are probably the directions corresponding to near-surface collisions with least energy loss.

At higher energies (above 1keV), $\langle 110 \rangle$ ejection became prominent which indicates that the channelling mechanism is becoming significant. Colombie et al (1966) found that at 80keV the order of effectiveness of ejection directions was $\langle 110 \rangle$, $\langle 112 \rangle$ indicating that the channelling mechanism is dominant.

2.1.9.3. Composition of sputtered deposits from compound semiconductors

TABLE 2.B. also shows the results by different observers for the chemical composition of sputtered deposits from single crystals of the III-V compound semiconductors GaAs, InAs and GaSb which show the covalent-bonded zinc-blende structure. The zinc-blende structure (see FIG.2.14.) exhibits several characteristic features which are important when interpreting sputtering results. These features, shown in FIG. 2.14.(a), are (i) the existence of rows of atoms along $\langle 110 \rangle$ and $\langle 100 \rangle$ directions consisting of one element (either III or V), (ii) the existence of rows of atoms along $\langle 111 \rangle$ directions where atoms of the two elements alternate, (iii) the absence of a centre of symmetry in the lattice, as the result of which the $\langle 111 \rangle$ directions form polar axes so that the $\langle 111 \rangle$ and $\langle \bar{1}\bar{1}\bar{1} \rangle$ directions differ. The $\{111\}$ and $\{\bar{1}\bar{1}\bar{1}\}$ planes also differ. This is evident from FIG. 2.14.(b) where $\{111\}$ planes and $\{\bar{1}\bar{1}\bar{1}\}$ planes are surfaced by atoms of different type.

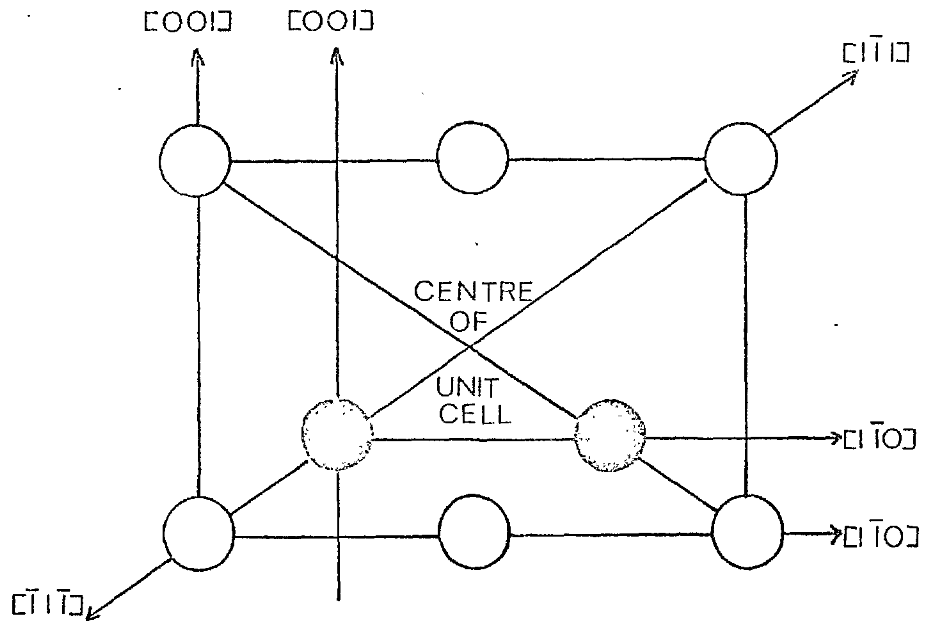

(a) SECTION IN (110) PLANE OF UNIT CELL

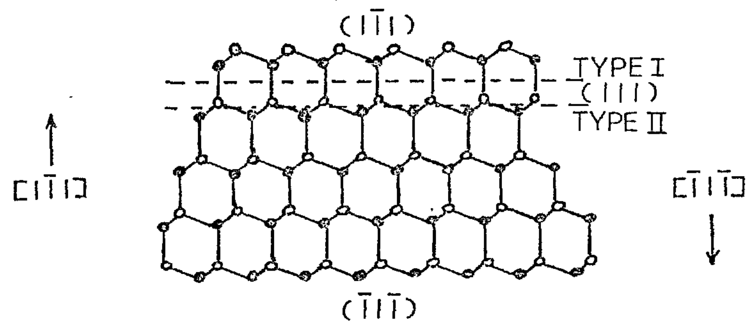

(b) PROJECTION OF THE STRUCTURE ON (110) PLANE. MATERIAL PREDOMINANTLY PARTS ON TYPE I PLANES SO THAT (1$\bar{1}$1) PLANE AND ($\bar{1}$1$\bar{1}$) PLANE ARE SURFACED BY ATOMS OF DIFFERENT TYPE.

FIG. 2.14. THE ZINC-BLENDE STRUCTURE.

Anderson and Wehner (1964) suspected that sputtered deposits in the polar directions $\langle 111 \rangle$ and $\langle \bar{1}\bar{1}\bar{1} \rangle$ were not identical. In a later study, Anderson (1966b) found that for GaAs the compositions of the spots in $\langle \bar{1}\bar{1}\bar{1} \rangle$ and $\langle 111 \rangle$ directions were Ga-55:As-45 and Ga-45:As-55 respectively. For a non-polar direction, Comas and Cooper (1968) found that the $\langle 110 \rangle$ spot contained equal amounts of Ga and As. In studies where a compositional analysis was made of the overall sputtered deposit from a single crystal an excess of the III-atom was generally found. Polycrystalline sources of the compound semiconductors produced stoichiometric deposits (Moulton 1962, Pearmain and Unvala 1971).

2.1.10. Pressure-dependent sputtering

A common feature of early sputtering experiments (pre 1950), particularly when the diode or glow discharge technique was used (typical operating pressure $\gtrsim 10^{-2}$torr), was that the mean free path of the sputtered particles was less than the distance from the target to some collector surface. In consequence many of the liberated atoms diffused back to the surface after collisions with gas atoms and were then either re-sputtered, or buried underneath subsequent returning particles.

With the advent of more sophisticated techniques this problem was overcome. Wehner and co-workers have used a plasma method which produced very high current densities (of the order of $10 mA/cm^2$) in a vacuum of 10^{-4} to 10^{-3}torr. Ion beam methods have also been used; current densities of up to $200 \mu A/cm^2$ were possible with the operating gas pressure usually less than 10^{-5}torr. The main disadvantage of the Wehner plasma method was that the angular dependence of sputtering could not be easily investigated and corrections for secondary electron emission were necessary. These disadvantages were overcome with ion beam methods, but, in certain instances, the ion beam method suffered from a further pressure-dependent sputtering effect. This was a result of the fact that ion beams in high vacuum are limited to low current densities because of the large space-charge effect of ions. In this case, the number of impurity

gas particles (eg. O_2) hitting the target was greater than the number of ions. This meant that sputtering was unable to overcome impurity surface-layer formation at the target. The criterion for a clean surface was that the arrival rate of primary ions (N_i) exceeded the combined arrival rate of background gases and impurities contained in the sputtering gas (N_g). ie. $N_i \gg N_g$ for a clean surface.

Southern et al (1963) bombarded Si and Ge targets with 1 to 5keV A^+ ions and used a bombardment ratio N_i/N_g of between 5 and 20. They found no evidence of a pressure effect on sputtering yields. At much lower energies (up to 400eV), Honig (1958) found that a bombardment ratio of between 0.2 and 2 was not sufficient to maintain a clean surface. Wolsky and Zdanuk (1961) bombarded Si with A^+ ions of energy up to 800eV. They estimated that the bombardment ratio was about 1 which, on the basis of Honig's work, was insufficient to maintain a clean surface.

2.1.11. Nature of the neutral sputtered particles

Mass-spectrometric methods have been used to determine the nature of neutral sputtered particles.

Honig (1958) bombarded a Ge single crystal with 30 to 400eV Xe^+, Kr^+, A^+ and Ne^+ ions and detected Ge, the simple atomic species, and in smaller concentrations Ge_2, the diatomic species. Neutrals due to gas molecules on the surface of the Ge target were also detected during sputtering. Relatively large numbers were found because the ion current density (up to $10\mu Acm^{-2}$) was not sufficiently high to overcome the formation of an impurity layer due to background gases on the target surface (see SECTION 2.1.10.).

Comas and Cooper (1967) used substantially larger ion current densities (up to $1.4mAcm^{-2}$) and appear to have overcome the formation of sputtered background-gas neutrals. They bombarded single crystals of GaAs with A^+ ions of energy up to 140eV and found that 99.4% of the particles detected were neutral Ga and As atomic species, the balance were neutral GaAs molecules. Within experimental limitations no neutral Ga_2, As_2, or $(GaAs)_2$ molecules were detected.

2.2. OTHER PARTICLES EMITTED

In the following sub-sections the emission of secondary charged particles (electrons, and positive and negative ions) is discussed. Another associated phenomena, for which there is no information for semi-conductor targets, is the emission of photons by excited atoms during ion bombardment. This process represents the group of secondaries which have either not quite reached, or, reach only temporarily, their ionised state during the exchanges leading to emission. The excited atoms or ions liberate their characteristic emission line as they decay again to the ground state.

2.2.1. Electrons

When a beam of ions strikes a target surface electrons are liberated. This process is known as secondary electron emission and a coefficient γ is defined as the number of electrons liberated per incident ion. It should be remembered that an ion travelling towards a target surface has both potential energy, due to its elevation to the ionised state, and kinetic energy, due to its velocity relative to the target material.

To a first approximation, for kinetic energies below about 1keV, the coefficient γ is independent of kinetic energy and a "Potential Ejection" process predominates. Several potential ejection mechanisms are possible but the mechanism where an ion approaching a surface is neutralised and electronic transitions occur is the most probable. The probability of electron production is related to the maximum energy available after neutralisation of the ion, which is equal to $E_i - \emptyset$, where E_i = ionisation energy of the ion and $\emptyset$ = work function of the surface. Hagstrum (1960) determined that the coefficient γ was fairly insensitive to the kinetic energy from 10eV to 1keV for clean (111) and (100) faces of Si. The results of Hagstrum also showed a marked dependence of γ on noble gas bombarding ion species. The ion giving the largest coefficient γ was He^+, followed by Ne^+, A^+, Kr^+ and Xe^+, respectively, in decreasing order of magnitude. This was expected because the corresponding values of E_i, and hence

the term $E_i - \emptyset$, decreased in the same order. Allen et al (1959) investigated the effect of surface cleanliness of a (100) Si target on the manner in which the coefficient γ varied with He^+ ion energy up to 1keV. Only after the surface was heated to 1250°C for a few minutes was the typical γ constant with ion energy characteristic of a perfectly clean surface obtained.

For ion energies above 1keV, kinetic energy considerations start to be important and the coefficient γ increases with increasing kinetic energy of the bombarding ions. Abroyan et al (1969) determined the manner in which γ for the (111) face of Ge increased for Kr^+ and Xe^+ ion energy of up to 15keV.

The dependence of the coefficient γ on the ion angle of incidence for polycrystalline targets shows the form

$$\gamma_\alpha = \frac{\gamma_0}{\cos\alpha} ,$$

where α = angle of incidence measured from the target normal,

γ_α = secondary electron emission coefficient at angle α,

and γ_0 = secondary electron emission coefficient for normal incidence.

When single crystals are used, the variation of γ with α shows strong anisotropy similar to that for the variation of sputtering yield with α (see SECTION 2.1.7.). Fagot et al (1966) determined the variation of γ with α for various monocrystals of Ge bombarded by 80keV A^+ ions. Minima in the values of γ corresponded to lattice directions more transparent to the ion beam. The coefficient γ was smaller in these cases because collisions occurred at greater depths and electrons could not escape so easily. An interesting feature of the investigations by Fagot was that after a period of a few minutes bombardment the anisotropy of the γ versus α curve disappeared and the resulting curve showed the $1/\cos\alpha$ variation characteristic of a polycrystalline target. This effect was due to the formation of an amorphous surface layer because the target temperature was not

sufficiently high to continually anneal out damage produced by bombarding ions (see SECTION 2.3.1.6.). The temperature determining the transition in the monocrystalline to polycrystalline behaviour of the γ versus α curve is called the critical annealing temperature, T_a, and the angular dependences of the secondary electron emission coefficient have been used to measure T_a (see SECTION 2.3.1.6.(b)).

2.2.2. Secondary positive ions

2.2.2.1. General trends.

Secondary positive ions are produced by ion bombardment due to (i) the reflection of the incident ion beam without neutralisation (this process is generally called ion reflection or scattering), (ii) the liberation of ionised species of the target atoms, and (iii) the ejection of ion species characteristic of gaseous impurity atoms adsorbed on the surface of the target. The formation of ion species characteristic of gaseous impurity atoms on reasonably clean surfaces is insignificant compared with the other two mechanisms.

A reflection coefficient R, expressed as ion/ion, is used to describe the reflection of ions at a surface. When clean surfaces are bombarded with the noble gas ions the coefficient R is virtually insensitive to the ion energy even up to the middle keV energy range. Typical values for R are from 10^{-4} to 10^{-3} ion/ion depending on the ion-target combination. When the ion attack approaches grazing incidence, the coefficient R increases rapidly. For example, in the case of ion bombardment of a polycrystalline Cu target with 27keV A^+ ions, the coefficient R is constant at about 0.05 ion/ion for angles of incidence α from 0° (normal incidence) up to 70°. However, at angles of α = 78°, 82° and 84° the corresponding values of R are 0.06, 0.17 and 0.22 ion/ion showing that the value of R for grazing incidence has increased markedly. When single crystals are used, minima in reflection coefficient occur when the ion beam direction is parallel to low index planes or low index directions. The presence of these minima is further

evidence for the phenomenon of channelling.

The energy spectra of scattered ions shows several interesting features. Firstly, all scattered ions have energies less than the primary ion energy due to energy losses by elastic and inelastic processes. The elastic process of energy loss is by collisions, either binary or multiple. The inelastic processes involve energy loss in the charge stripping of both the incident ion beam and the target atoms. Secondly, the structure of the energy spectra is highly dependent on primary ion energy, ion angle of incidence, collection angle and the type of crystal bombarded. Typically for ion energies greater than 10keV and incidence at grazing angles, the spectra shows, for polycrystalline targets, single peaks due to single two-atom collisions superimposed on a general background due to multiple collisions. The general background disappears when the collection angle with respect to the surface becomes small and some of the peaks show a high energy shoulder indicating that scattering due to multiple collisions is still present. Similar effects are observed with single crystals but, in this case, the shoulder on the high energy side of some of the peaks is transformed into a second peak. The main peak is usually referred to as the single-scattering peak and the second peak as the double-scattering peak.

A yield K_+, expressed as ion/ion, is used to describe the emission of positively charged target ion species. Not surprisingly, the conditions controlling the emission of sputtered atoms are found to control the emission of "sputtered" target ions. Beyond a critical threshold value, the yield K_+ increases rapidly with increasing ion energy and reaches a maximum at about 10keV or more. Yield values also increase with increasing mass of the incident ion. The dependence of the yield K_+ on the ion angle of incidence similarly shows a striking resemblance to that for sputtered atoms. The yield K_+ increases monotonically with angle of incidence α for polycrystalline targets, and for single crystal targets the yield curve shows minima corresponding to low index directions which

is yet further evidence for the phenomenon of channelling. Furthermore, "sputtered" target ions are also ejected from single crystals in the same preferred crystallographic directions as observed for sputtered atoms. Finally "sputtered" target ions have energies that are of the same order of magnitude as sputtered atoms. The distribution shows that the most probable ejection energy is usually between 1 and 10eV (the same result for sputtered atoms). A long high-energy tail is present in the distribution, similarly found for sputtered atoms and extends beyond a few hundred eV.

2.2.2.2. Semiconductor targets

Honig (1958) bombarded Ag, Ge and Ge-Si alloy surfaces with various noble gas ions at energies between 30 and 400eV. Secondary positive ions were identified as being due to the reflection of primary ions, the ejection of target ion species and the liberation of ion species characteristic of background gases adsorbed on the surfaces. Honig's experiments yielded large numbers of ion species characteristic of gaseous impurities because the ion bombardment current density was insufficient to overcome impurity surface layer formation and produce a clean surface. (see SECTION 2.1.10.) For the Ag sample bombarded with Xe^+ ions, the secondary positive ions detected, in order of decreasing magnitude, were Xe^+, Ag^+, Xe^{2+}, $Ag_2{}^+$, $Ag_3{}^+$ etc., excluding ions due to hydrocarbon contamination of the Ag surface. With the Ge sample, the Ge ion species detected were Ge^+, $Ge_2{}^+$, GeH^+, $GeOH^+$ and Ge_2O^+, the presence of the last three indicating the severity of the contamination of the Ge surface. Roughly 1 in every 100 sputtered Ge atoms was singly ionised, and 1 in 50 of these ionised particles was of the diatomic species. The most probable energy of the Ge^+ species was about 2eV. The major secondary positive ions found for the Ge-Si crystal (11% Si by density) were Ge^+, GeH^+, $GeOH^+$, $Ge_2{}^+$, Ge_2O^+, Si^+, SiH^+, $SiOH^+$, $GeSi^+$ and $GeSiO^+$.

Beske (1967) has investigated the emission of positive secondary ions from Si targets bombarded with higher energy ions. Targets were bombarded with 12keV A^+

ions at 45° incidence, the current density was 1mA cm^{-2}, and the positive Si ion species detected were Si^+, Si^{2+}, Si^{3+}, Si^{4+}, SiH^+, SiO^+, Si_2^+ and Si_3^+. The yield K_+ of Si^+, Si^{2+}, Si^{3+} and Si^{4+} was 10^{-2}, $4x10^{-3}$, $7x10^{-5}$ and 10^{-6} ion/ion respectively.

Hennequin (1968) determined the nature and energy distribution of the Si ion species, Si^+ and Si^{2+}, for bombardment with A^+ ions of energy up to 8keV. The most probable ejection energy of the Si ion species was about 10eV but Hennequin has quoted figures for the mean energy of ejection ($\bar{E}_2$) which is a good bit larger than the most probable ejection energy because of the presence of the high energy tail in the distribution. The variation of $\bar{E}_2$ for Si^+ with ejection angle and primary ion energy was investigated. At 8keV, and for an ejection angle of 30°, $\bar{E}_2$ for Si^+ was about 70eV. The corresponding value for Si^{2+} was about 160eV.

Mashkova and Molchanov (1968) have investigated the complete energy spectra of reflected and sputtered positive ions from Ge(111) single crystals. A typical spectra with single and double peaks for 30keV A^+ ions at grazing incidence is shown in FIG. 2.15. The effect of grazing ion incidence resulted in, firstly, Ge sputtered ions with keV energies and, secondly, the formation of double-scattering peaks characteristic only of single crystal targets. The existence of double-scattering peaks in the energy spectra from single crystal targets of semiconductors has been used to monitor the degree of crystal damage produced in semiconductors by ion bombardment and enabled values for the critical annealing temperature, T_a, to be determined (see SECTION 2.3.1.6.(c)). At comparatively low temperatures, the energy distributions are similar to those usually observed for polycrystals (ie. without the double-scattering peak). Apparently, at these temperatures, the temperature is not sufficiently high to continually anneal the damage created by the ion bombardment and prevent the formation of an amorphous surface layer. As the target temperature is increased, the spectral shape changes sharply, and double-scattering peaks appear. This

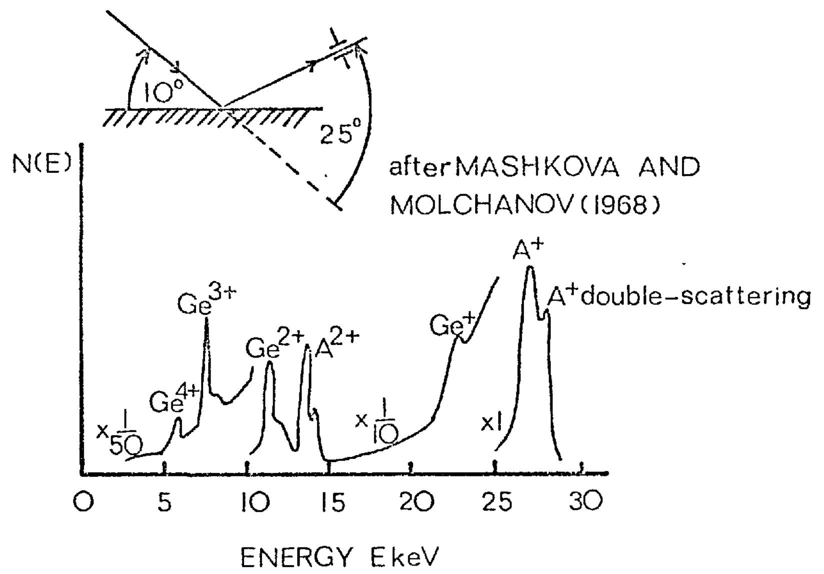

FIG. 2.15. ENERGY SPECTRA OF SECONDARY POSITIVE IONS FROM A Ge(111) SURFACE AT 550 °C DUE TO 30keV A^+ IONS AT GRAZING INCIDENCE.

conversion occurs within a narrow temperature range around the annealing temperature, T_a. This double-peaked shape persists with increasing temperature up to a certain temperature which is determined by the combination of the ion and target atom. Above this temperature, the double-scattering peak begins to smooth out because the increased thermal vibration of the lattice atoms disturbs the regular arrangement of the atoms in the crystal.

2.2.3. Secondary negative ions

Secondary negative ions are produced by ion bombardment due to (i) the liberation of ionised species of the target atoms, and (ii) the ejection of ion species characteristic of gaseous impurity atoms adsorbed on the surface of the target.

The factors controlling the emission of sputtered atoms, and positively-charged target ion species (see SECTION 2.2.2.1.), are also found to control the emission of negatively-charged target ion species. However, the yield K_-, expressed as ion/ion, of negatively-charged target ion species is much smaller than the yield, K_+, of the positive species for the same bombardment conditions. Typical values for K_- are from 10^{-6} to 10^{-5} ion/ion for perfectly clean and heated metal targets. Under these conditions about the same number of ion species characteristic of gaseous impurity atoms are also released. For targets not deliberately heated during bombardment, about an order of magnitude increase in the number of gaseous impurity ion species is produced.

The sensitivity of the emission of negatively-charged target ion species to the target temperature and bombardment conditions has been shown for semiconductor targets by several observers.

Honig (1958) bombarded Ag and Ge surfaces with various noble gas ions at energies between 30 and 400eV. For the Ag sample, the secondary negative ions detected were in order of decreasing intensity, excluding hydrocarbon combinations, Ag_2O^-, O^-, OH^-, Ag_2^- and $Ag_2O_2^-$. For the Ge sample, the only negative ions detected were gas ions excluding O^-. The absence of negative ions characteristic of the Ge sample and the preponderance of

negative gas ions was due to insufficiently clean surfaces maintained during bombardment. Honig did not specify target temperatures but they were almost certainly at or near room temperature. A low bombardment ratio N_i/N_g of 0.2 to 2 (see SECTION 2.1.10.), insufficient for overcoming the pressure-dependent sputtering effect, was clearly inadequate for the release of negative ions characteristic of the target.

In later work, Honig (1964) again bombarded Ge targets but this time after the surfaces had undergone an ethylation treatment before 400eV A^+ bombardment. In the negative ion spectrum, GeO_2^-, characteristic of the target, was detected. A vast number of impurity ion species characteristic of the ethyl-covered surface was also observed.

Ayukhanov and Abdullaeva (1966) bombarded Si surfaces with Cs^+ ions at energies between 700 and 1000eV. The detected target ion species were in order of decreasing intensity SiO_2^-, SiO_3^- and Si^-, the peaks of which, after a certain period of bombardment, became comparable in height with the peaks due to impurity gas ions (eg. H^-, O^-, OH^-, Cl^-, O_2^-, O_2H^- etc.).

Comas and Cooper (1967) bombarded single crystals of GaAs with A^+ ions of energy up to 140eV and found that the only ions detected in the negative ion spectrum were due to gas ions (eg. O^-, N^- etc.). No signals of the negative ions Ga^-, Ga_2^- or $(GaAs)^-$ were detected even though a relatively high bombardment ratio N_i/N_g of between 20 and 50 was used. Target temperatures in general did not exceed 100°C. Comas and Cooper concluded that if the negative ions characteristic of the target were present then their number was less than 0.05% of the detected sputtered neutral atoms from the target. Correspondingly, the value of K_- was less than about 10^{-4} ion/ion.

2.3. TARGET EFFECTS

2.3.1. Ion Bombardment damage

2.3.1.1. Formation of damage

As a consequence of elastic collisions between energetic particles and lattice atoms, those lattice atoms which recoil with kinetic energy in excess of the displacement energy threshold (13eV for Si atoms - Loferski and Rappaport 1959) are permanently displaced. Generally, the lattice recoil energy after the first collision is many times greater than the displacement energy threshold and this excess energy is dissipated via a cascade of secondary collisions within which many atoms receive sufficient energy to remain displaced. The majority of these displaced atoms are contained within an approximately spherical volume. Spherical damaged regions of 50 to 100 Å diameter representing roughly 50 displaced lattice atoms have been observed in Si by Mazey et al (1966), (1968) and Large and Bicknell (1967), and in Ge by Bacchilega et al (1965) and Parsons (1965) when samples, thinned prior to ion bombardment with 80 to 100keV ions, were examined in the electron microscope. Parsons (1965) deduced that the individual damaged regions had a structure which was amorphous and less dense than the crystalline matrix in which they were located. These less-dense regions are surrounded by isolated interstitials and vacancies which even for room temperature bombardments migrate away into the undamaged crystal, where either mutual annihilation, trapping at impurity sinks or agglomeration occurs. As the bombardment dose builds up the number of damaged regions increases until they eventually overlap to form a continuous surface layer which electron diffraction shows to be amorphous. Nelson et al (1966) found that in the case of Si the formation of the amorphous surface phase was characterised by a change in reflectivity due to Rayleigh scattering which gave rise to a milky appearance of the Si surface. Gianola (1957) was the first observer to report for Si a complete change of surface structure to the amorphous state when single crystals were bombarded with 30keV He^+

ions to a dose of $2\frac{1}{2}\times10^{15}$ ions cm^{-2}.

2.3.1.2. Critical ion doses for damage in Si and Ge

TABLE 2.C. shows the results of several investigators who determined the threshold dose for damage and the dose necessary for the formation of a continuous amorphous surface layer in Si and Ge single crystals at or near room temperature. Even for a wide variety of ion/target combinations surprisingly similar critical dose values were reported.

A factor which clearly affects the situation is the channelling phenomenon for under conditions where the incident beam is aligned with a major channelling direction, the probability of large energy transfer to the lattice atoms is significantly reduced with the inevitable consequence that the rate of buildup of disordered regions is also reduced. Nelson and Mazey (1968) have shown that a reduction in bombardment damage by a factor of 8 was inferred when a Si(111) crystal was oriented so as to present its $\langle 110 \rangle$ channels to an incident ion beam of 80keV Ne^+ ions.

2.3.1.3. Extent of surface disorder

Jacobson and Wehner (1965) determined the state of surface disorder in Ge(111) crystals after bombardment with A^+ ions of energy 10eV to 1keV to total doses of up to 10^{16} ions cm^{-2} using the sensitive surface monitor of low-energy electron diffraction (LEED). Their results suggested that each ion disordered a certain surface area which increased with ion energy as far as 1keV. For example 100eV ions were believed to disorder about 2 surface atoms whilst 1keV ions disordered about 50 atoms. Jacobson and Wehner predicted that beyond 1keV the surface damage perincident ion would decrease because ions penetrating further into the target could not be expected to transfer energy so easily to surface lattice atoms.

Depths of ion bombardment damage in Ge(111) crystals were determined by MacDonald and Haneman (1966a and 1966b) after subjecting the crystals to bombardment with He^+, Ne^+, A^+ and Kr^+ ions of energy from 200eV to 1keV at total doses of up to 2×10^{17} ions cm^{-2}. MacDonald and Haneman determined that the total depth of damage (a) increased

REFERENCE	METHOD OF EXAMINATION	MATERIAL BOMBARDED	BOMBARDING IONS	ION ENERGY	THRESHOLD DOSE FOR DAMAGE IONS cm^{-2}	DOSE FOR CONTINUOUS AMORPHOUS SURFACE LAYER IONS cm^{-2}
JACOBSON AND WEHNER (1965)	LEED	Ge(111)	A^+	100eV 250eV 1keV	$\sim 10^{13}$ $\sim 5\ 10^{12}$ $\sim 10^{12}$	$\sim 10^{16}$ $\sim 10^{15}$ $\sim 10^{14}$
ABROYAN AND TITOV (1969)	ANGULAR DEPENDENCES OF SECONDARY ELECTRON EMISSION	Ge Single crystals	K^+	6keV	$\sim 10^{13}$	$\sim 10^{14}$
PARSONS (1965)	TEM	Ge Single crystals	O^-	100keV	$\sim 10^{12}$	$\sim 10^{15}$
DAVIES et al (1964)	RANGE DEPTHS	Si (111)	Xe^{125}	40keV	$\sim 10^{13}$	
MAYER et al (1968)	1MeV He^+ ION SCATTERING	Si Single crystals	Ga^+, As^+, Sb^+, In^+, P^+	40keV	$\sim 10^{13}$	$\gtrsim 10^{14}$
DEARNALEY et al (1969)	TEM	Si Single crystals	P^+ B^+	60keV 60keV		$\sim 5\ 10^{13}$ $\sim 5\ 10^{15}$
MAZEY et al (1968)	TEM	Si Single crystals	Ne^+	80keV	$\sim 10^{13}$	$\gtrsim 10^{14}$
LARGE AND BICKNELL (1967)	TEM	Si Single crystals	B^+	150keV	$\sim 10^{14}$	

TABLE 2.C. CRITICAL DOSES FOR DAMAGE IN Si AND Ge

with decreasing ion size, except for the case of He^+ ion bombardment where limitations of the experimental method were prominent, (b) increased with increasing damaging ion dose up to a saturation value, the magnitude of which increased with decreasing ion size (the saturation ion dose for 1keV A^+ ions was about $6x10^{16}$ ions cm^{-2}), and (c) increased with increasing ion energy (eg. the saturation depths were 16 and 35 Å for A^+ ion energies of 500eV and 1keV respectively). Furthermore, the damaged layer was deduced to consist of two main regions. The one nearer the surface consisted mainly of severe lattice disorder plus trapped gas, which extended to a depth of approximately 17 Å at 1keV ion energy with most disorder occurring at the surface. The second, lower region consisted mainly of gas atoms trapped in a more ordered lattice, the depth of this region increasing with decreasing ion mass. The gas atoms trapped in the lower region were at a depth beyond the theoretical range predicted by Nielsen (1956) and Lindhard and Scharff (1961) and were believed to be atoms "knocked-on" by ions incident after trapping had occurred. Therefore, ion bombardment had led to an increase in the sorption properties of the lattice. Saturation of the lattice with gas atoms occurred when the rate of release of trapped gas atoms by erosion of the surface by sputtering equalled the rate of trapping of incident ions. The sorption properties of ion bombarded crystals is discussed in SECTION 2.3.2.2. in more detail.

At higher energies, Mazey et al (1968) found that bombardment of Si with 80keV Ne^+ ions to a total dose of $\geqslant 10^{14}$ ions cm^{-2} resulted in an amorphous surface phase approximately to the depth of the random penetration of ions. Parsons (1965) and Large and Bicknell (1967) confirmed that the damaged layer was confined to the front bombarded surface.

With 200keV P^+ ions, Irving (1969) found that the amorphous layer grew out from a depth corresponding to the expected range of ions, where the most severely damaged material was formed initially, until eventually its thickness was about 2 times the depth of the expected range of the ions. The observation that the most severely

damaged material occurred beneath the surface of a material bombarded with very high energy ions was a direct consequence of the prediction made by Jacobson and Wehner (1965).

2.3.1.4. Annealing behaviour of bombarded crystals and the structural defects remaining

Parsons (1965) and Bacchilega et al (1965) examined the thermal stability of the spherical damaged regions in Ge introduced by 100keV O^- ions by annealing room temperature bombarded specimens in the electron microscope.

Parsons observed that as a specimen was annealed up to 665°C, the damaged regions near crystal boundaries disappeared first and then in thicker regions of the crystal but dislocation loops formed in the thicker crystal and these finally annealed. Parsons deduced that recrystallisation of the damaged regions occurred above 300°C, and, because of the less dense character of the damaged regions, the matrix subsequently became supersaturated with vacancies. These vacancies, now mobile, migrated to existing sinks and trapping centres. The largest sink was the upper and lower surface of the specimen and the most prevalent trapping centres were the 1 in every 5 incident 100keV O^- ions that were stopped in the specimen. Thus, in thin specimen regions a defect free zone was formed as practically all of the excess vacancies in this region migrated to the crystal boundaries. In thicker regions of the specimen vacancies were retained in the form of dislocation loops which were most likely nucleated on the bombardment-induced oxygen atom impurities. The final disappearance of these dislocation loops at annealing temperatures of 665°C was explained by the migration of vacancies from the loops to the specimen surfaces.

Bacchilega et al (1965) observed that during heating some damaged regions annihilated by mutual reaction and others reacted to give rise to defects interpreted as being due to vacancies and interstituals. These defects were jogged dislocations to a high density, hexagonal loops showing stacking fault contrast, and twofold images of the

type encountered with symmetrical coherency strains around inclusions.

Short and long range vacancy movement was proposed by Jacobson and Wehner (1965) as the mechanism by which Ge(111) crystals bombarded with A^+ ions of energy up to 1keV annealed. The effect of heating room temperature bombarded specimens was found to accelerate room temperature reordering effects and at the reordering temperature occluded ions were also released. Jech and Kelly (1969) used the phenomenon of inert gas release as a marker for studying the annealing of damage in single crystals of Ge and Si subjected to 10keV Kr^+ ion bombardment.

Mazey et al (1966), and in more detail Mazey et al (1968), Large and Bicknell (1967), Dearnaley et al (1969), and Irving (1969) have used the electron microscope and determined the annealing behaviour of ion bombardment damage in pre-thinned Si samples. In most cases doping ions were used to determine the extent of damage produced in the process of ion implantation (see SECTION 2.3.2.)

Mazey et al (1968) observed that individual damaged regions were stable in the lattice up to temperatures around 400 to 500°C when they recrystallised epitaxially onto the surrounding lattice, presumably with a release of vacancies due to the increase in density on recrystallisation. Annealing experiments by Irving (1969) at temperatures between 700 and 800°C have shown that point defects, probably due to clusters of vacancies, resulted. The concentration of point defects was greatest at a depth below the surface corresponding to the expected range of ions where the most severely damaged material was formed initially.

On the other hand, Mazey et al (1968) have shown that once the small damaged regions overlapped to form a continuous amorphous layer, complete recrystallisation did not occur until about 630°C. In regions where the ion range was greater than the foil thickness (eg. near the edge of a thin tapering section), epitaxial recrystallisation could not occur and this region was found to contain small randomly oriented crystallites. In intermediate

thickness regions, micro-twinning sometimes occurred in the bombarded areas. This was more likely when (111) Si slices were examined owing to the relative ease of double position twinning about the (111) normal (Large and Bicknell 1967). In thicker regions, where the Si was thick enough for only the surface to have become amorphous, the structure which evolved consisted of an array of dislocation loops and dipoles. Dearnaley et al (1969) reported that a defect free region extending to a depth of about 500 Å overlaid the region containing the dislocation loops and dipoles, the depth of which was approximately equal to the depth of the amorphous phase. Mazey et al (1968) found that the loops coalesced and grew when annealing was carried out at temperatures between 700 and 850°C and loops occurred in all annealed specimens after ion doses $\geqslant 3 \times 10^{14}$ ions cm^{-2}, at energies between 10keV and 90keV, irrespective of ion species used, ie. Ne^+, P^+, Si^+ or B^+, and of the conductivity type of the Si. The loops finally annealed at temperatures in excess of 1000°C (Dearnaley et al 1969).

Large and Bicknell (1967) found that beneath regions which exhibited micro-twinning, there was again a high density of dislocation loops, some approximately circular and others which formed very long narrow dipoles, the type and size of which was dependent on the bombardment and annealing schedule. Analysis of the loops indicated they were of interstitual or vacancy type. Beneath the dislocation loops a region containing long straight dislocations was found. Irving (1969) has shown that even in specimens subjected to a 1000°C aneal an extremely high concentration of dislocations and sometimes stacking faults remained.

Another type of defect which gave very similar diffraction results to the small dislocation loops was the strain occurring around precipitates in a crystal, as reported by Ashby and Brown (1963). These defects were prominent when the dose of doping ions represented a concentration level greater than the solid solubility of the doping ions in the lattice. Higher post-implantation

annealing temperatures were also necessary when the concentration level of doping ions was greater than the solid solubility level (Mayer et al 1968).

A summary of the previously mentioned results for the post-bombardment annealing temperature required to restore the single crystal surface of Si or Ge is shown in TABLE 2.D.

2.3.1.5. Defects remaining in crystals bombarded at elevated temperatures

Parsons (1965) investigated the thermal stability of the damaged regions in Ge created by 100keV O^- ions for bombardments at 210 and 320°C. Specimens heated to 210°C and subsequently ion bombarded exhibited damaged regions. However, no visible damaged regions were retained in specimens heated to 320°C and subsequently bombarded with ion doses which would normally have resulted in the formation of an amorphous surface layer. The absence of damaged regions showed that at 320°C epitaxial crystallisation of each amorphous damaged region occurred during bombardment.

Mazey et al (1968) investigated the nature of damage produced in Si during bombardment at temperatures above 200°C. Pre-thinned discs were heated to temperatures of 200 and 510°C and bombarded with Ne^+ ions. A high-dose bombardment at 200°C with 3.6×10^{16} 30keV Ne^+ ions cm^{-2} resulted in a dense dislocation entanglement. The diffraction pattern of the bombarded area showed a [001] spot pattern characteristic of single-crystal material, and streaking between the reciprocal lattice spots in the ⟨220⟩ directions, but no sign of the diffuse rings associated with the presence of amorphous Si which would have occurred at much lower doses at room temperature. After bombardment at 510°C with 1.8×10^{16} 30keV Ne^+ ions cm^{-2}, dislocation networks and narrow lamellar regions (about 500 Å in length) of disorder were observed in a [110] oriented specimen. No rings were present in the diffraction pattern, but streaking occurred between the reciprocal lattice spots, in the ⟨111⟩ and ⟨200⟩ directions. Dearnaley et al (1969) reported that in most cases the number of dislocations found in material bombarded at

REFERENCE	MATERIAL BOMBARDED	BOMBARD-ING IONS	ION ENERGY	STATE OF CRYSTAL AFTER BOMBARDMENT BY DOSE ions cm^{-2}	POST-BOMBARDMENT ANNEALING TEMP. TO RESTORE SINGLE CRYSTAL SURFACE
JACOBSON AND WEHNER (1965)	Ge(111)	A^+	10eV to 1keV	AMORPHOUS LAYER 10^{16} 1keV ions cm^{-2} INDIVIDUAL DAMAGED REGIONS 10^{13} 500eV	RE-ORDERING BEGINS AT 250°C, COMPLETE BY 400°C. ~300°C
PARSONS (1965)	Ge single crystals	O^-	100keV	INDIVIDUAL DAMAGED REGIONS 10^{13}	$\gtrsim$300°C
JECH AND KELLY (1969)	Si and Ge single crystals	Kr^+	10keV	AMORPHOUS LAYER $7x10^{13}$ to $4x10^{16}$	470 ± 45°C (Ge) 720 ± 70°C (Si)
MAYER et al (1968)	Si single crystals	Ga^+, As^+ Sb^+, In^+ P^+	40keV	INDIVIDUAL DAMAGED REGIONS~10^{13} AMORPHOUS LAYER. $>10^{15}$ (As^+ and P^+) $>10^{15}$ (Ga^+ and Sb^+)	260°C 550°C to 650°C 900°C
MAZEY et al (1968)	Si single crystals	Ne^+	80keV	INDIVIDUAL DAMAGED REGIONS~10^{13} AMORPHOUS LAYER $>10^{14}$	400 to 500°C 630°C

TABLE 2.D. POST-BOMBARDMENT ANNEALING TEMPERATURE OF DAMAGE IN Si AND Ge

elevated temperatures was more than the number remaining after annealing room temperature bombarded material.

2.3.1.6. The critical annealing temperature, T_a

The critical annealing temperature, T_a, is defined as the temperature of the sample during bombardment just sufficient to retain the single crystal properties of the sample to the outermost surface layers and prevent the formation of the amorphous surface phase. For temperatures less than T_a, the rate of defect production is greater than the annealing rate and the surface is essentially amorphous. At temperatures greater than T_a, the annealing rate predominates and the surface is always ordered.

Authors have used several ion-impact phenomena, sensitive to the degree of lattice arrangement, to determine T_a and its variation with ion dose, rate of ion dose, ion energy and ion mass for example. The phenomena, which have been used, are

(i) atom ejection patterns (see SECTION 2.1.9.2.)

(ii) the angular regularities of the secondary electron emission (see SECTION 2.2.1.)

(iii) the energy distribution of scattered ions (see SECTION 2.2.2.2.)

and (iv) sputtering yield (see SECTION 2.1.6.2.)

The onset of the milky appearance (for Si) (see SECTION 2.3.1.1.) has also been used as a monitor of surface structure in the determination of T_A, the amorphisation temperature.

2.3.1.6(a) Determination of T_a from atom ejection patterns

Anderson et al (1963), Anderson and Wehner (1964) and Anderson (1966b) determined values of T_a and the variation with ion mass for Ge, Si and GaAs single crystals respectively. The ion energy was less than 1keV, the rate of dose about 1mAcm^{-2} ($6x10^{15}$ ion sec^{-1} cm^{-2}), and the total dose about $6x10^{16}$ ions cm^{-2}. Values of T_a for Ge were 230°C (Ne), 290°C (A), 300°C (Kr) and 320°C (Xe); for Si, T_a was 350°C (Ne) and 430°C (A); for GaAs, T_a was 130°C for both Ne and A. It would appear that higher annealing temperatures were necessary for

larger bombarding ions. Presumably the larger ions do not penetrate the crystal so far and a more concentrated region of damage is present near the surface requiring a higher annealing temperature.

In the earlier studies (Anderson et al 1963, and Anderson and Wehner 1964), it was reported that spot patterns characteristic of a single crystal surface could persist even for temperatures less than T_a if the bombarding-ion energy was less than some critical energy in the range 200 to 400eV. Anderson (1966b) established that this was an erroneous conclusion resulting from the method used for pattern study, and no such critical energy existed.

2.3.1.6(b) Determination of T_a from the angular regularities of the secondary electron emission coefficient

Evdokimov et al (1967) and Mashkova and Molchanov (1968) determined values of T_a and the variation with ion mass for Ge and Si single crystals respectively. Ne^+, A^+ and Kr^+ ions of energy 30keV were used at a rate of dose of between 0.25 and 0.5 mAcm^{-2} (1½ to 3×10^{15} ion sec^{-1} cm^{-2}). The total dose was not stated. A typical angular and temperature dependence of the secondary electron emission coefficient γ from the Si(111) surface for 30keV A^+ ions is shown in FIG. 2.16. The γ versus temperature curve shows two characteristic temperatures, T_A and T_a; T_A is the amorphisation temperature where the structure completely disappears in $\gamma(\alpha)$, and T_a is the temperature at which the function $\gamma(\alpha)$ begins to smooth out. The values of T_a for Si were about 390°C (Ne), 400°C (A) and 460°C (Kr). Values of T_a for Ge were 240°C (Ne), 310°C (A) and 320°C (Kr), which were similar to those determined by Anderson et al (1963) at much lower energies and higher rates of dose using atom ejection patterns. A higher T_a was again necessary for the larger bombarding ions.

Abroyan et al (1969) used significantly lower rates of dose between 1 and 8μA cm^{-2} (6×10^{12} to 5×10^{13} ion sec^{-1} cm^{-2}) when bombarding Ge single crystals with

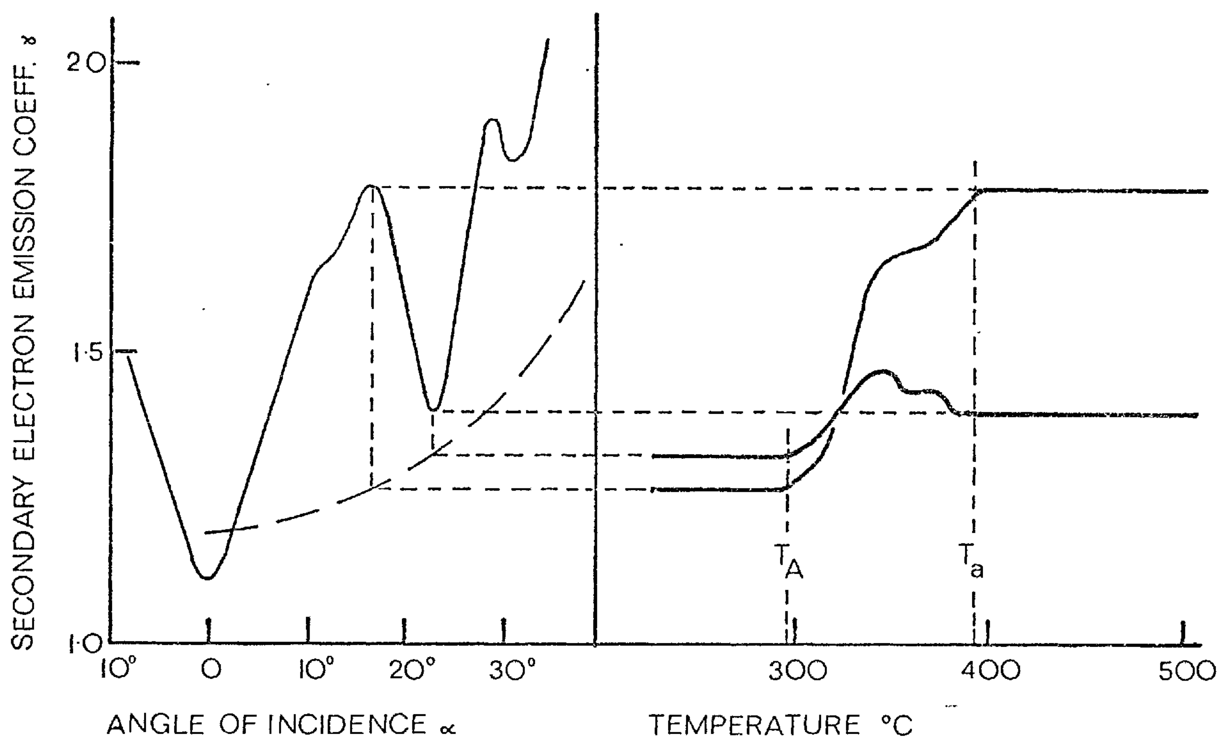

FIG. 2.16. ANGULAR AND TEMPERATURE DEPENDENCE OF THE SECONDARY ELECTRON EMISSION COEFFICIENT FROM A Si(111) SURFACE UNDER ION BOMBARDMENT BY 30keV A^+ IONS.

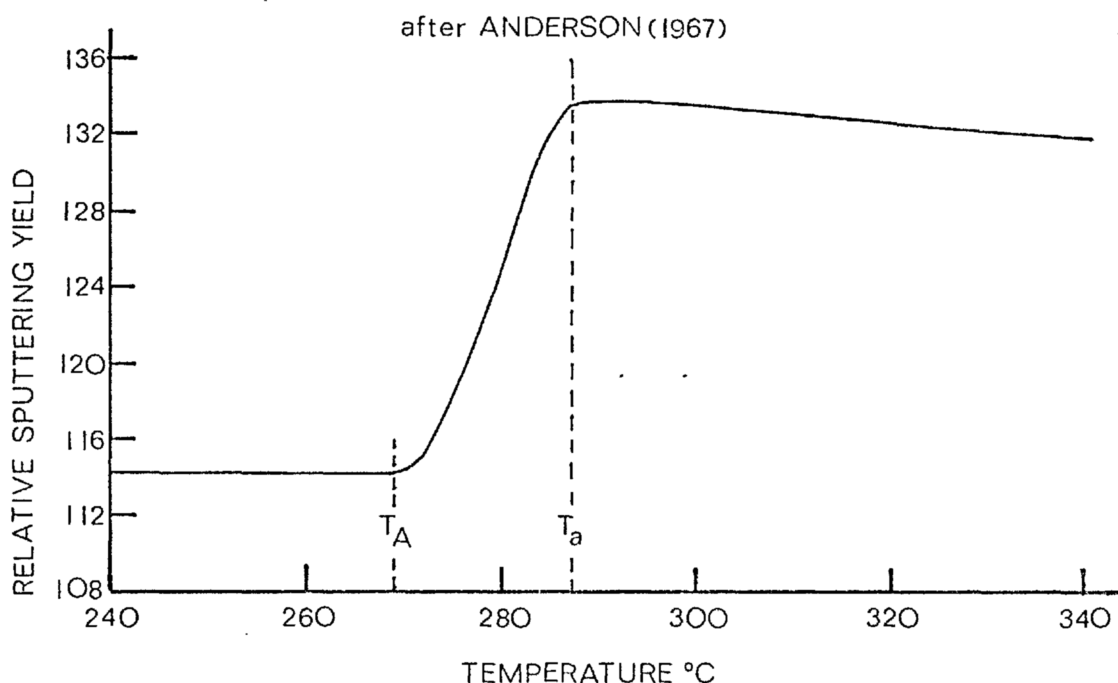

FIG. 2.17. TEMPERATURE DEPENDENCE OF THE RELATIVE SPUTTERING YIELD FROM A Ge(100) SURFACE UNDER ION BOMBARDMENT BY 600eV A^+ IONS AT ABOUT 3.8mA cm^{-2}.

10keV Xe^+ ions and found that the logarithm of the rate of dose decreased linearly with an increase in the reciprocal of the annealing temperature, T_a. At 1μA cm^{-2}, T_a was about 300°C increasing to 340°C at 8μA cm^{-2}. The difference T_a-T_A amounted to 10 to 12°C. A further significant observation was that annealing temperatures were independent of the crystallographic orientation of the single crystal Ge samples.

2.3.1.6(c) Determination of T_a from the energy distribution of scattered ions

Mashkova and Molchanov (1968) determined values of T_a for Ge and Si single crystals by monitoring the temperature dependence of the double-scattering peak in the energy spectrum of scattered ions. 30keV ions were used at a rate of dose of between 0.25 and 0.5mA cm^{-2} (1½ to $3x10^{15}$ ion sec^{-1} cm^{-2}) and the values of T_a were 320°C (A) and 380°C (Kr) for Ge, and between 300 and 600°C (A) for Si. These values of T_a were similar to those found under identical bombardment conditions using the angular regularities of the secondary electron emission coefficient as a monitor of the surface structure.

2.3.1.6(d) Determination of T_a from sputtering yields

Anderson (1967) determined values of T_a for Ge single crystal surfaces by monitoring the temperature dependence of sputtering yields of the (100) and (110) surfaces. Both the (100) and (110) surfaces showed differences in sputtering yield for temperatures above and below the critical annealing temperature, T_a (see SECTION 2.1.6.2.). The (111) surface showed no change in sputtering yield for temperatures above and below T_a.

Anderson (1967) used a spectroscopic emission technique which enabled a series of relative sputtering yield values to be obtained over a wide temperature range without interrupting the ion bombardment. A typical result for the Ge(100) surface is shown in FIG. 2.17, where T_A is the amorphisation temperature, T_a is the temperature where the single crystal begins to lose its

single crystal properties, and T_a-T_A is the temperature width of the transition. The variation of T_a with ion mass (Ne, A and Kr), ion energy (200 to 800eV), and rate of ion dose (0.7 to 4mA cm^{-2}; 4 to $24x10^{15}$ ion sec^{-1} cm^{-2}) was investigated. Values of T_a between 200 and 300°C were recorded. No difference in annealing temperature appeared to exist between the different surface orientations. T_a was found to increase with increasing ion mass, ion energy and rate of ion dose; the logarithm of the ion energy and the logarithm of the rate of ion dose both decreased linearly with an increase in the reciprocal of the annealing temperature, T_a. The temperature width of the transition (T_a-T_A) decreased as T_a increased.

Comparison of results with those by other surface structure monitoring techniques were encouraging. For example, 400eV ions at a rate of dose of about 1 to 2mA cm^{-2} resulted in values of T_a of 200°C (Ne), 290°C (A) and 300°C (Kr), which were almost identical to the values obtained under similar bombardment conditions by Anderson et al (1963) using atom ejection patterns.

2.3.1.6(e) <u>Determination of T_A, the amorphisation temperature</u>.

Nelson and Mazey (1968) used the onset of the milky appearance of Si as a criterion for the existence of an amorphous surface phase and studied the influence of bombardment temperature on its formation for 60keV Ne^+ ions. Irving (1969) used the more sensitive surface monitor of reflection electron diffraction and similarly studied the temperature dependence of amorphous surface phase formation using 100keV P^+ ions. The results of these two seperate investigations are depicted in FIG. 2.18, which shows the threshold dose for the appearance of an amorphous surface phase plotted logarithmically as a function of the inverse of the amorphisation temperature, T_A. The results of Nelson and Mazey were apparently independent of rate of ion dose as this was varied by more than two orders of magnitude. Analysis of the curve in FIG. 2.18. produced by Nelson and Mazey suggested an activation energy of 0.3 ± 0.0 5eV, which was very nearly

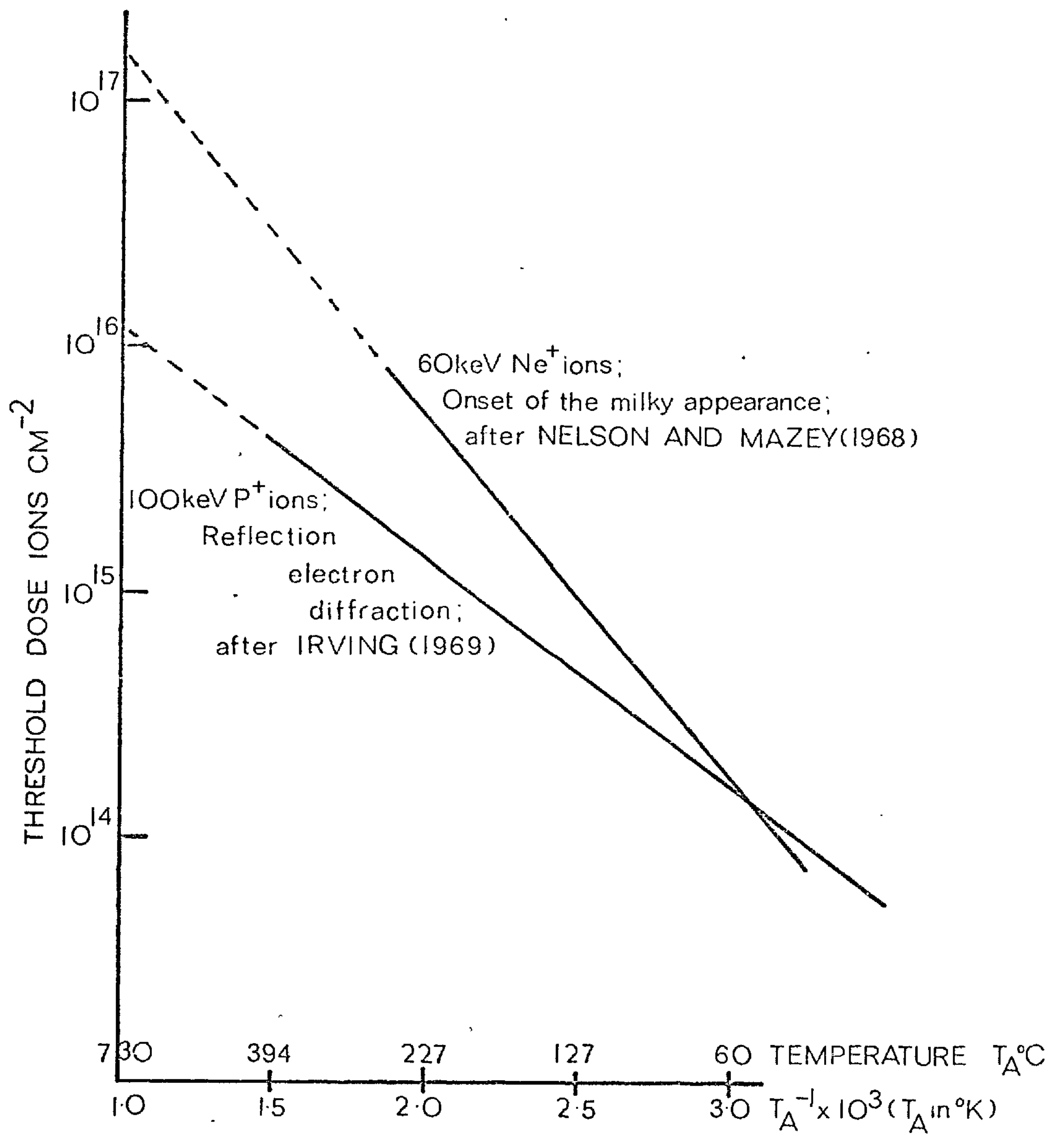

FIG. 2.18. GRAPH OF THE THRESHOLD DOSE TO PRODUCE AN AMORPHOUS SURFACE PHASE IN (111) Si, PLOTTED AS A FUNCTION OF TEMPERATURE AND RECIPROCAL TEMPERATURE.

equal to the measured activation energy for migration of a single vacancy in Si of 0.33eV. This result was further evidence that the formation of the disordered regions depended on their loss of vacancies to the surrounding lattice.

2.3.2. Ion implantation

The two aspects of ion bombardment which have received the most attention are the studies of ion penetration and ion sorption during ion bombardment. This has resulted in the development of P-N junction devices by ion implantation.

2.3.2.1. Ion penetration

Ion penetration studies have been stimulated from the discovery by Nelson and Thompson (1963) that enhanced ion penetration occurred along open channels of a crystal lattice. For Si, the order of penetrability is

$[110] \gg [111] > [100]$ (Davies et al 1964)

ie. the [110] direction is the easy direction for implanting.

Under conditions of good collimation of the ion beam along channelled directions, the ions come to rest in a narrow and well-defined band, sometimes at channelled ranges greater than ten times the statistical range. The statistical range of 40keV P^+ ions in Si is about 600 Å.

In most bombardment studies the problems presented by radiation damage are quite considerable. However, with channelling this damage is minimised. For example, if a single crystal is implanted along a good channelling direction, many incident ions are steered between the rows of atoms which form the channel walls. The probability of energetic recoils is greatly reduced, so there is correspondingly less radiation damage. Nelson and Mazey (1968) have shown that a reduction in radiation damage by a factor of 8 was inferred when the crystal was oriented so as to present its $\langle 110 \rangle$ channels to the incident ion beam.

2.3.2.2. Ion sorption

Channelling is particularly sensitive to the presence of ions which have become trapped in the lattice as atoms during bombardment. Each implanted atom has two alternatives;

it can come to rest squeezed into the space between adjacent atoms as an interstitial impurity or it can replace a lattice atom as a substitutional impurity. This trapping of atoms is called sorption, and Brown and Davies (1963) have examined the effect of sorption on the ranges of ions incident subsequently. Sorption can ultimately lead to saturation of the target with gas atoms. Beyond saturation, precipitation of implanted atoms occurs.

The degree of saturation is directly related to the sputtering yield. The sputtering yield imposes an inherent limit upon the number of atoms that can be implanted because a steady state is reached when the concentration is, to a first approximation, numerically equal to the inverse of the sputtering yield. In the case where sputtering yields are low (eg. 2 atoms/ion), implantation will build up to 50 atomic per cent of the saturation concentration in a depth approximately equal to the range (either channelled or statistical). Therefore, targets with particularly low sputtering yields (eg. Si) are ideal for producing high impurity saturation by bombarding ions.

2.3.2.3. P-N junction devices

The most important technical application of ion implantation is in the manufacture of semiconductor devices. By introducing the doping elements, generally boron and phosphorus, into Si by ion implantation along channelled directions controlled junction depths are possible. Junctions as deep as 12,000 Å have been produced by 80keV P^+ ions channelled along the ⟨110⟩ direction (for a review see Dearnaley et al 1969).

However, even with channelled trajectories, radiation damage is inevitable. The nature of the structural damage together with its annealing behaviour has been described in SECTION 2.3.1. The amorphous surface phase was stable up to temperatures of about 630°C where it recrystallised epitaxially onto the underlying undamaged Si; a defect-free region extending to a depth of about 500 Å below the surface overlaid a region containing dislocation loops and dipoles to the depth of the original amorphous surface

phase. The extent of the electrically-active dislocation damage in ion-implanted and annealed devices is generally less severe than in devices doped by thermal diffusion of impurities where dislocations emanate from the strain introduced into the lattice during the diffusion process and extend from the surface to a depth beyond the doped regions.

2.3.3. Surface topography of target after ion bombardment

Wehner (1956), (1957) and (1958) bombarded single crystal and polycrystalline targets of Si and Ge at temperatures of about 300°C with Hg^+ ions of 100 to 300eV energy at current densities from 10 to 20 mA cm^{-2}. A microscopic inspection of surfaces after up to 20 hr. bombardment revealed several pronounced effects which indicated that sputtered surfaces resembled in many cases those obtained with certain chemical etchants. Grain boundaries were more easily attacked than the perfect surface and appeared as grooves. Differently oriented crystal grains were attacked at different rates and appeared at different elevations. Etch pits were observed in single crystals, the abundance and size of which depended on target temperature and ion energy. These pits were not correlated with pits developed by CP-4 which would have brought out edge dislocations. The conditions of Wehner's experiments were such that preferential ejection of sputtered atoms was present and the formation of the amorphous surface phase was prevented.

Meckel and Swalin (1959) used bombardment conditions which probably resulted in the formation of an amorphous surface phase. Ge single crystal targets were bombarded with 350eV A^+ ions at a current density of 2mA cm^{-2} with target temperatures less than 100°C. Hillocks were observed having the shape of truncated cones with a spiral pattern on their tops. Meckel and Swalin (1959) concluded that the hillocks formed at the sites of intersection of screw dislocations with the surface. On the other hand, Wolsky and Zdanuk (1961) proved that, for Si at least, hillocks were not necessarily indicative of the existence

of screw-type dislocations in the bulk. This is hardly surprising if an amorphous surface phase is present.

Dillon and Oman (1960) have observed the appearance of etch patterns for a Ge sample under different conditions. For both 500 and 100eV A^+ ion bombardment at a current density of 100μA cm^{-2} for prolonged periods a number of tiny pits were detected only by the electron microscope. This type of etching presumably represented the initial stages of the gross characteristic pitting reported by Wehner. Bombardment at 500eV and 1mA cm^{-2} eventually produced etching patterns of a different nature. Hillocks were observed which were thought to be associated with the accumulation of mobile surface atoms at locally active centres on the amorphous surface layer. Honig (1958) attributed the presence of hillocks on (111) Ge and (221) Ge-Si, which were several hundred Å in height, to aggregates of C atoms which, because of their low sputtering yield, served to mask off parts of the surface which were left standing as hillocks. Meckel (1966) interpreted the presence of strange hillocks found on sputtered Ge surfaces as being due to small electrically insulating particles covering the surface. The positive ions charged the dielectric material positive and, therefore, the ions were deflected away from the region hence preventing the sputter erosion of the microscopic area beneath each insulating particle.

Hillocks have also been observed on Si surfaces in the form of conical protrusions after high energy (5 to 8keV) A^+ ion bombardment by Stewart and Thompson (1969) in the scanning electron microscope. These conical protrusions were formed with their axes along the direction of ion incidence (45° to surface normal) and were interpreted as being due to either the presence of foreign inclusions in the specimen or the presence of fine dust particles on the surface which apparently shielded the surface immediately beneath them. In all cases the specimen was near 25°C during bombardment and the shape of the spikes did not seem to be a function of current density from 100uA cm^{-2} to 5mA cm^{-2}. If the diffusion of mobile surface atoms to impurity centres was the dominant

mechanism in the formation of the conical protrusions (as concluded by Dillon and Oman 1960) then a dependence on ion current density would have been expected.

CHAPTER 3

EQUIPMENT AND EXPERIMENTAL TECHNIQUES

3.1. GENERAL ARRANGEMENT

The experimental arrangement for the homo-epitaxial deposition of Si layers by ion beam sputtering is shown schematically in FIG. 3.1.

An argon ion beam is extracted from the ionisation chamber of the ion beam source and strikes the central region of a Si target, the source material, at an angle of incidence of about 60° to the target normal. The usual total energy of the ion beam is 12keV and, according to Lindhard (1965) (see SECTION 2.1.7.), the optimum angle to give maximum sputtering yield and hence maximum deposition rate is then about 80°. The angle of ion incidence is fixed at 60° in this investigation due to the extent of spreading of the ion beam (see SECTION 4.2.2.) and limited sizes of targets available. The other requirement to ensure a useful deposition rate is that the ion beam current is sufficiently large. Mass-analysed ion beams (for example, Yonts et al 1960, Rol et al 1960a, Almén and Bruce 1961a, Molchanov et al 1961) are not suitable because currents of up to only about 1mA are possible. With ion beams which are not mass analysed currents far in excess of 1mA are possible (for example, Yurasova et al 1960, Pleshivtsev 1960) and useful sputtering and deposition rates can be obtained. In this investigation a typical non-mass-analysed extracted ion beam current is 4mA and the purity of a mass-analysed ion beam has been retained by suitable modifications to the ion beam source to ensure that original metal contamination in the beam is minimal.

During the initial stages of bombardment of the target when the target is cleaned, the shutter is in a position above the target shielding the heated (111) Si substrate so as to prevent sputtered atoms reaching it. Contamination of the substrate with impurity atoms originating from the target and contamination of the target with impurity atoms

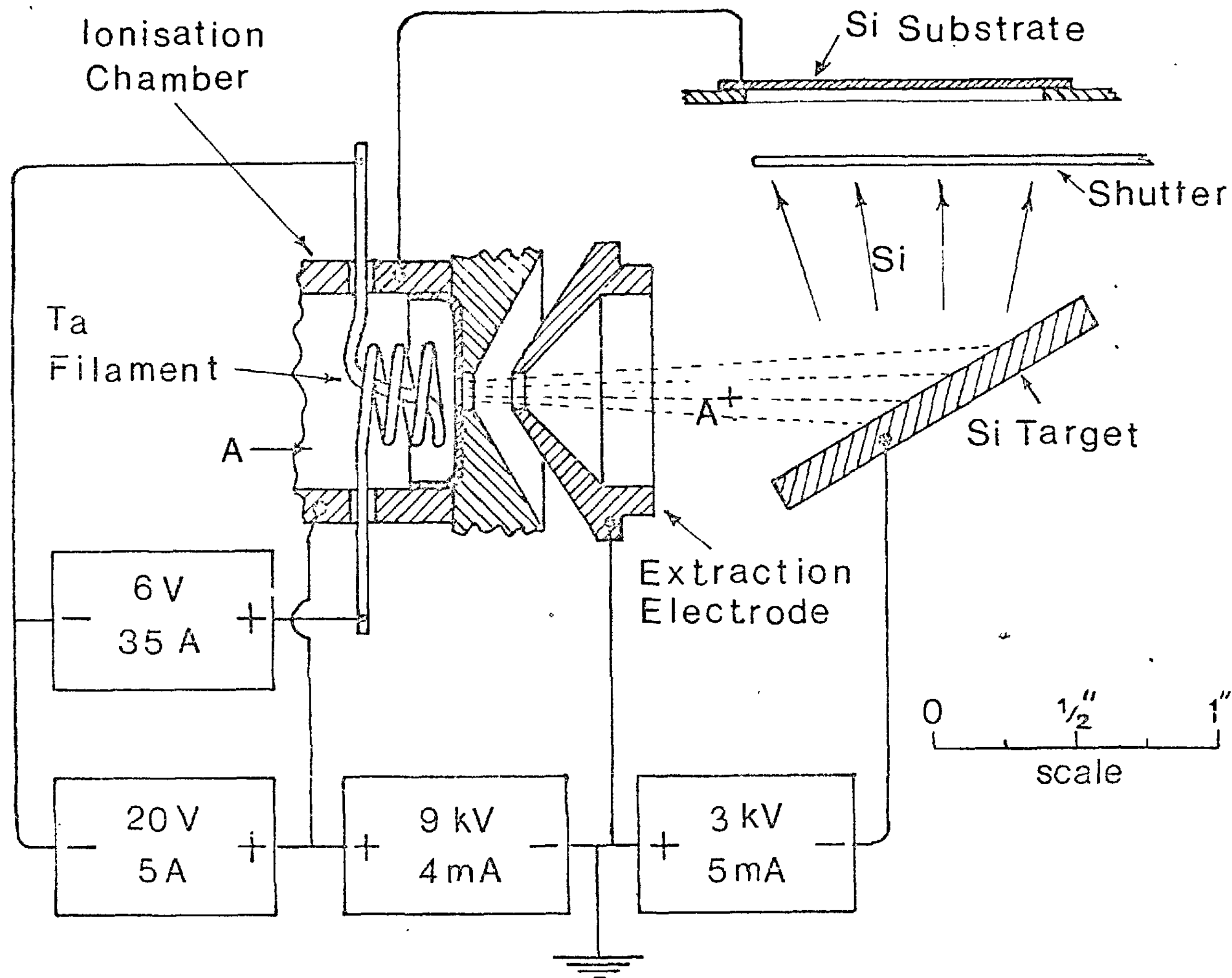

FIG. 3.1 ION BEAM SPUTTERING ARRANGEMENT

originating from the substrate is thus prevented. After the target has been cleaned for a few minutes, the shutter is opened and deposition of sputtered atoms onto the heated substrate commences. To achieve a maximum deposition rate the substrate is required to be as near as possible to the target. The minimum seperation tolerated is about 1in. before it becomes impossible to use the shutter between the target and substrate satisfactory.

The effect of ion bombardment of the substrate during deposition on the structural quality of the resulting Si layer is determined by suitable substrate biasing. In FIG. 3.1. the substrate is shown biased at the same potential as the ion beam source thus repelling secondary positive ions but attracting secondary negative ions.

In cases where a detailed study is made of the angular distribution of sputtered atoms from Si and GaAs targets, the Si(111) substrate is replaced by a series of glass microscope slides which, when deposition is complete, are analysed for thickness and rate variations across them.

3.2. THE VACUUM SYSTEM

The vacuum system (see FIG. 3.2.) consists of a 12in diameter stainless steel chamber with a number of ports with Varian type flanges. The detachable water-cooled top plate and the 6in pyrex dome are sealed by L-shaped viton gaskets.

The chamber is pumped by titanium sublimation, a liquid helium cryopump and a 2in mercury diffusion pump through an all metal valve, a liquid nitrogen trap and a Peltier baffle. The initial roughing out and the backing of the diffusion pump is done by two sorption pumps and a vacuum resevoir for overnight operation. The cryopump built (see FIGS. 3.3. and 3.4. and APPENDIX 1) consists of a 5cm. diameter 5cm. high liquid helium container surrounded by a liquid nitrogen cooled copper shield. The helium container "views" the vacuum chamber through a chevron baffle in the copper shield and with the mercury diffusion pump gives an effective chamber pumping speed of about 180 l/sec. Without the cryopump, the effective chamber pumping speed is only 15 l/sec.

The pressure in the vacuum chamber is measured by a nude ion gauge and individual residual gases are identified by an A.E.I. MSIO mass spectrometer.

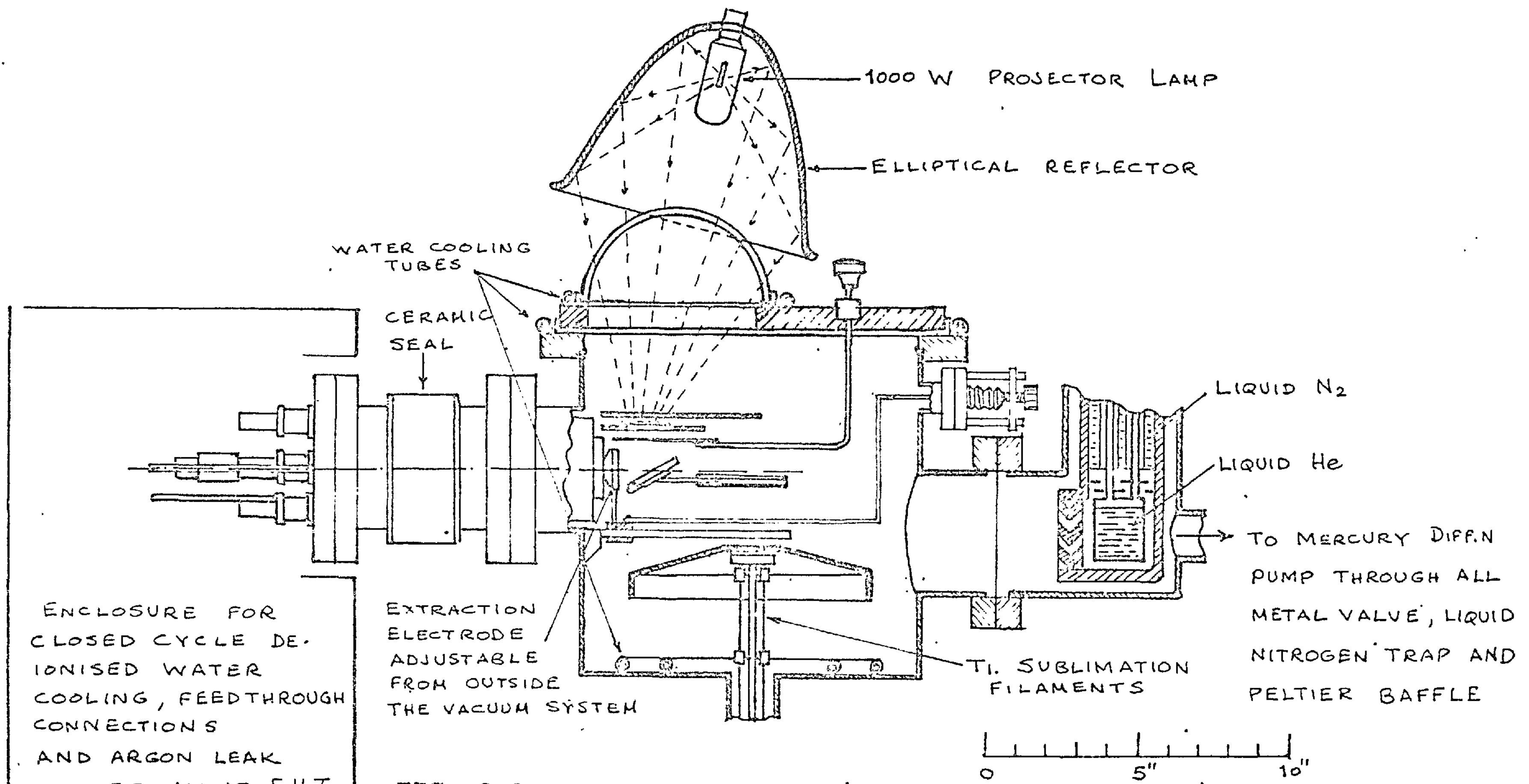

FIG. 3.2 EXPERIMENTAL ARRANGEMENT SCHEMATIC

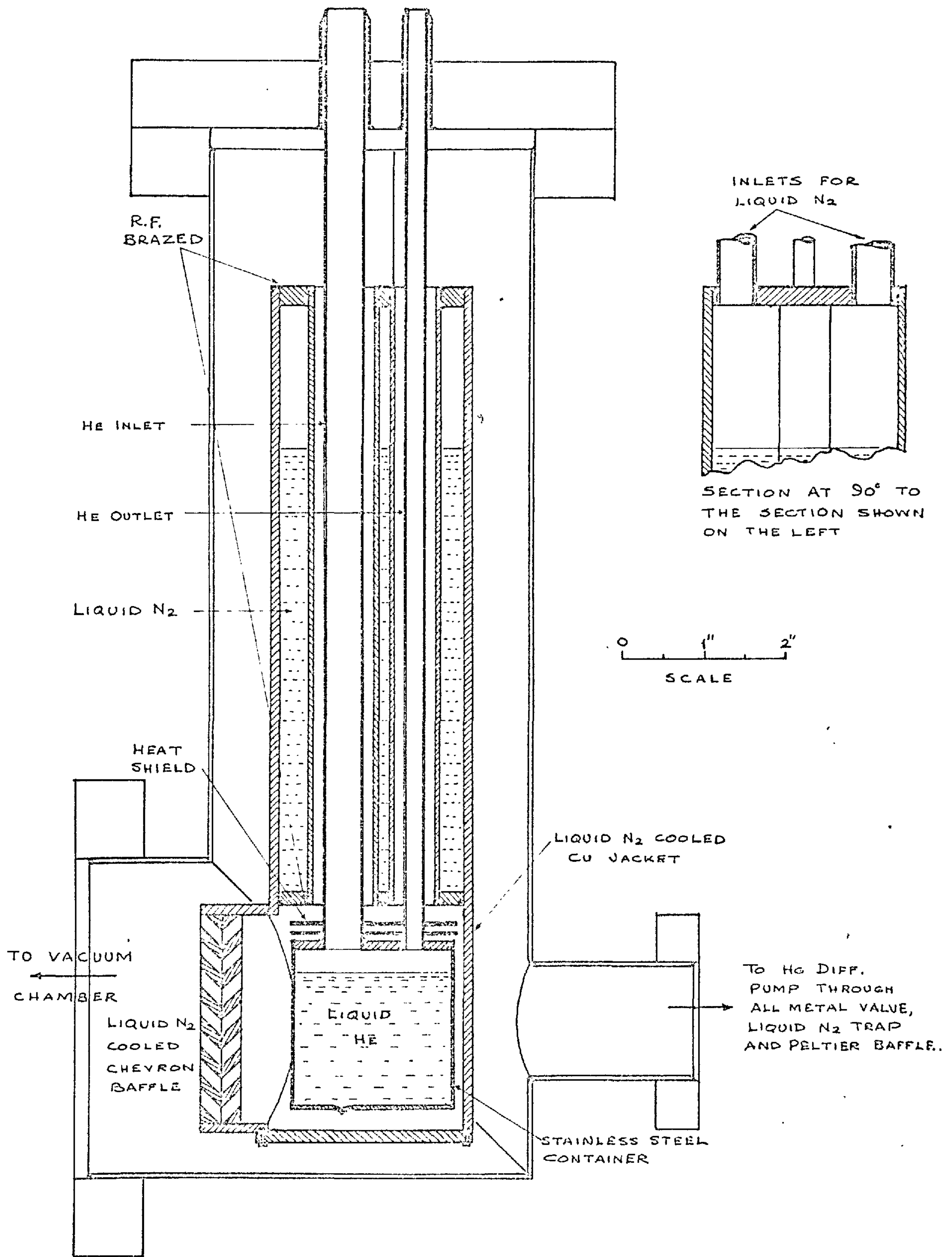

FIG. 3.3 LIQUID HELIUM CRYOPUMP

METALLURGY DEPT.,
IMPERIAL COLLEGE,
LONDON S.W.7.

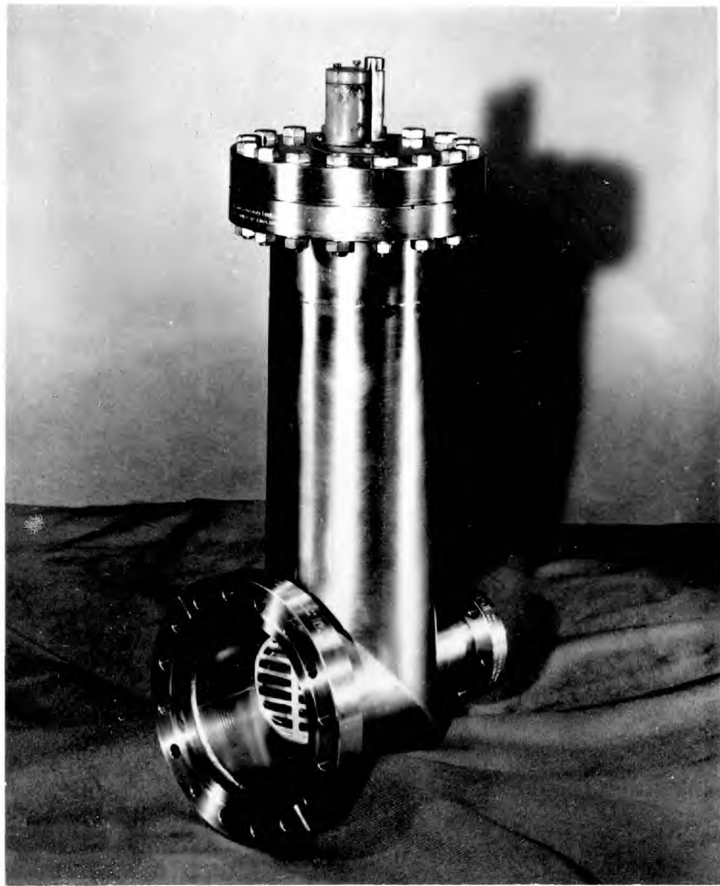

FIG. 3.4. LIQUID HELIUM CRYOPUMP

3.3. ION BEAM SOURCE

3.3.1. Choice of type of source

An ion beam source was necessary which would satisfy the following specification;

(i) it must be capable of producing ions of the noble gases and solids, in particular, Si. It was hoped to use the poor self-sputtering properties of Si (see SECTION 2.1.5) to an advantage and investigate the possibility of depositing deaccelerated Si ions onto Si substrates epitaxially.

(ii) it must produce a "clean" beam with unwanted impurities kept to a minimum.

(iii) the source must produce a few milliamps of the required ions in a narrow beam.

(iv) provision must be made for quick servicing.

The "sputtering ion source", described by Hill and Nelson (1965), satisfied these requirements. Moreover, these authors have reported the extraction of several hundred microamp beams of Al, Cu, Fe, Au and Ag, and milliamp beams of A and Xe for their source which is installed on the Heavy Ion Accelerator at A.E.R.E. Harwell.

The original design and the operation of the Harwell source was modified considerably to reduce contamination from the source to a minimum and to increase the A or Xe extracted ion beam current to several milliamps. All viton gaskets were dispensed with so that the modified source could be baked to over 400°C; the modified source was water-cooled instead of compressed-air cooled during operation; metal contamination from the source was minimised by a change in the operating conditions and selecting optimum values of angles of electrodes. With the optimum electrodes less divergent beams were extracted. Denser beams were possible with larger electrode apertures. The modified source was then capable of giving the purity needed for the production of semiconductor layers without mass analysis of the ion beam. The modified ion beam source is shown in FIG. 3.5. together with the general sputtering arrangement.

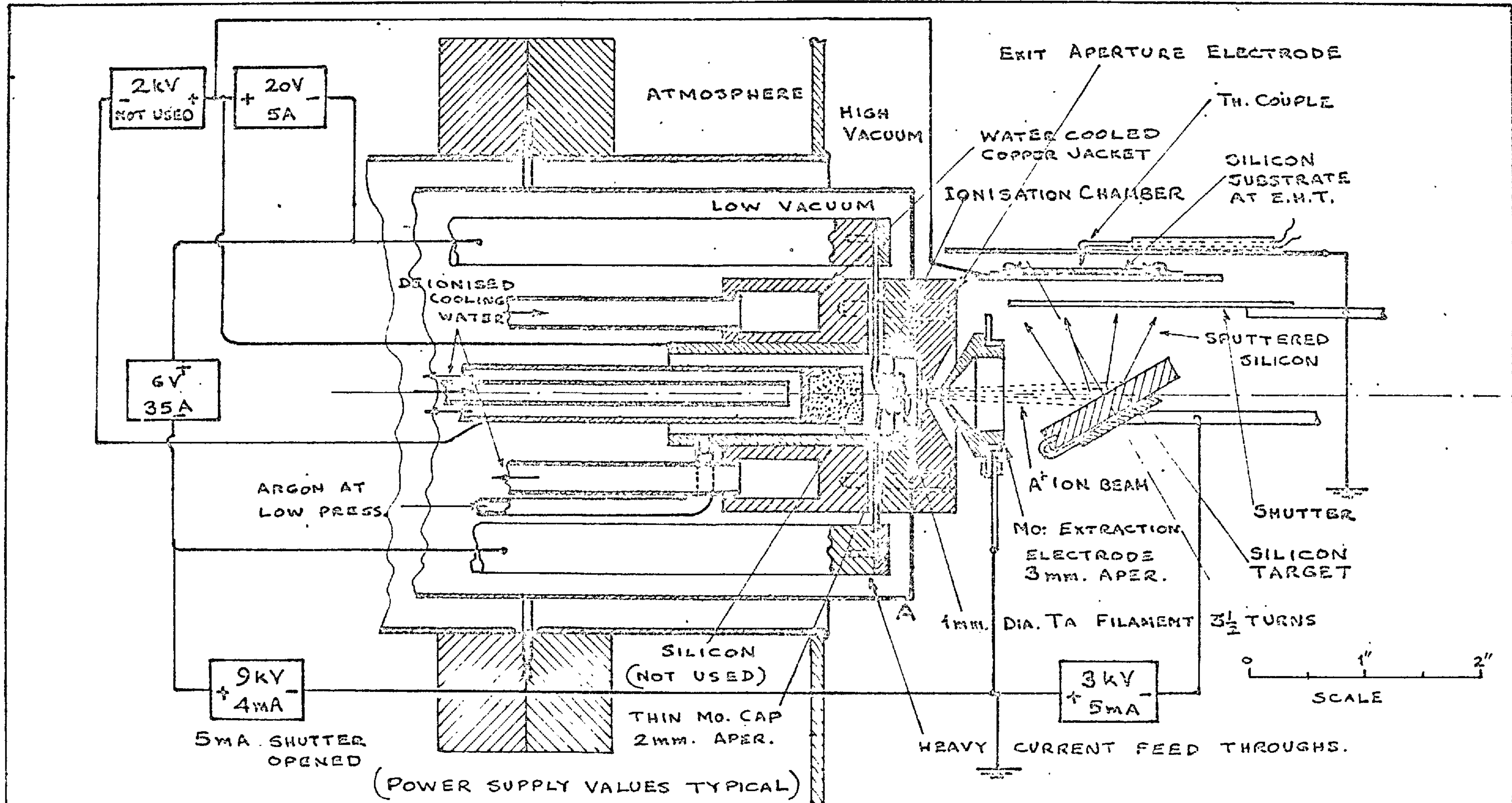

FIG. 3.5 ION BEAM SOURCE AND SPUTTERING ARRANGEMENT

METALLURGY DEPT.,
IMPERIAL COLLEGE
LONDON S.W.7.

3.3.2. Operation of source

The operation of the ion beam source for the production of an A^+ ion beam is shown in FIG. 3.5.

Argon at a pressure of a few hundred microns is leaked into the ionisation chamber. Electrons emitted from the hot Ta filament are attracted to the ionisation chamber by a potential of +20v and argon atoms are ionised. Only singly-charged ions are formed because for argon the first ionisation potential is 15.7v and the second ionisation potential 27.8v. The corresponding values for xenon are 12.1v and 21.1v respectively. The magnetic field set up by the large current flowing though the filament increases the number of ionising collisions by changing the linear path of electron flow into a helical path. The concentration of ions is greatest along the central axis of the ionisation chamber because the magnetic field is greatest here (about 170 oersteds at centre of filament). The extraction electrode at earth potential extracts a fraction of these singly-charged ions from the source at positive EHT.

If it is required to introduce Si^+ ions in the beam, the Si held in the water-cooled pedestal is biased negatively (eg. -2kV). It is then bombarded by the A^+ ions, resulting in sputtered Si atoms which are ionised in the plasma region at the centre of the filament. The emerging ion beam then consists of A^+ and Si^+ ions. Hill and Nelson (1965) were able to make Fe and Cu ionisation self-supporting without the necessity of a support gas. This was not possible with Al where the highest ratio of Al ions to support gas ions obtained was 20%. These results were not surprising because the self-sputtering yields (see SECTION 2.1.5.) for Cu and Fe were greater than 1, whereas for Al it was less than 1. More recently, Hill et al (1968) found that in some cases the magnetic field produced by the filament was insufficient for the ionisation to be made self-supporting. They have overcome this problem by increasing considerably the concentric magnetic field along the axis of the ionisation chamber with the aid of an external magnet. Efficiency of ionisation of noble

gas atoms and sputtered atoms was therefore improved.

3.3.3. Construction of source

The entire ion beam source (FIG. 3.5.) together with all its feed-throughs and cooling tubes was mounted on a standard 6in. O.D. Varian type flange and fitted to the vacuum chamber through a Ferranti ceramic-to-metal seal which electrically insulated the ion source assembly from earth (see FIG. 3.2.).

Quick servicing of the ion source was possible using an ionisation chamber and cooling jacket which split into two sections at the point where the filament entered the chamber. The filament could then easily be replaced. The ionisation chamber was made a push-fit inside its cooling jacket so that when necessary it could be removed and thoroughly cleaned. With the ionisation chamber removed, access was possible to the Si button mounted on the fixed sputtering electrode.

The photographs in FIG. 3.6. show the ion source at various stages of assembly.

The first photograph (FIG. 3.6.(i)) shows the dismantled ion source removed from the vacuum system with the ceramic-to-metal seal still bolted on and a Si button mounted on the sputtering electrode. Current to the filament was supplied via two 12½in. long ½in. diameter Cu rods connected through Ferranti high-current EHT feed-throughs. Current to the sputtering electrode was supplied through a water-cooled 12½in. long ½in. diameter Cu pipe also through a Ferranti high-current EHT feed-through. The Si button was secured to the sputtering electrode by means of a tungsten wire clip which passed through an ultrasonically-drilled hole in the button and connected to a clamp fastened around the exterior of the electrode a short distance away from the button. The photograph in FIG. 3.6.(i) also shows the water-cooled Cu jacket for the ionisation chamber which was vacuum-brazed (see APPENDIX 1) to a stainless steel jacket onto which was argon arc-welded the stainless steel pipes. These pipes acted as flow and return pipes for cooling water and physically supported the cooling jacket.

(i)

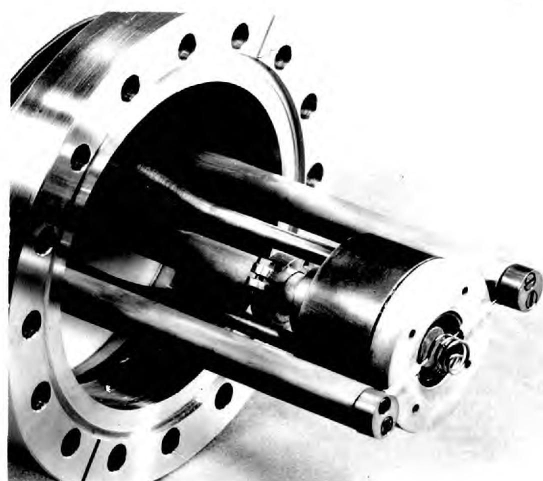

(ii)

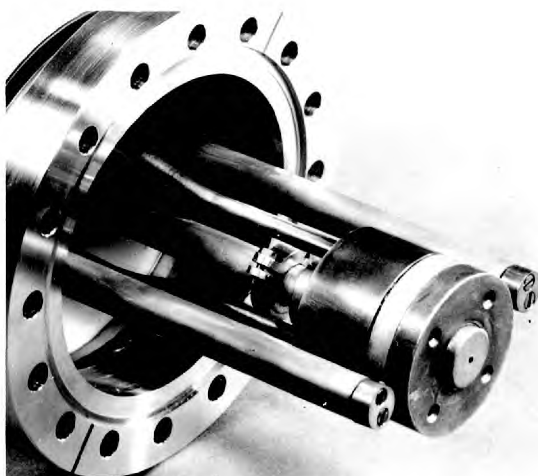

(iii)

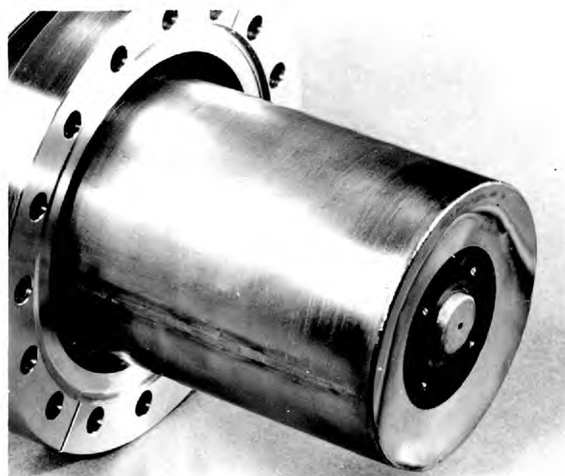

(iv)

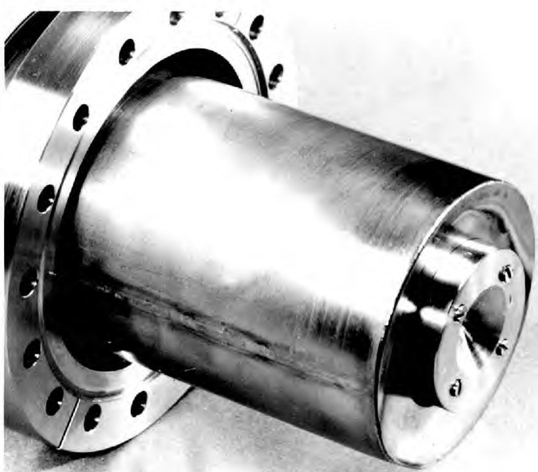

(v)

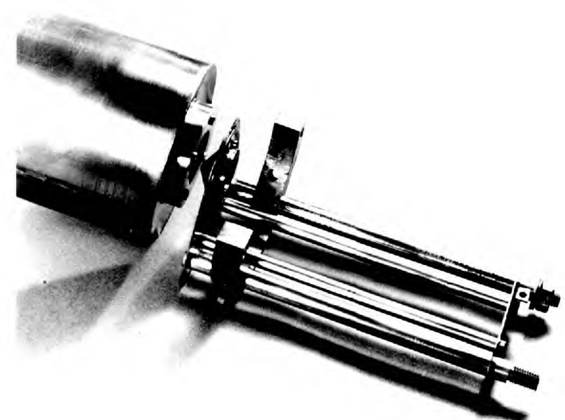

(vi)

FIG. 3.6. ION SOURCE AT VARIOUS STAGES OF ASSEMBLY

Finally the stainless steel pipe for leaking in inert gas is also shown in the photograph in FIG. 3.6.(i).

The second photograph (FIG. 3.6.(ii)) shows, firstly, the main part of the ionisation chamber pushed inside its cooling jacket and fixed in place by the gas pipe and, secondly, a filament mounted. Where the filament passed through the ionisation chamber and cooling jacket, silica insulators were used to eliminate the possibility of an electrical short.

In the next photograph (FIG. 3.6.(iii)), the remainder of the ionisation chamber and cooling jacket was fitted and the 0.005in. thick Mo cap with a 2 mm. aperture pushed inside the ionisation chamber.

In the next photograph (FIG. 3.6.(iv)) the can, which limits gas leakage from the ion source solely to that from the 2 mm. aperture, was fitted.

The stainless steel exit aperature electrode was now mounted and this assembly was secured using four 4BA screws which protruded into the Cu cooling jacket of the ionisation chamber (FIG. 3.6.(v)). The can, shown as the casing A in FIG. 3.5., was in pressure contact with the Varian flange when the screws were done up tightly.

The final photograph, FIG. 3.6.(vi), shows the Mo extraction electrode with a 3 mm. aperture and the stainless steel assembly for adjusting its position with respect to the ion source with the source operating. The fixed part of this assembly, the semicircular ring, was bolted to two flanges welded onto the inside of the vacuum chamber. Movement of the extraction electrode from outside the vacuum system was possible using a micrometer controlled linear drive feedthrough of ½in. stroke through a UHV bellows. The position of the extraction electrode was then accurately repositioned.

3.3.4. Equipment used with the ion source

3.3.4.1. Power supplies

FIG. 3.5. shows the power supplies used with the ion source with the figures in the squares representing typical operating values during a run. The full rating of each power supply was 10V 100A (fiament), and 300V 5A

(ionisation chamber), 20kV 10mA (EHT), and 3kV 500mA (target or ion source sputtering electrode).

All supplies were designed to give capacitance-smoothed DC output from current rectification of a single-phase AC supply. A cascade voltage doubler circuit was used for the EHT supply and conventional full-wave bridge circuits for the other three supplies. Because ion currents are very susceptible to changes of environment, unstable currents can result. This aspect of instability can be controlled by making the regulation of the power supply poorer. ie. larger output currents are only possible at severely reduced output voltages. The feature of poor regulation was included in all the power supplies built, except the filament supply where it was unnecessary, by using a suitable high-wattage resistor in series with the load.

The other important feature of the design of the power supplies was that, by virtue of the EHT supply, at least 20kV insulation of the outputs of each of the other supplies from earth was needed. This was achieved by mounting all diodes, heat sinks, meters etc. on paxolin panels and using suitable EHT cable. Insulation between each output circuit and its mains input circuit was achieved using an isolation transformer.

3.3.4.2. Water cooling

A unit was constructed which circulated deionised water in a closed loop through the ionisation chamber cooling-jacket and the pedestal holding a Si button.

Deionised water was used because its resistivity is approximately 600 times greater than that for tap water. Long lengths of plastic pipe were used between the ion source (at EHT potential) and earth to keep the leakage current at a value which was small compared to the extracted ion current. With the system constructed a typical leakage current was about 18μA at 16kV.

The disadvantage of using long lengths of plastic pipe was that flow rates were significantly reduced and heat could not be extracted so easily. However, using a flow rate of 1 gall/min. and fan-cooled heat exchangers

in the return line from the ion source, no appreciable rise in water temperature was noticed during a run.

3.3.4.3. Inert gas supply

Inert gas was leaked into the ion source via two Edwards type LB2B leak valves mounted at the same potential as the ion source by virtue of the copper pipe connections. It was essential that the leak valves were at EHT potential and not at earth potential to ensure that a gas discharge did not occur between them and the ion source. The gas leakage rate could then only be adjusted safely with the EHT turned off. The second leak valve was connected to the inert gas supply by rubber tubing. If the gas supply was now at earth potential breakdown could not occur because the critical voltage needed for breakdown at this pressure was much higher.

Spectroscopically pure argon or xenon was used in this investigation which was supplied by B.O.C. in 1 litre pyrex glass containers filled to a pressure of 1 atmosphere. The argon purity was 99.9995% (N_2<5vpm, O_2<1, H_2<1, Co_2<0.5, Hydrocarbons < 0.5vpm) and xenon 99.99% (Kr<50vpm, N_2<25, O_2<5, H_2<5, Hydrocarbons < 5vpm).

3.3.5. Performance of ion source

The magnitude of the ion current extracted from the ion beam source depended on (i) the pressure in the ion source, (ii) the ionisation chamber current, (iii) the applied EHT potential, and (iv) the seperation of the extraction electrode from the exit aperture of the ion source.

When either larger pressures or larger ionisation chamber currents were used, increased extraction currents resulted because the density of ions in the ionisation chamber was also increased. The filament current and filament bias voltage controlled the initial number of electrons available for ionising gas atoms.

The maximum pressure possible in the ion source was determined by the highest value of chamber pressure tolerated. For chamber pressures greater than $1x10^{-3}$torr mean free path considerations were becoming prominent so the maximum permissible chamber pressure was $1x10^{-3}$torr. At $2x10^{-3}$torr glow discharge breakdown occurred between the electrodes anyway. A high pressure difference between

the ion source and vacuum chamber was achieved by pumping the chamber with the 180 l/sec cryopump and limiting gas leakage from the ion source solely to its ion exit aperture.

A limit was also set on the maximum ionisation chamber current possible. The ionisation chamber current was the sum of the ion and electron currents to and from the filament. The total current could not exceed 5A because this was the current limit set by the power supply. The ionisation potential was set at 20V throughout this investigation to ensure, firstly, that only singly-charged ions were extracted, and secondly, to minimise metal contamination in layers due to sputtering of the filament material (see SECTION 3.3.6.). The total power dissipated by ions and electrons was 100 watts. Under these conditions the ionisation chamber current remained constant throughout a run. On the other hand, in initial experiments where the power dissipated was 500 watts. (100V and 5A) ionisation chamber currents were unstable and showed an overall increase as the run proceeded. The thin Mo cap was also observed to be glowing when no exit aperture electrode was used indicating the instabilities in current were a direct result of severe outgassing at temperatures much greater than the usual ion source baking temperature of 400°C. Therefore, even if a 20V power supply with a current capability of greater than 5A had been available it was not suitable for use here because of the severe outgassing and possible contamination evolved at high powers.

As the applied EHT was increased the extracted ion current also increased. A limit to the maximum EHT was set eventually by sputtering and deposition rates. Values of EHT less than 12kV were used because the peak in the sputtering yield versus ion energy curve occurred for ion energies less than 12keV (see SECTION 4.2.1.).

At any applied EHT, the closer the extraction electrode to the ion source the higher the extracted ion current. However, for very small seperations the extracted beam was highly divergent and a smaller number of ions reached the target. In all cases, for set

operating conditions and a fixed geometry, the position of the extraction electrode was adjusted so that a peak value of the ratio of target current to extracted ion current occurred.

With the aforementioned parameters at their maximum permissible values, up to 8mA beams have been extracted from the ion source using apertures of 3 and 2 mm. for the extraction electrode and the ion source exit aperture electrode respectively. These values of aperture sizes were about the optimum values for obtaining maximum ion current with all other parameters kept constant. In the Harwell design of ion source 1½ and 1 mm. apertures were used.

When Si^+ ions were introduced into the extracted beam, the highest ratio of Si^+ ions to Xe^+ support gas ions recorded was 20% without the help of an extra magnet to increase ionisation efficiency. The ionisation could not be made self-supporting because, according to Almen and Bruce (1961b), the self-sputtering yield of Si was less than 1 and appeared to be zero (see SECTION 2.1.5.). The possibility of depositing extracted deaccelerated Si^+ ions onto Si substrates epitaxially appeared difficult at this stage and was not continued. Mass analysis of the ion beam would have been necessary to seperate noble gas ions from Si^+ ions and only slow deposition rates would have been possible. The facility to produce ion beams of a required material was built into the source but was not used for growing sputtered Si layers.

3.3.6. Minimisation of metal contamination from the source

Voltage and current values used during a typical run with a 4mA A^+ ion beam extracted from the ion beam source are shown in FIG. 3.5. In initial experiments a voltage of 200 to 300V was used between the filament and the ionisation chamber (as in the Harwell design). This caused sputtering of the filament material and metal contamination was detected in Si layers by electron probe analysis, having been transferred through the ion beam. A typical level of metal contamination was 0.6% with

A^+ ions. The limit of Ta detection with the electron probe was 0.05%. By lowering the filament bias to 20V no Ta impurity could be detected. This improvement was offset by the need for higher pressures in the ionisation chamber and consequently in the vacuum chamber to maintain the same ion beam current. A filament bias of 20V was below the threshold voltage for sputtering of Ta which was 26V for A^+ ions and 30V for Xe^+ ions (Stuart and Wehner 1962).

Another source of metal contamination was sputtering of the aperture edge in the extraction electrode as high current density ion beams tended to diverge. For this work high beam currents were required to obtain useful rates of sputtered atom deposition. Contamination resulting from excessive beam spreading was minimised by careful choice of electrode angles. The optimum values of angles for the electrodes were determined experimentally from the ratio of the target current to the extracted ion current for various electrode angles (see FIGURE 3.7.) The target current measured represented the sum of the ion current to the target and the electron current away from the target due to secondary emission. When beam spreading was insignificant all extracted ions reached the target and the target current was greater than the extracted ion current by the factor $(1+\gamma)$. γ represented the secondary electron emission coefficient for singly charged ions. The value for γ was about 0.3 ± 0.1 for a 12keV A^+ ion beam incident at 60° to the target normal on a Si surface. On the other hand, when beam spreading was excessive, sputtering of the extraction electrode occurred and a smaller number of ions left the ion source. Some of these emerging ions even missed the target and resulted in further unwanted sputtering. The target current was then less than the extracted ion current when beam spreading was excessive. The optimum values for the electrodes were $\emptyset_1 = 30°$, $\emptyset_2 = 32°$ and $\emptyset_3 = 42°$. Unfortunately, for Xe^+ ion beams it was still not possible to collect all extracted ions and eliminate entirely sputtering from the edge of the aperture of the extraction electrode. In the original

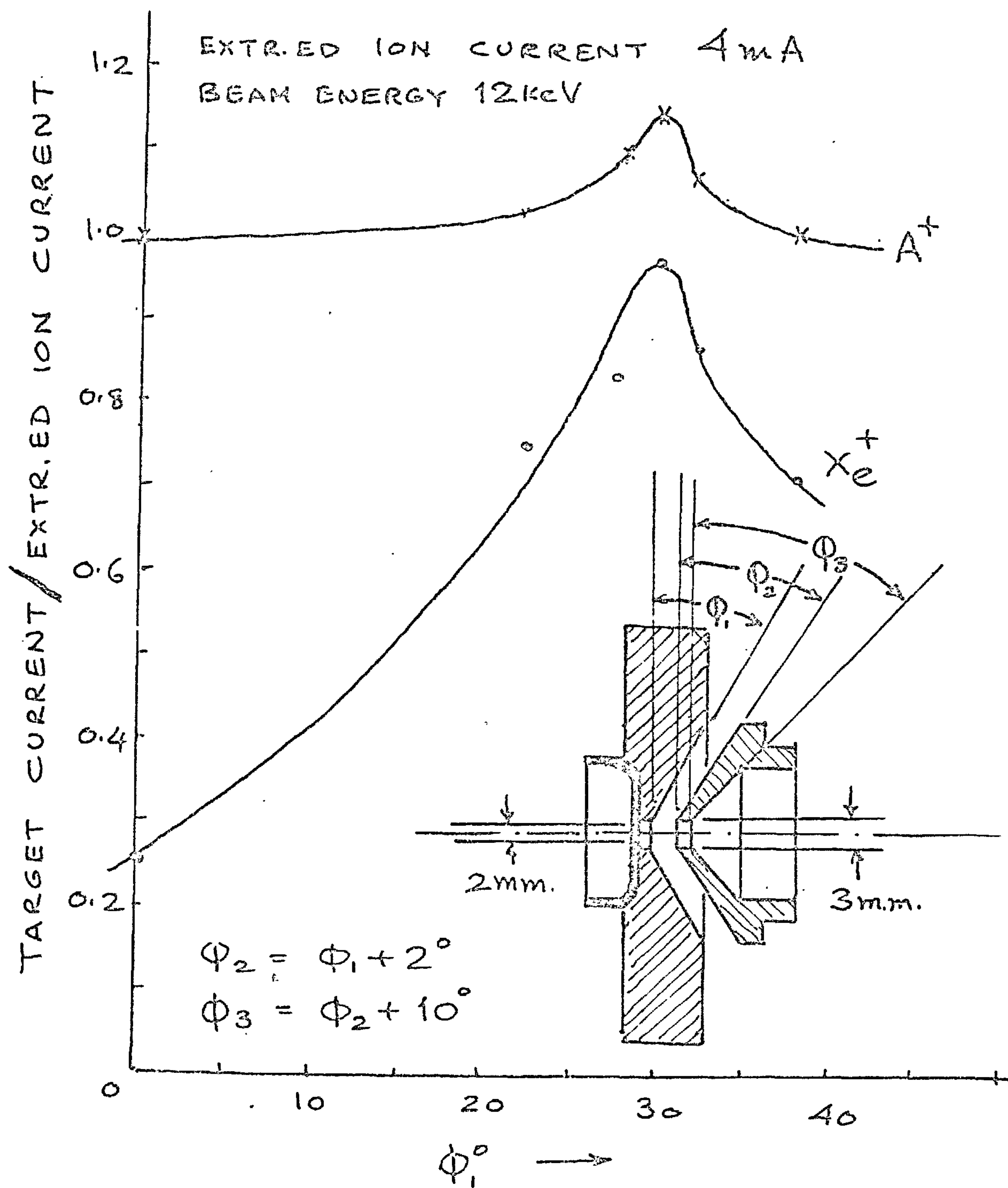

FIG. 3.7 DETERMINATION OF THE OPTIMUM ANGLE OF THE EXIT APERTURE ELECTRODE.

Harwell design of ion source, the angle $\emptyset_1$ was set at $22\frac{1}{2}°$ which was perfect for the extraction of electrons (Pierce 1941) and suitable only for low current density ion beams.

A further cause of metal contamination in Si layers was unwanted sputtering due to misalignment in the assembly of the ion source. It was essential that all electrodes and apertures were aligned perfectly. Misalignment and contamination problems also occurred when Ta filaments were operated continuously for more than 2 hours. In this case appreciable sagging of the filament took place. Therefore, the duration of use of any Ta filament was restricted to 2 hours. Attempts at making suitable coiled filaments of tungsten were unsuccessful.

No level of metal contamination detectable by electron probe was now introduced at the substrate for well-aligned A^+ ion beams with the filament bias set at 20V, using the optimum electrode angles, and the filament operated for no more than 2 hours.

3.4. TARGETS AND TARGET HOLDERS

3.4.1. Si Targets used

For sputtering yield and sputtered atom distribution studies both single crystal and polycrystalline targets were used. The single crystal targets were (111) Si slices 32 mm in diameter and 0.25 mm thick either 0.01 ohm-cm N-type or 25 ohm-cm P-type supplied by Texas Instruments. Bombardment of these thin slices was limited to 60 mins. because for 4 to 5mA 12keV A^+ bombardments in excess of 100 mins. the central region of the slice was completely eroded away and a small hole formed. When polycrystalline Si was used as the target material, 5 mm. thick samples were used.

For studies of the epitaxial deposition of Si, 32 mm diameter 5 mm thick Si samples were used. These were either 0.01 ohm-cm N-type or 25 ohm-cm P-type (111) samples or a polycrystalline sample predominantly of P-type conductivity.

3.4.2. GaAs targets used

A (111) single crystal and a polycrystalline sample were used as target for sputtering yield and sputtered atom distribution investigations. Both of these GaAs targets were about 5 mm thick so that heat generated by bombarding ions was dissipated more easily and the possibility of dissociation reduced.

3.4.3. Target holders

The holder used for supporting Si targets is shown in the photograph in FIG. 3.8. A shaped Mo plate was spot-welded to a rigidly supported $\frac{1}{8}$ in stainless steel rod and insulated from its support at earth potential by silica tubing. The target was positioned on the plate by two Ta clips at the bottom. When thick targets (eg. 5 mm thick) were used the securing clips were pushed into ultrasonically-drilled holes in the side of the target. Targets larger than the holder were used to ensure that unwanted sputtering of the holder was avoided. Sputtering of the securing clips was unlikely because they were well out of the path of the ion beam.

A similar design holder was used for GaAs targets

FIG. 3.8. TARGET AND SUBSTRATE HOLDERS FOR THE EPITAXIAL DEPOSITION OF Si

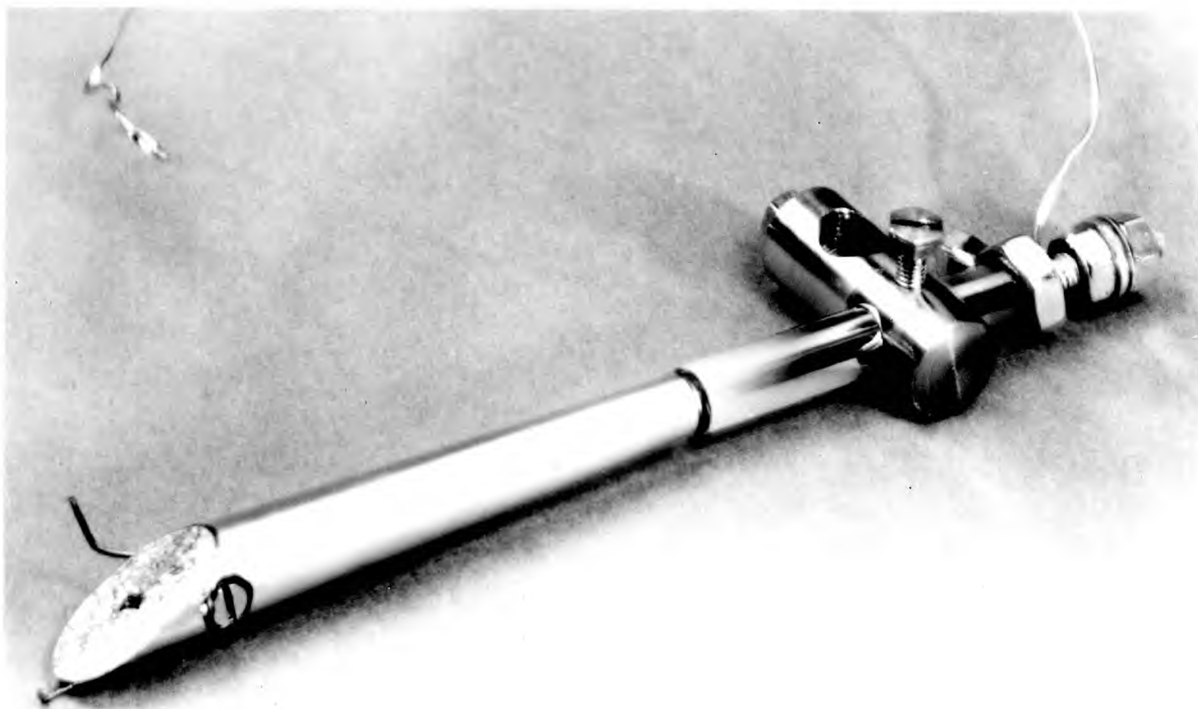

FIG. 3.9. GaAs TARGET HOLDER

(see FIG. 3.9.). In this case a tapered bar of Cu was used for supporting the target to ease the dissipation of heat generated by bombarding ions and reduce the possibility of dissociation.

3.5. SHUTTER BETWEEN TARGET AND SUBSTRATE

The shutter between the target and substrate was made from a Mo disc connected to a stainless steel rod and could be turned to one side from outside the vacuum system by operating the rotary feedthrough in the water-cooled top plate of the vacuum system (see FIG. 3.2.). Because it was connected to earth, the shutter could not be placed closer than 1/5 in. to the substrate at ion source potential otherwise an electrical breakdown occurred. The seperation of the shutter from the centre of the target was limited to about 4/5 in. by the size of the target and the need for the shutter not to interfere with the passage of the ion beam to the target. The minimum seperation tolerated between the substrate and the target was then about 1 in. before it became impossible to use the shutter satisfactory.

3.6. SILICON SUBSTRATES; METHODS OF SUPPORT AND HEATING

3.6.1. Substrates used

The Si substrates used were (111) slices 32 mm. in diameter and 0.25 mm. thick either 0.01ohm-cm N-type or 25ohm-cm P-type supplied by Texas Instruments.

3.6.2. Substrate holder and measurement of layer thickness

The holder for 32 mm. diameter Si slices was a Mo plate with a 28 mm. aperture rigidly connected to an EHT feedthrough. The plate is shown in FIG. 3.8. just below the mask which prevented coverage of the pyrex dome with sputtered Si. Slices were held in a central position on the Mo plate by four Ta tags spot-welded to the plate at about 33 mm. diameter. When slices were maintained at ion source potential it was also necessary to use four Ta wire clips pressing down on the surface to prevent movement by electrostatic attraction.

The thickness of the deposited layer was determined using the Talysurf across the step produced on the slice at a 28 mm. diameter.

3.6.3. Experimental considerations for substrate heating

It was necessary to heat the substrate to at least 1250°C for a few minutes (Allen et al 1959) to clean the surface and then reduce the temperature to the operating temperature before deposition commenced.

The design considerations were:

(i) uniform heating of the whole area of the substrate

(ii) efficiency of heating was important to minimise the area of the heated material other than the substrate and to reduce the chances of the substrate being contaminated during the outgassing process

(iii) a facility to maintain the substrate at ion source potential

(iv) metal contamination should be minimal

Therefore, radiant heat from hot metallic strips, plates, cylinders or filaments was undesirable because of

the direct line of sight between the source of metallic impurity and the substrate.

3.6.4. Methods of heating

The methods of heating attempted were electron bombardment heating and radiation heating.

FIG. 3.10. shows the electron bombardment heater constructed, roughly drawn to scale, which produced uniform substrate heating up to temperatures of 700°C. A uniform temperature of 700°C was reached with the EHT 5kV and the beam current 10mA. The problem of possible metallic contamination from the hot filament, which acted as the source of electrons, was minimised since there was no direct line of sight between the annular filament and the substrate. Attempts to obtain uniform temperatures in excess of 1000°C were unsuccessful because excessive beam divergence caused the formation of an annular focus.

The two methods of radiation heating tried were, firstly, radiation from a tungsten halogen lamp placed near the substrate and, secondly, focusing radiation from outside the vacuum system through a pyrex dome onto the substrate. In fact the second method was adopted in this investigation and is outlined in SECTION 3.6.5.

FIG. 3.11. shows the tungsten halogen lamp and reflector assembly used as a radiation heater. The tungsten halogen lamps used were supplied by G.E.C. and rated at 230V 800 watts. These lamps were chosen because the filament length was about the same value as the substrate diameter (ie. 32 mm.). The reflector assembly developed for use with the lamps was constructed entirely from thin Mo sheet. The temperature distribution in the substrate plane was uniform and temperatures as high as 1200°C have been recorded with the lamp operating at about 700 watts. No water cooling of the ends of the lamp was used and the reflector was observed to glow when the lamp was operated near or at full power. This observation was thought to explain why the life of each lamp was restricted to little more than 1 hr. because the manufacturers state that lifetimes are reduced drastically if the lamp seals exeeed 450°C.

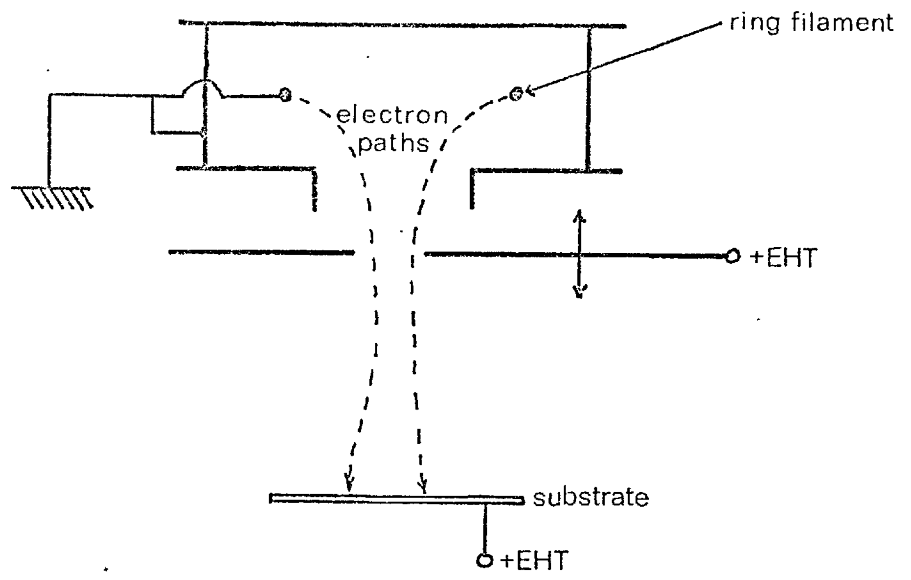

FIG. 3.10. ELECTRON BOMBARDMENT SUBSTRATE HEATER

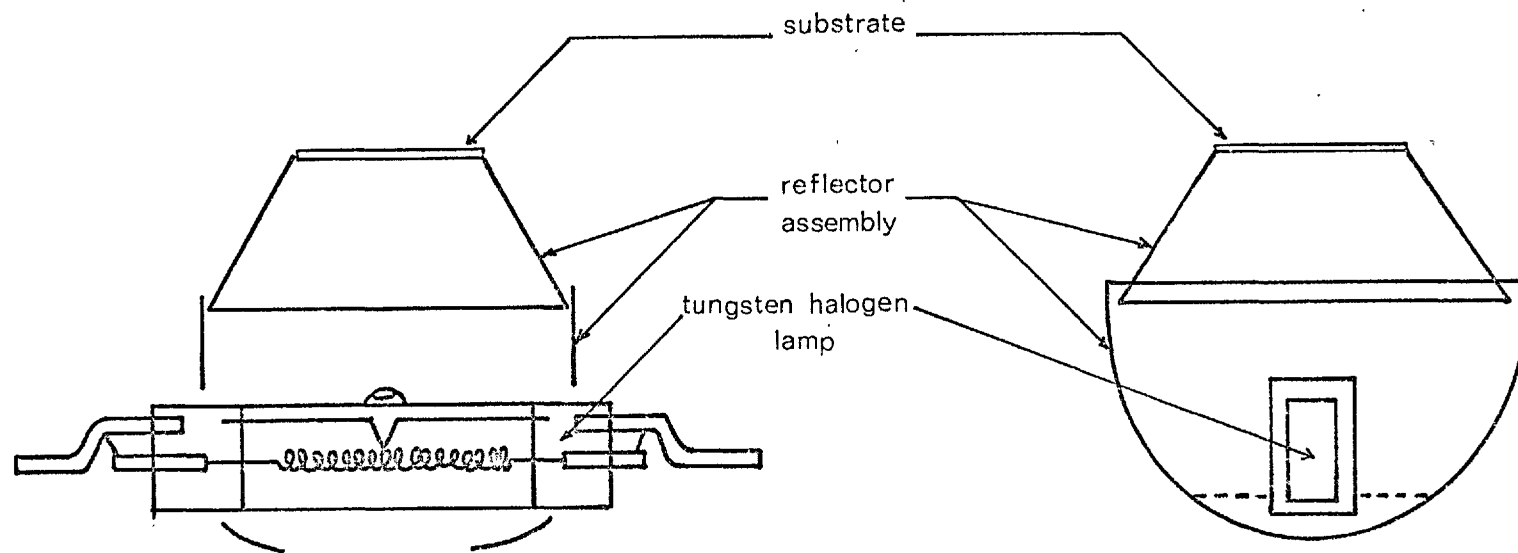

FIG. 3.11. SUBSTRATE HEATING BY RADIATION FROM TUNGSTEN HALOGEN LAMP AND REFLECTOR ASSEMBLY.

3.6.5. <u>The substrate heater used</u>

The radiation heater used for heating the Si substrate from outside the vacuum system is shown in FIG. 3.2. The advantages of a heater operating from outside the vacuum system were:

(i) electrical feedthroughs into the vacuum system were not needed

(ii) outgassing and possible contamination effects from internal heaters were eliminated

(iii) electrical insulation between the heater and the substrate, possibly at ion source potential, was no problem.

An Al elliptical reflector focused radiation from a G.E.C. 240V .1 kwatt projection lamp held at one of the foci of the ellipse onto the Si substrate placed at the other focus. The ellipse was constructed with a long radius of 6.808 in. and a short radius of 4.011 in. so that for focused radiation the seperation of the lamp from the substrate was about 10.8 in. For the set-up shown in FIG. 3.2. all light paths through the pyrex dome were unobstructed and reasonably uniform temperatures were obtained up to about 1100°C. The pyrex dome was prevented from becoming covered with sputtered Si by the stainless steel mask at earth potential, shown in the photograph of FIG. 3.8. just above the substrate holder. This mask also acted as support for the thermocouple insulator. During operation of the substrate heater the pyrex dome was kept cool by compressed air directed onto it.

3.6.6. <u>Measurement of substrate temperatures</u>

The substrate temperature was varied by changing the lamp voltage of the heater with a variac and the temperature measured by a T_1-T_2 thermocouple placed about 2 mm. above the substrate. The thermocouple leads entered the vacuum system through an EHT feedthrough so that when the substrate was at ion source potential the temperature measuring device was disconnected and the thermocouple allowed to "float". Substrate temperatures were then only measured when the slice was at earth potential.

The readings of the thermocouple were calibrated in

terms of the temperature of the side of the substrate onto which deposition was intended. This temperature was measured by a T_1-T_2 thermocouple pressed against the surface of the substrate and by a near-focusing optical pyrometer. When the pyrometer readings were corrected for the emissivity of Si at 0.65µ wavelength using the data of Allen (1957), they virtually coincided with the readings from the thermocouple pressed against the Si surface. The discrepancy in temperature between the substrate and the thermocouple placed just above it was then less than 20°C over the temperature range 700 to 1000°C. The temperature variation across the heated Si substrate was up to 50°C at a temperature of 1000°C; the temperature being higher at the centre of the substrate.

3.7. PROCEDURE FOR A TYPICAL RUN FOR PRODUCING EPITAXIAL SILICON LAYERS

Prior to positioning in their respective holders, the Si target and Si substrate are chemically polished by the standard 3-15-5 (CH_3 COCH- HNO_3 - HF) etch for a period of a few minutes with continuous agitation followed by quenching in deionised water and drying in hot air.

The vacuum system is initially evacuated by liquid nitrogen sorption pumps to a pressure better than 0.05 torr, as indicated by a Pirani gauge attached to the sorption pumps. Sorption pumping is then ceased and the vacuum chamber pumped by the mercury diffusion pump through a liquid nitrogen trap and a water-cooled Peltier baffle. The diffusion pump is continuously backed by a sorption pump through a resevoir so that the backing pressure is about 0.02 torr. When the system pressure is reduced below 5×10^{-6} torr a mild overnight bake is begun. Periodic titanium sublimation keeps the pressure in the 10^{-6} torr range during the bakeout.

During the early part of the bakeout the ion beam source filament is outgassed by flashing it close to the normal operating current of 35A at 6V. Occasionally the entire ion beam source is baked at about 400°C by initially operating the filament at about 1.5V 15A with no circulating cooling water. The temperature of the source is monitored by a T_1-T_2 thermocouple pushed inside one of the cooling water pipes as far as the ionisation chamber cooling jacket. As soon as the ion beam source reaches a temperature of 400°C the filament voltage and current are reduced and adjusted periodically to suppress any further increase in temperature.

When the bakeout is complete and the system has cooled sufficiently, the liquid nitrogen container of the cryo-pump is filled and the pressure in the system reduced to 2×10^{-8} torr with the aid of periodic titanium sublimation. The vacuum system is cooled quickly after the bakeout by tap water flowing through cooling tubes attached to the base and top flange of the vacuum chamber (see FIG. 3.2.)

The substrate is now heated close to 1000°C and the

heater repositioned to give maximum substrate temperature readings. The ion beam source filament is reflashed and the system pressure returns to $5x10^{-8}$ torr after this last outgassing procedure.

Liquid helium is now transferred to the cryopump and within ten minutes the helium container of the pump is full. Continuous transfer of helium is required from now on to accommodate the high gas load on the cryopump when inert gas is eventually leaked into the ion source.

The system now reaches an ultimate pressure of $2x10^{-8}$ torr with the cryopump in operation. A mass scan with the MSIO mass spectrometer shows that the principal residual gas is water vapour (see FIG. 3.12.)

The substrate is now reflashed at 1100°C for two minutes. This is the time required for the SiO (m/e=44) peak on the mass spectrograph to reach a maximum ($1x10^{-7}$ torr) and then start dropping indicating that the oxide layer on the Si surface is being removed. The total pressure peaks at about $2x10^{-7}$ torr and the oxygen partial pressure increases by a factor of two to $6x10^{-9}$ torr during this flashing operation. The substrate is then reduced to its normal run temperature of between 700 and 950°C and the temperature measuring device disconnected. The total pressure in the system is about $3x10^{-8}$ torr.

Argon is now leaked into the ion beam source and the leak rate adjusted to give a pressure in the vacuum chamber of about $7x10^{-4}$ torr (ARGON). Ion beam source cooling is now commenced with circulating deionised water. The ion beam source filament is turned on, an ionisation potential of 20V applied and an ionisation chamber current of 5A established. An A^+ ion beam emerges from the ion beam source when positive EHT is applied to the source. The substrate is usually maintained at the same potential as the ion beam source by a common connection. A typical extraction voltage is 9kV which gives about a 4mA A^+ ion beam. The corresponding target current is about 5mA. The target is now cleaned by bombarding it with the ion beam with the shutter closed.

FIG. 3.13. shows an MSIO mass scan when a Si target was being cleaned in a vacuum of $1x10^{-4}$ torr (ARGON)

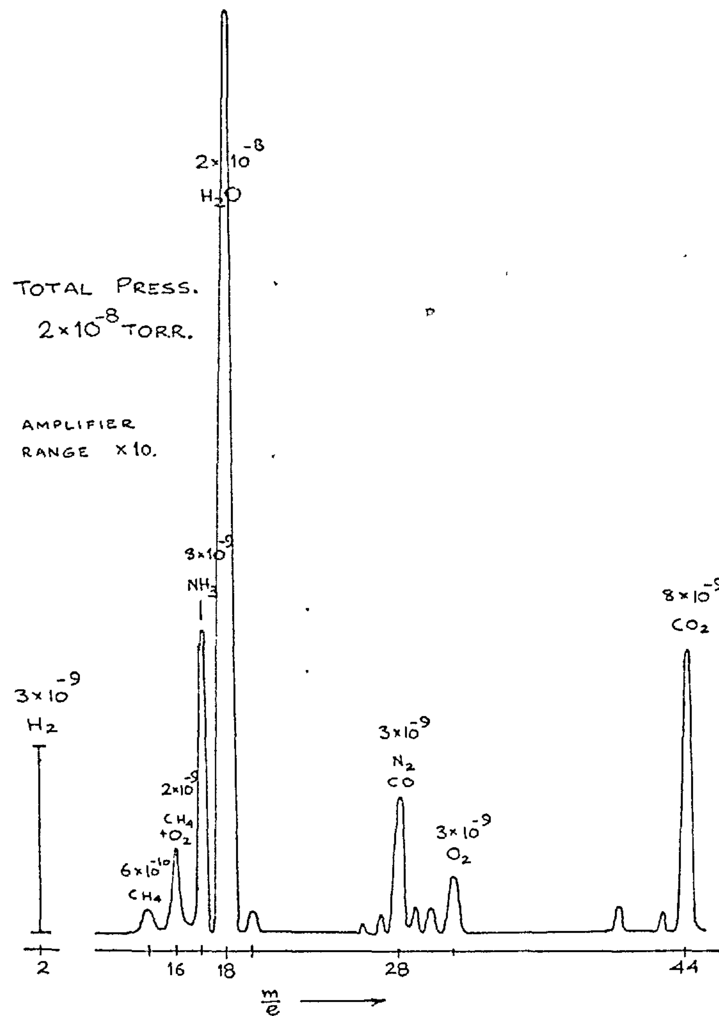

FIG. 3.12 ANALYSIS OF PARTIAL PRESSURES IN THE SYSTEM; Before operation of ion beam source.

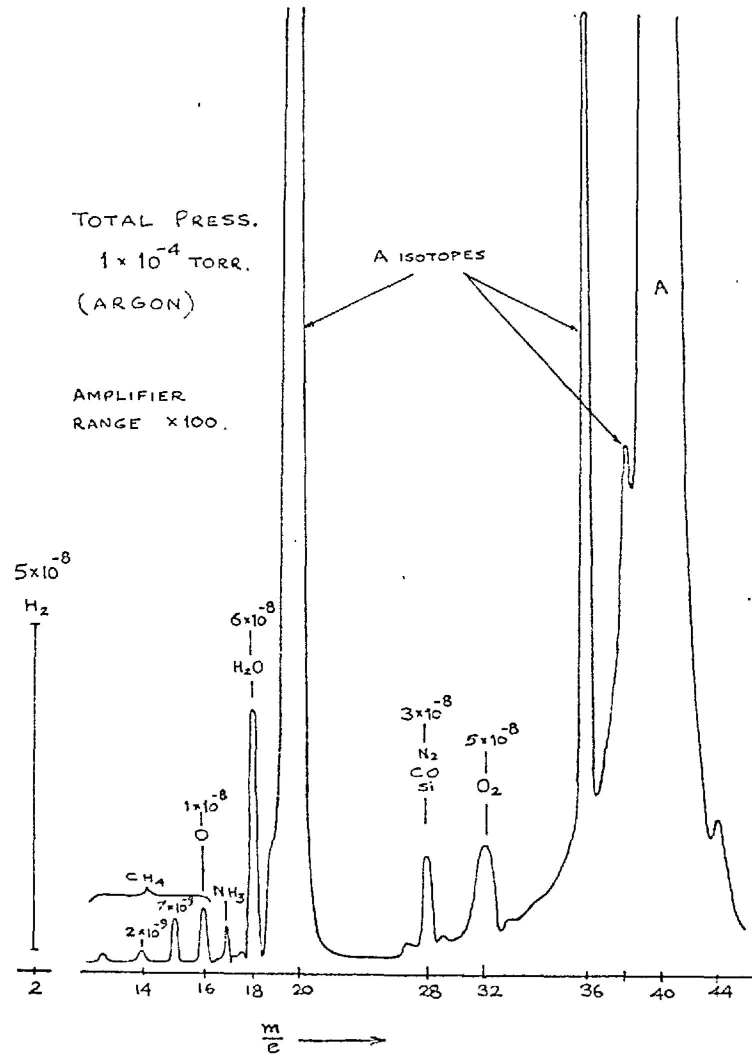

FIG. 3.13 ANALYSIS OF PARTIAL PRESSURES IN THE SYSTE
During operation of ion beam source.

by a 1.0mA 9kV argon ion beam. Individual values of partial pressure have not been corrected for the drop in sensitivity of the MSIO at high pressures. A pressure of 1×10^{-4} torr is about the maximum safe working pressure of the MSIO. Comparison of FIG. 3.13. with FIG. 3.12. shows that the partial pressures of all the background gases have increased. Any increase in the CO_2 and SiO (44) level is undetected because the peak is swamped by the main argon (40) peak. The partial pressure of oxygen is estimated to be 5×10^{-7} torr when the total chamber pressure is 7×10^{-4} torr (ARGON).

After the target has been cleaned for at least ten minutes with a 4mA beam, the shutter is opened and deposition of sputtered Si atoms onto the heated substrate commences. The extraction current now increases to almost the value of the target current (5mA) because the majority of electrons emitted from the target are attracted to the substrate.

The shutter is closed after about 60 minutes bringing the deposition to an end. Within a few minutes of closing the leak valves the pressure in the chamber recovers to 1×10^{-7} torr. After 5 minutes the heating of the substrate is ceased and a few minutes later the helium transfer is stopped. When the cryopump has recovered, the vacuum chamber is isolated and the substrate with a deposited Si layer removed.

The thickness of the layer is determined using the Talysurf and the layer is studied by transmission in an A.E.I. EM6G electron microscope operating at 100kV, and also by reflection in an A.E.I. electron diffraction camera type EDC2 operating at 100kV. Layer resistivity measurements are made and junction characteristics are also investigated.

3.8. ASSESSMENT OF QUALITY OF SILICON LAYERS

3.8.1. Structural assessment by transmission electron diffraction (TED) and microscopy (TEM)

3.8.1.1. Preparation of specimens for the electron microscope

Si samples need to be less than 1 micron thick and preferably 3 mm. in diameter before they are suitable for examination in an A.E.I. EM6G electron microscope. The method used for thinning specimens from the Si substrate initially 250 microns thick was similar to that developed by Booker and Stickler (1962) and is shown in FIG. 3.14. As the sputtered Si layer was to be examined, the specimen was jet etched from the substrate side only.

Before thinning commenced, several 3 mm. discs were ultrasonically cut from the substrate using a stainless steel tube cutter and mounted on glass microscope slides. Each disc was fixed to a glass slide by pushing it layer-side-down into a globule of acetone collodion on the glass surface. Etch solution was prevented from creeping around the edge of the 3 mm. disc and attacking the layer by lacomit solution painted around the edge of the disc.

Jet thinning of the disc was then begun and continued until a small hole appeared, usually after a period of 15 minutes, when the specimen was quickly removed from the thinner and immediately rinsed in deionised water. The thinned disc of Si, now ready for examination in the electron microscope, was removed from the glass slide by carefully peeling off the lacomit around the edge of the disc. The profile of the disc after thinning was as shown in FIG. 3.15.

The progress of the thinning during the last few minutes was observed through the optical microscope placed above the thinner. When a small dark red spot appeared in the centre of the disc the thickness left was only about 1 micron. As the polishing was continued the spot changed to light red, orange and pale yellow and then the small hole appeared. The time interval between the orange and hole stages was only a few seconds so rapid removal of specimen

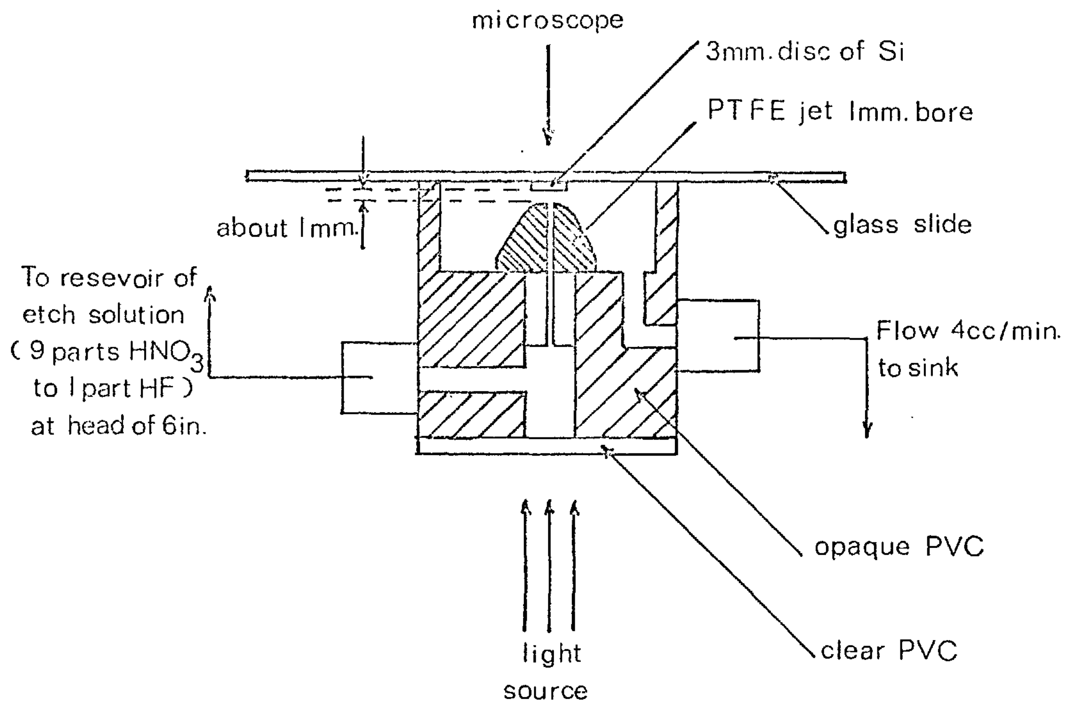

FIG. 3.14. METHOD OF THINNING SILICON

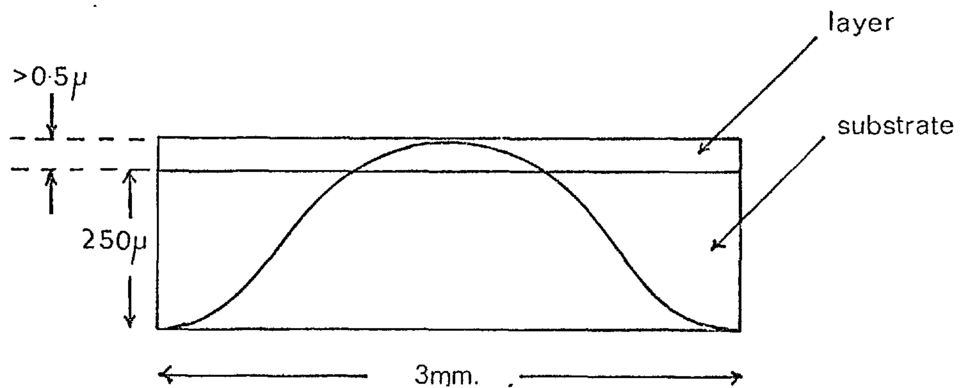

FIG. 3.15. PROFILE OF 3 mm. DISC AFTER THINNING.

for rinsing was required. The pale yellow regions around the hole were ideal for examination by the electron microscope because they were only about 0.2 micron thick. The layers examined were always initially thicker than 0.5 micron to ensure that the material of the layer and not the substrate was being examined.

3.8.1.2. Electron microscopy of Si layers

In most cases thinned 3 mm. discs of Si were examined in the A.E.I. EM6G electron microscope operating at 100kV with the layer side uppermost in the microscope. The orientation relationship between the layer and (111) Si substrate was determined directly from diffraction patterns. In diffraction paterns where individual matrix spots were surrounded by "satellite" spots or where "streaking" between matrix spots occurred, the special technique of dark field microscopy was used to establish conclusively the origin of a particular spot or streak.

For the analysis of defects in epitaxial Si layers, a specimen-tilting goniometer stage was used in the microscope so that individual defects could be tilted in and out of contrast. Using the method outlined by Hirsch et al (1965), the displacement vectors ($\bar{R}$) of stacking faults and the Burger's vectors ($\bar{b}$) of dislocations could be determined. The criterion for invisibility of a stacking fault is $\bar{g}.\bar{R} = 0, \pm 1, \pm 2$ etc. A dislocation is invisible when $\bar{g}.\bar{b} = 0$. In both cases $\bar{g}$ is the diffraction vector.

3.8.2. Structural assessment by reflection high-energy electron diffraction (RHEED)

The surfaces of some of the layers were examined by glancing-angle RHEED using an A.E.I. electron diffraction camera type EDC2 operating at 100kV. The advantages of glancing-angle RHEED were that no elaborate preparation procedure was needed before layers could be examined and whole substrates could beaccommadated in the specimen stage if required. The disadvantage of glancing-angle RHEED was that only the top few atomic layers of the layer were probed by the electron beam so that an assessment of the structural quality of the layer surface, and not the layer bulk, could only be made. Finally, the only surface defects in epitaxial layers which the technique could

identify were twins, if they were present.

3.8.3. Electrical measurements

Attempts were made at depositing either N-type epitaxial layers on 25 ohm-cm P-type substrates or P-type epitaxial layers on 0.01 ohm-cm N-type substrates. It was hoped that the conductivity-type and resistivity of the target would be reproduced in the layer each time. The original resistivity of the target was either 0.01 ohm-cm N-type or 25 ohm-cm P-type.

The resistivity of sputtered epitaxial layers was checked using the 2-point probe method (Mazur and Dickey 1966) which was particularly suitable for thin layers about 1μ thick. The error in each individual measurement was about 15%.

Junction characteristics were displayed on a Solartron C.R.O. using an Elliot curve tracer after suitable "mesas" about 1 mm. diameter had been produced. Contact was made to the mesa with a probe pressing on the layer surface.

3.9. Si AND GaAs SPUTTERING EXPERIMENTS

3.9.1. Measurement of sputtering yield

Apparent sputtering yield values were determined for Si and GaAs from the weight loss of the target and integrated target current measurements (see SECTION 2.1.3.)

A Unimatic CL41 balance was used to measure the weight of the target before and after bombardment. The accuracy of each measurement was ± 0.1 mgms. The average target current during a typical 60 minute bombardment was computed from at least ten readings of target current taken at equal time intervals. Usually the largest deviation in target current values was ± 0.2mA.

For Si, apparent sputtering yield

$$S^* = \frac{56.3dM}{It} \text{ atoms/ion}$$

and for GaAs, apparent sputtering yield

$$S^* = \frac{21.8dM}{It} \text{ atoms/ion,}$$

where dM = weight loss of the target in mgms. (accuracy ± 0.2 mgms.),

I = target current in mA (typical accuracy ± 0.2mA),

and t = bombardment time in minutes, usually 60 minutes.

The overall accuracy in each apparent sputtering yield value was then about 7%.

3.9.2. Topography of target surfaces after bombardment

The macrotopography of bombarded Si targets was determined using the Talysurf and the microtopography investigated using a Cambridge Instruments "Stereoscan" scanning electron microscope (SEM) type 96113 Mk. 2A.

3.9.3. The angular distribution of sputtered atoms

The angular distribution of sputtered atoms ejected from Si and GaAs targets was investigated by depositing the sputtered material onto a number of closely-spaced microscope slides in a plane $2\frac{3}{8}$ in. above the target. A Siemens microdensitometer was then used to scan the deposited layer and determine density and hence thickness variations. Ejection maxima, and in some cases ejection minima, were pin-pointed to an accuracy of ± 1°. Absolute

measurements of thickness were determined to an accuracy of 10% using the Talysurf. From this data it was possible to show in polar and contour map form the variation of deposition rate over the deposited layer. The values of deposition rate were not corrected for the slightly non-linear dependence of thickness on density.

3.9.4. Chemical composition of sputtered deposits from GaAs targets

Several samples about $1cm^2$ were cut from the glass slides used for determining ejection directions and chemically analysed using an electron probe analyser. Each sample was compared directly with a GaAs standard to ensure that the resultant atomic percentage measured was independent of sample layer thickness. The accuracy of the measurement was0.4 atomic percentage for either Ga or As.

3.9.5. Procedure for a typical run when determing the sputtering properties of Si and GaAs

A target of Si or GaAs, previously chemically polished, rinsed, dried and weighed, is mounted in its appropriate holder and 4 glass microscope slides are positioned in a plane $2\frac{3}{8}$ in. above it. The standard 3-15-5 (CH_3COOH-HNO_3-HF) etch is used for chemically polishing Si targets whereas a mixture of ½% bromine methanol to 99½% water is used for GaAs targets. The experimental run is now identical to that described in SECTION 3.7. for epitaxial Si layers minus the parts concerned with Si substrates.

At the end of the experimental run, normally restricted to 60 minutes, the target is removed and re-weighed. The apparent sputtering yield is then determined from the average value of target current recorded during the run, the run time and the weight loss of the target due to ion bombardment. The surface topography of Si targets after bombardment is investigated, firstly, by the Talysurf and, secondly, by examination in the scanning electron microscope.

Before the glass slides are removed from the vacuum system their position relative to the target is accurately

measured. Thickness and deposition rate variations across the glass slides are determined using the Talysurf and microdensitometer. GaAs deposits are also investigated for stoichiometry.

CHAPTER 4

EXPERIMENTAL RESULTS AND DISCUSSION OF RESULTS

4.1. ANALYSIS OF HOMO-EPITAXIAL SPUTTERED SILICON LAYERS

4.1.1. Conditions of growth

About 40 Si layers of measured thickness between 0.9 and 1.5μ were grown at deposition rates between 150 and 250 Å/min (corresponding A^+ ion beam currents were 3 and 5mA respectively) in the temperature range 650 to 950°C. Individual measured values of thickness were up to 33% below maximum values (see SECTION 4.3.3.). Layers were grown with the substrate maintained at either ion source or earth potential. FIG. 3.1. shows the arrangement for the growth of epitaxial layers with the substrate at ion source potential. In this case, secondary positive ions originating at the target were repelled by the substrate whereas all secondary negative ions and electrons were attracted. In the second case, where the substrate was at earth potential (+3kV relative to the target), the growing layer was bombarded with those secondary positive ions with energy greater than 3keV together with secondary negative ions and electrons. The rate of substrate ion dose has been estimated for both substrate biasing conditions when the ion beam current to the target was 4mA or $2\frac{1}{2}\times10^{16}$ ions sec^{-1} (see APPENDIX 2). In the first case, with substrates at ion source potential, the rate of ion dose was estimated to be less than $2\frac{1}{2}\times10^{12}$ ions sec^{-1}, and in the second case, with substrates at earth potential, it was estimated to be about 10^{15} ions sec^{-1}.

4.1.2. Analysis of diffraction patterns

TED patterns of selected areas were used to identify the orientation of epitaxial layers and determine the epitaxial temperature. A typical series of diffraction patterns for both substrate biasing conditions at different substrate temperatures is shown in FIG. 4.1. and FIG. 4.2. together with corresponding RHEED patterns, which only gave information of the orientation of the top few atomic layers of the layer.

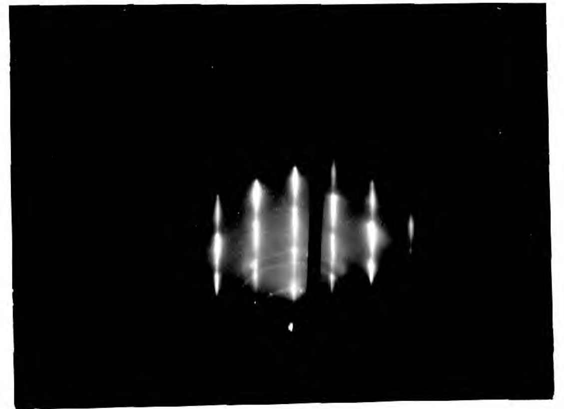

(111) pattern Single crystal layer grown at 840°C (110) pattern

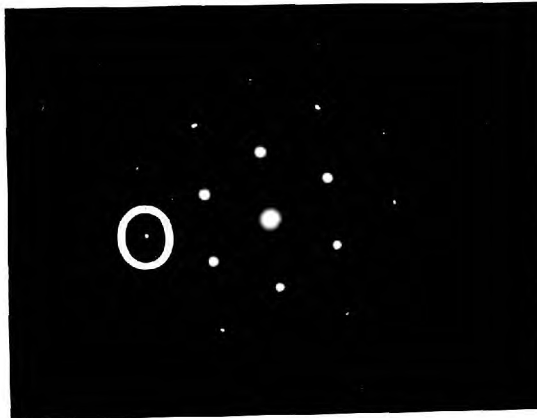

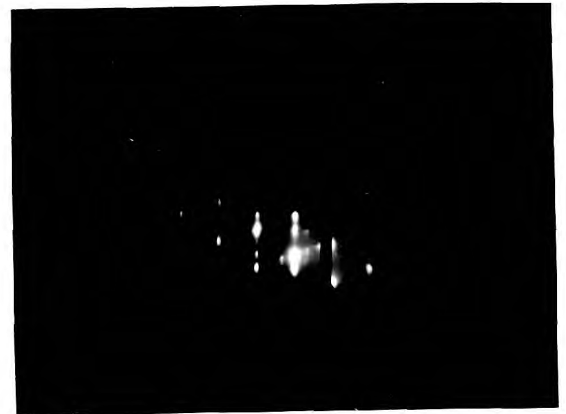

(111) pattern (110) pattern

Single crystal layer grown at 730°C whose TEDP shows split and streaked spots (an example is circled)

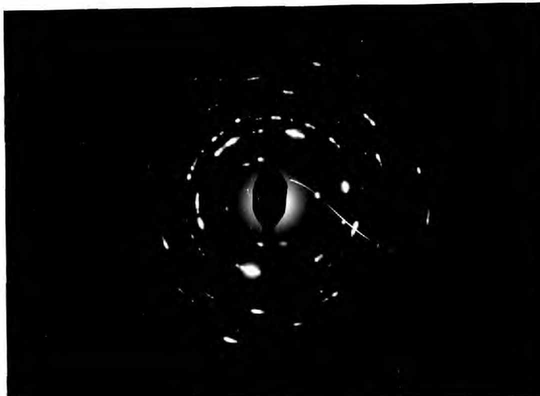

Polycrystalline layer grown at 700°C

TRANSMISSION ELECTRON DIFFRACTION PATTERNS

REFLECTION HIGH-ENERGY ELECTRON DIFFRACTION PATTERNS

FIG. 4.1. DIFFRACTION PATTERNS OF SPUTTERED Si LAYERS GROWN WITH SUBSTRATES AT ION SOURCE POTENTIAL

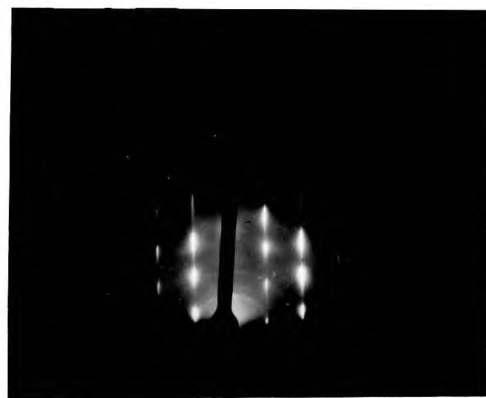

(111) pattern (110) pattern

Single crystal layer grown at 920°C

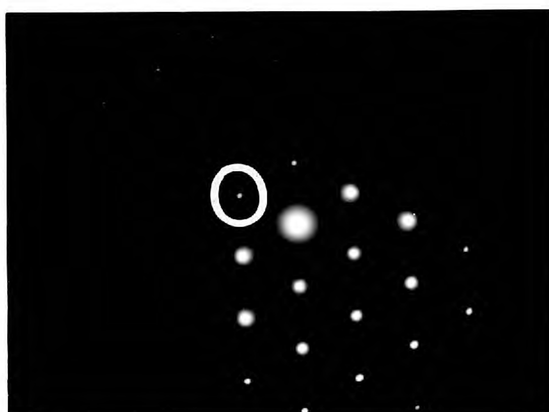

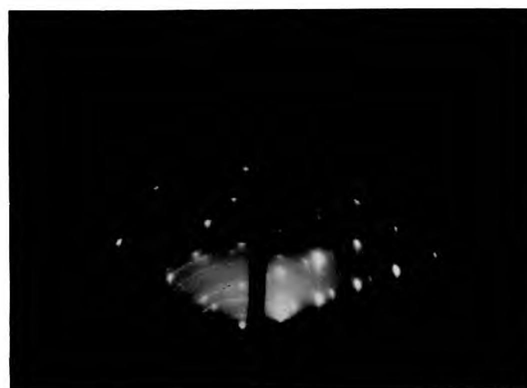

(111) pattern (110) pattern

Single crystal layer grown at 860°C whose TEDP shows split and streaked spots (an example is circled)

Polycrystalline layer grown at 650°C

TRANSMISSION ELECTRON DIFFRACTION PATTERNS

REFLECTION HIGH-ENERGY ELECTRON DIFFRACTION PATTERNS

FIG. 4.2. DIFFRACTION PATTERNS OF SPUTTERED Si LAYERS GROWN WITH SUBSTRATES AT EARTH POTENTIAL

4.1.2.1. TED patterns and the epitaxial temperature

The epitaxial temperature for layers grown at ion source potential was between 700 and 730°C. No layers were grown at earth potential close to the epitaxial temperature and so an accurate value for the epitaxial temperature for this biasing condition could not be reported. However, it lay somewhere between 650 and 850°C. All epitaxial layers reproduced the (111) orientation of the substrate. A feature of diffraction patterns for epitaxial layers grown at temperatures less than 800°C for substrates at ion source potential, and less than 900°C for substrates at earth potential, was that matrix spots were split and streaked along $\langle 11\bar{2} \rangle$ directions. This phenomenon was not consistent with conventional twinning on $\{111\}$ planes which would have given the (111) diffraction pattern with satellite spots shown in FIG. 4.3. Mazey et al (1968), Large and Bicknell (1967), and Irving (1969) similarly observed split matrix spots in diffraction patterns from annealed ion-bombarded Si and interpreted their presence as being due to defects lying parallel to the electron beam. In this work, defects producing split matrix spots were believed to be microtwins which disappeared at a particular temperature depending on the ion bombardment conditions of the substrate during deposition (see SECTIONS 4.1.3.1. and 4.1.3.2.).

4.1.2.2. RHEED patterns

RHEED patterns of epitaxial layers, shown in FIGS. 4.1. and 4.2., were considerably different from the corresponding TED patterns. (110) RHEED patterns of (111) epitaxial layers showed, firstly, matrix spots surrounded by prominent satellite spots and, secondly, rings running through matrix and satellite spots.

The satellite spots were in positions expected for twinning on $\{111\}$ planes; a complete (110) diffraction pattern with all expected satellite spots due to twinning on $\{111\}$ planes is shown in FIG. 4.3. However, there was a possibility that these extra spots were not genuinely representative of a twinned surface-structure. Multiple reflection and diffraction of the electron beam at

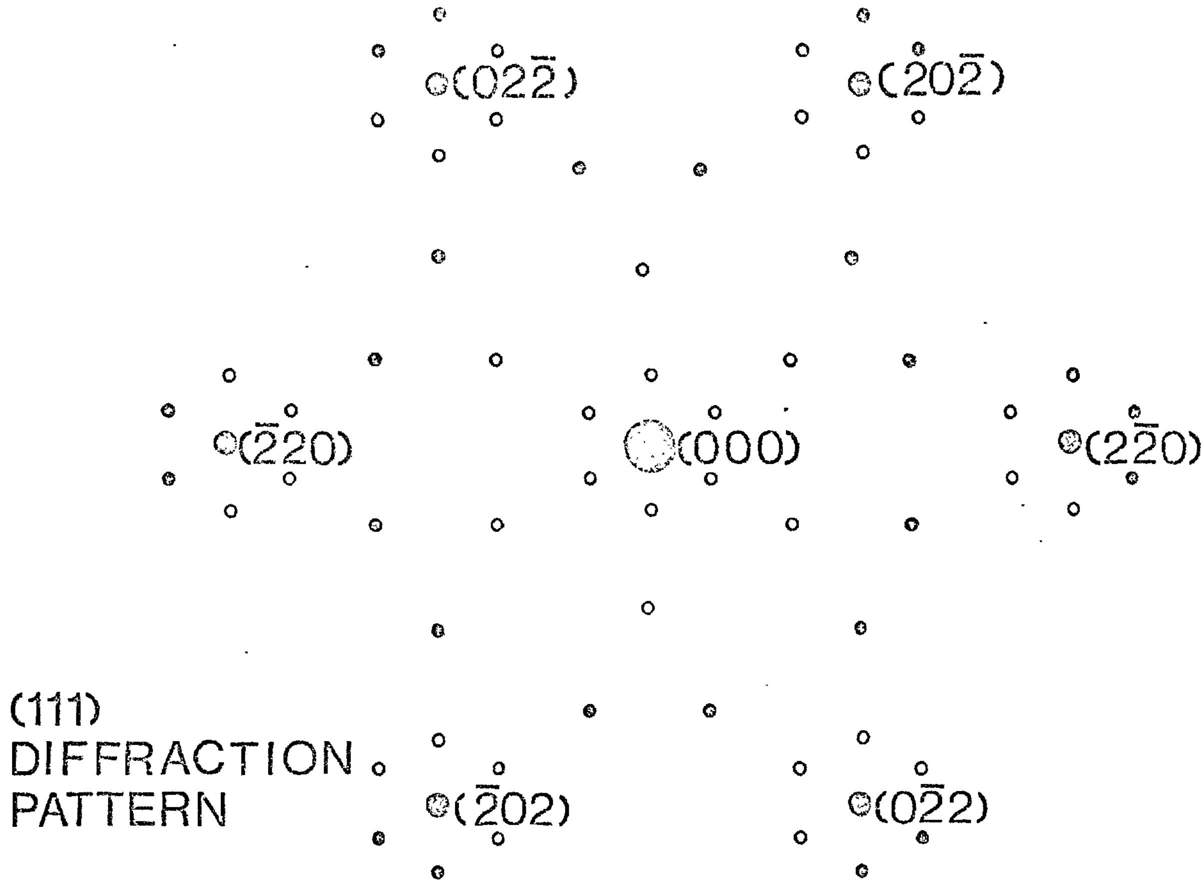

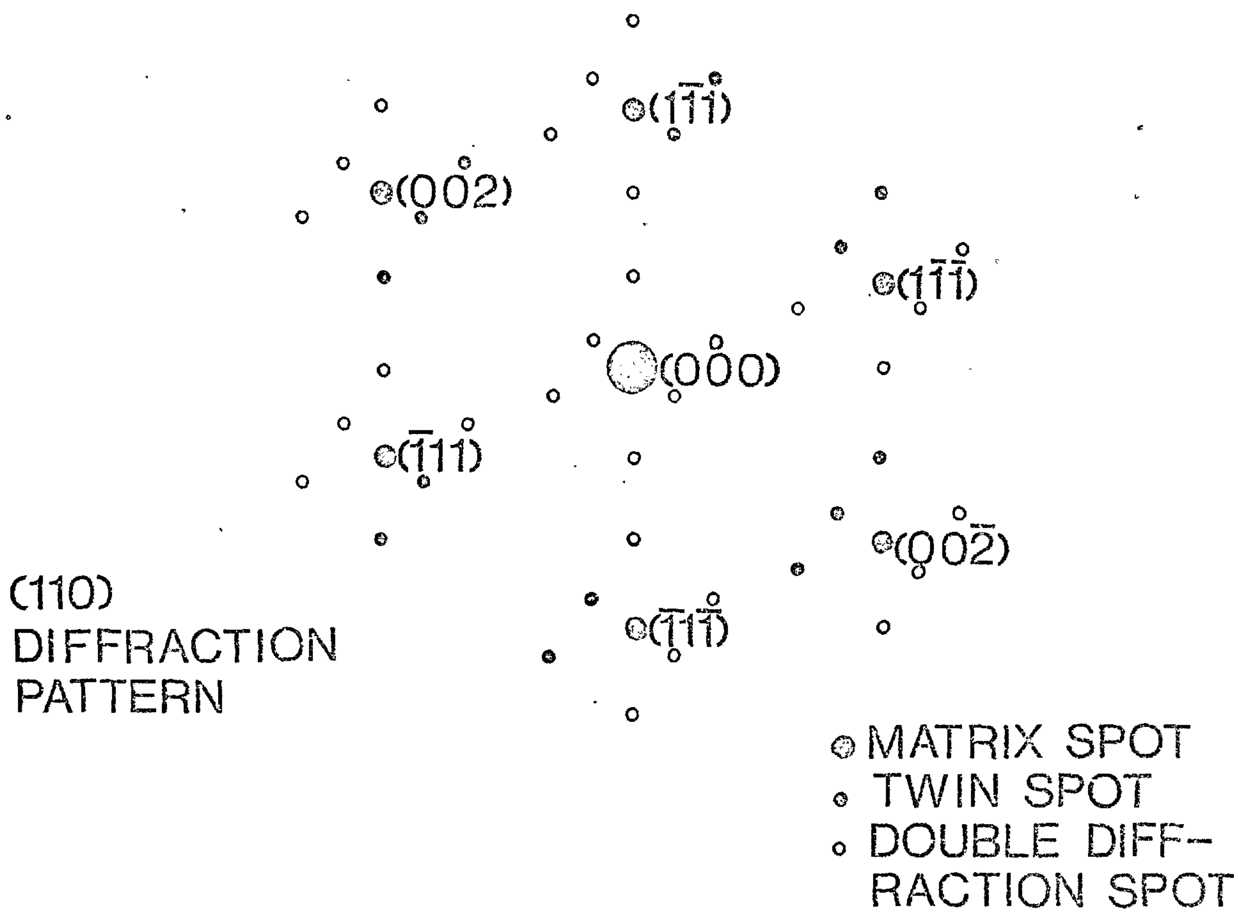

FIG. 4.3. DIFFRACTION PATTERNS WITH TWINNING ON {111} PLANES.

misoriented surface protrusions might have produced the same effect. The degree to which "surface-roughness" contributed to the formation of satellite spots could not be determined precisely because the same value of glancing angle was not reproduced for each diffraction pattern.

On the other hand, the presence of rings in RHEED patterns coincident with matrix and satellite spots indicated the presence of polycrystalline Si at the surface of the epitaxial layer. The top few atomic layers of the epitaxial layer was therefore different from the bulk.

4.1.2.3. TED patterns of very thin regions and an estimate of the thickness of surface disorder

TED patterns of very thin regions at the edges of the hole in jet-thinned epitaxial layers exhibited diffuse haloes concentric with the central spot. A typical example is shown in FIG. 4.4.a. and the distinct halo , which almost coincided with the $\{2\bar{4}2\}$ Si single crystal matrix spots, was almost certainly indicative of polycrystalline or amorphous Si on the surface of the epitaxial layer and not contamination as a result of the electron microscope examination. The formation of haloes by contamination could be discounted because none of the Si-hydrocarbon combinations would have given a halo which was as close to the $\{2\bar{4}2\}$ Si single crystal matrix spots as the halo shown in FIG. 4.4.a. If the halo did not result from contamination then the only other cause of its origin was disordered Si at the surface. This appeared to be the case because the non-coincidence of high-order haloes and spots due to disordered and crystalline Si respectively has been explained by rotation of the atomic bonds (Large and Bicknell 1967). The existence of a disordered structure of Si occurring at the surface of epitaxial layers was also established by RHEED patterns (SECTION 4.1.2.2.).

An estimate of the thickness of surface disorder in epitaxial layers has been made by assuming that if the thickness of the disorder was at least one tenth of the total thickness studied in transmission then a diffraction halo would show up on the basis of relative intensities.

(a) Diffraction from edges of hole

(b) Diffraction from region of thickness about 2000 Å

FIG. 4.4. TRANSMISSION ELECTRON DIFFRACTION FROM VERY THIN REGIONS OF EPITAXIAL LAYER

The absence of haloes in diffraction patterns of regions about 2000 Å thick (FIG. 4.4.b.) indicated therefore, that the disordered surface was less than 200 Å thick and probably only about 100 Å thick.

In some cases, thinned 3 mm. disc specimens were inverted in the electron microscope so that the electron beam was first transmitted through the ordered crystal before the top surface of the epitaxial layer. If a disordered surface region was present, strong single crystal reflections would now act as the sources for inelastic scattering in the disordered region giving diffraction patterns with haloes concentric around matrix spots other than the central spot. This double diffraction effect has been observed in Ge by Parsons (1965) when the depth of surface disorder was about 600 Å but could not be reproduced here because the disordered surface region was too thin.

4.1.3. Defects in epitaxial layers

4.1.3.1. Substrates at ion source potential

A series of typical transmission electron micrographs and diffraction patterns corresponding to epitaxial layers grown at different temperatures on substrates at ion source potential is shown in FIG. 4.5. The defects depicted in the micrograph of the layer grown at 940°C (FIG. 4.5.(i)) exhibited contrast effects associated with dislocations. The number of dislocation defects was estimated to be about $8x10^{9}$ cm^{-2}. At a lower temperature (840°C) and for a more intense ion beam, the resulting micrograph showed smaller but more numerous dislocations (FIG. 4.5.(ii)). The density of dislocations in this case was $2x10^{10}$ cm^{-2}. At the same temperature (840°C) but for a further increase in the ion beam current, the micrograph showed a dense dislocation network accompanied by fringe contrast characteristic of stacking faults in $\langle 1\bar{1}0 \rangle$ directions (FIG. 4.5.(iii)). In conclusion, defects were less numerous, and larger in the case of dislocations, for higher substrate temperatures during growth and small bombarding ion currents. A smaller ion beam current to the target meant a proportionally smaller rate of ion dose to the substrate.

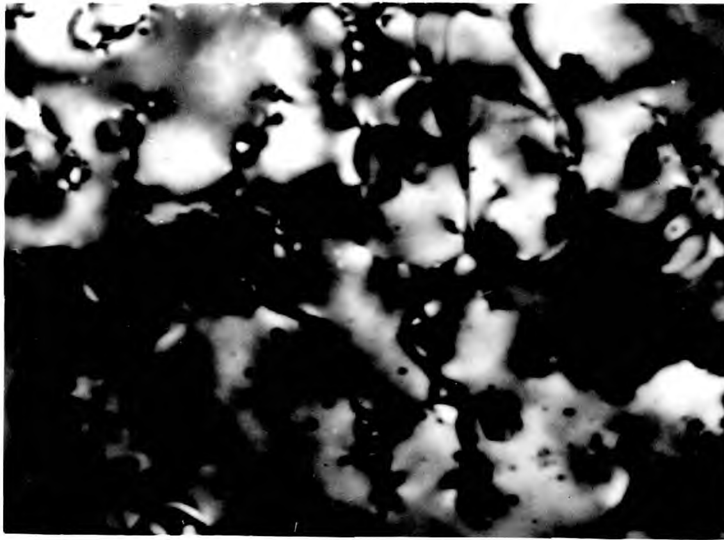
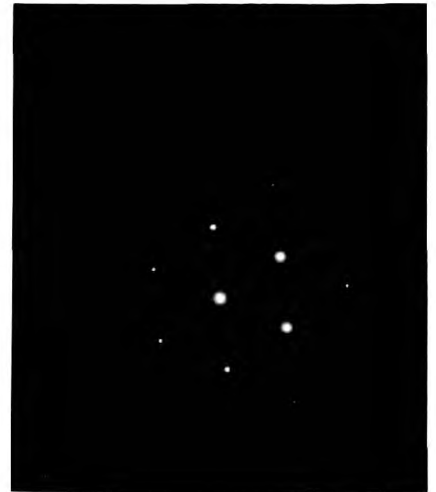

⊢ 0·1μ ⊣

(i) Ion beam 6keV 2.5mA, temperature about 940°C

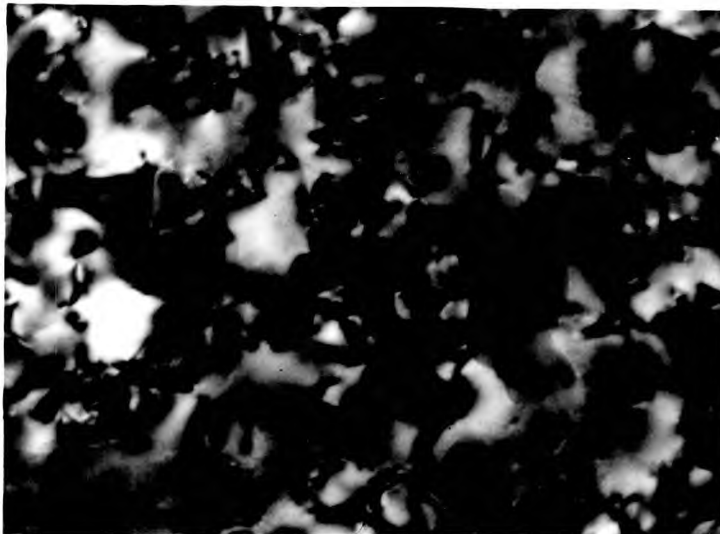

⊢ 0·1μ ⊣

(ii) Ion beam 12keV 4.5mA, temperature about 840°C

FIG. 4.5. TRANSMISSION ELECTRON MICROGRAPHS AND DIFFRACTION PATTERNS FOR LAYERS GROWN WITH SUBSTRATES AT ION SOURCE POTENTIAL

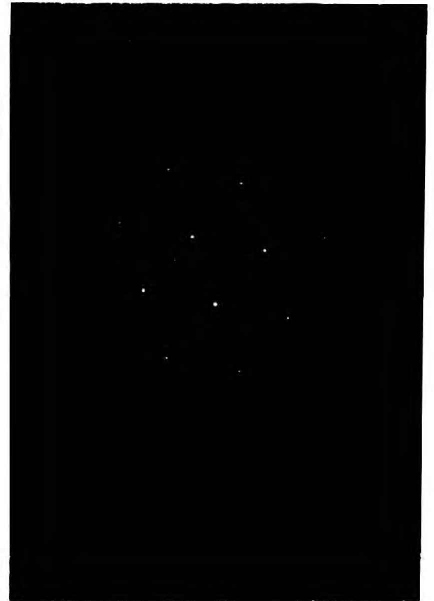

(iii) Ion beam 10keV 5.8mA, temperature about 840°C

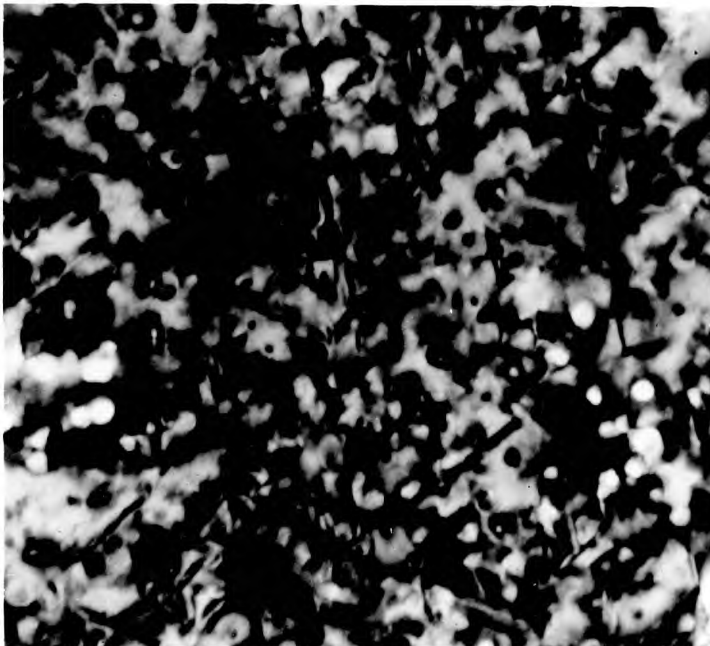

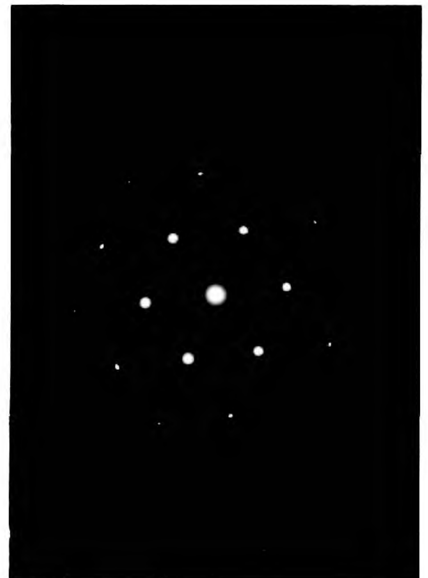

(iv) Ion beam 12keV 4.5mA, temperature about 730°C

FIG. 4.5. (contd.) TRANSMISSION ELECTRON MICROGRAPHS AND DIFFRACTION PATTERNS FOR LAYERS GROWN WITH SUBSTRATES AT ION SOURCE POTENTIAL

Below 800°C, the diffraction patterns of epitaxial layers, exhibited matrix spots which were split and streaked, the origin of which could not be determined precisely with dark field microscopy owing to the low intensity of these streaks. However, the appearance of split and streaked matrix spots appeared to coincide with the introduction of long thin lamellar regions lying along $\langle 1\bar{1}0 \rangle$ directions believed to be microtwins. A typical micrograph showing microtwins and small loop-type dislocations is presented in FIG. 4.5.(iv).

There would appear to be some correlation between the type of defects observed here to those observed in ion bombarded and annealed Si specimens. The defects also showed similar temperature behaviour patterns. In cases where the anneal temperature was not sufficient or when (111) specimens were chosen, microtwinning occurred (Mazey et al 1968, and Large and Bicknell 1967). Increasing the anneal temperature resulted in small dislocation loops which coalesced and grew (Mazey et al 1968, and Large and Bicknell 1967) and finally disappeared at 1000°C (Dearnaley et al 1969). Stacking faults could also result sometimes in ion bombarded and annealed Si specimens (Irving 1969).

4.1.3.2. Substrates at earth potential

Similar defects were observed in layers grown on substrates at earth potential to those in layers grown at ion source potential. However, in this case a particular defect persisted at higher substrate temperatures. Microtwinning (FIG. 4.6.(ii)) did not disappear until about 900°C and in a layer grown at 920°C the visible defects were stacking faults to a density of about $5\text{x}10^{7}$ cm^{-2} and dislocations mainly loop-type. Two overlapping stacking faults and a typical dislocation array are shown in the micrograph in FIG. 4.6.(i). At about the same substrate temperature, no stacking faults were observed in layers grown at ion source potential and this observation, together with the fact that microtwinning persisted to a higher substrate temperature in layers grown at earth potential, could possibly be attributed to the increase in rate of ion

(i) Ion beam 12keV 5.5mA, temperature about 920°C

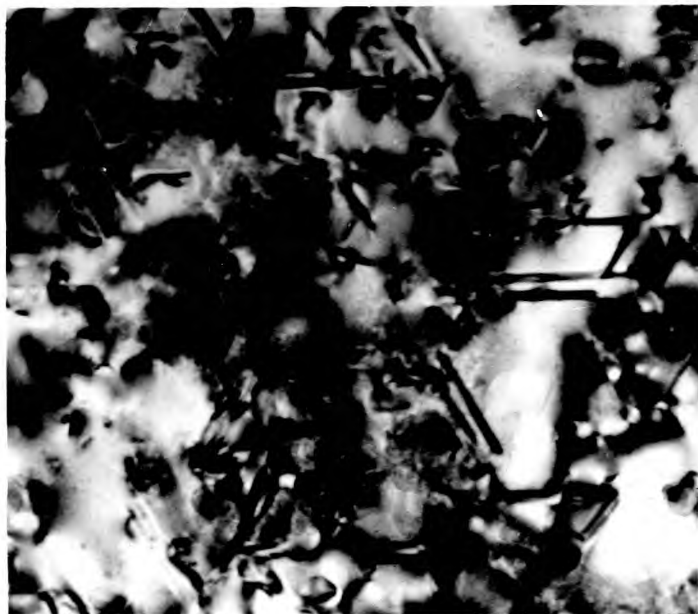

(ii) Ion beam 12keV 4.6mA, temperature about 860°C

FIG. 4.6. TRANSMISSION ELECTRON MICROGRAPHS AND DIFFRACTION PATTERNS FOR LAYERS GROWN WITH SUBSTRATES AT EARTH POTENTIAL

dose to the substrate during deposition (see SECTION 4.1.1.) Recently, Censlive (1971) has shown that a very marked increase in the number of stacking faults in evaporated epitaxial layers of Si could result if the growing layer was bombarded with energetic ions.

4.1.3.3. Substrates at earth potential with no shutter between the target and substrate

The effect of not using a shutter between the target and substrate was to result initially in a large number of impurity atoms and ions reaching the substrate at the beginning of the deposition. Epitaxial layers grown in this manner were usually more heavily faulted than if a shutter had been used and the target subjected to the usual 10 minutes clean before the shutter was opened and deposition could commence. Two typical micrographs for an epitaxial layer grown at 990°C illustrating the types of faults encountered in epitaxial layers grown at earth potential with no shutter are shown in FIG. 4.7. The faults observed are (a) stacking faults to a density of about $2x10^8$ cm^{-2}, (b) dislocation loops of three types; "elliptical", "parallel" and "circular" (according to Bicknell 1971 the "elliptical" and "circular" loops are both faulted types of loops, and the "parallel" loops are un-faulted prismatic loops), and (c) tetrahedra of various sizes which showed the same contrast effect and orientation of stacking faults. Stacking faults were probably more numerous for this layer grown with no shutter between the target and substrate because initially a larger number of impurity atoms and ions was incident at the substrate surface. Dislocation loops of different types can result in an ion bombarded and annealed Si specimen due to vacancies and interstituals (Mazey et al 1968, Large and Bicknell 1967). They can also result in a crystal subjected to a concentration level of impurity atoms higher than the solid solubility level of the lattice due to the strain occurring around precipitates (Ashby and Brown 1963). No detailed analysis was undertaken to distinguish the origin of the different types of dislocation loop depicted in the micrographs in FIG. 4.7. but it would not be unreasonable

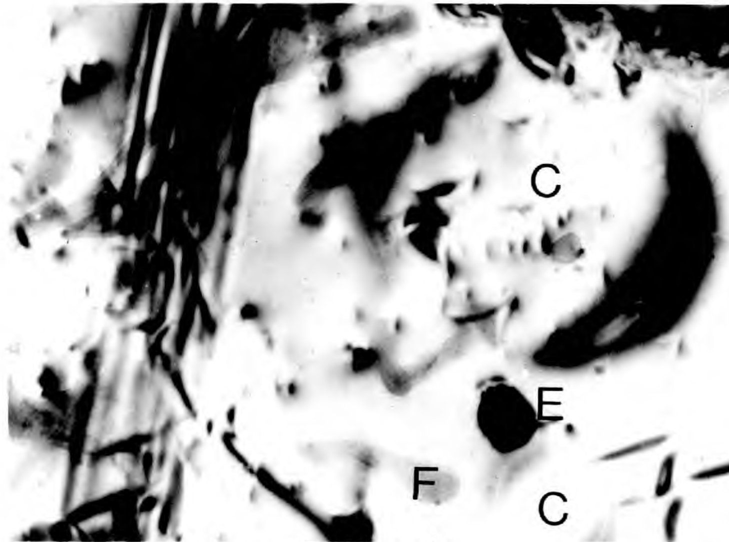

FIG. 4.7. TRANSMISSION ELECTRON MICROGRAPHS OF LAYER DEPOSITED AT 990°C ONTO SUBSTRATE AT EARTH POTENTIAL WITH NO SHUTTER BETWEEN TARGET AND SUBSTRATE (ION BEAM 12keV 4.4mA)

(i) shows:

(a) stacking faults bounded by dislocations,

(b) dislocation loops of 3 types; "elliptical" faulted loops eg. A, "parallel" prismatic loops eg. B, and "circular" faulted loops eg. C (better examples of C are shown in (ii),

(c) stacking-fault tetrahedra of various sizes eg. D

Black blobs (eg. E) and stains (eg. F) represented impurities introduced by a change in the jet-thinning procedure. For this case 3mm discs were mounted in vacuum grease during thinning which was not completely removed before examination.

to suppose that vacancies, interstituals and foreign atoms could all be present as inclusions here because this layer was subjected to a high rate of ion dose and impurity level during the initial stages of growth. The stacking-fault tetrahedra of varying sizes showing stacking fault contrast could possibly also represent regions containing large numbers of vacancies, interstituals and impurity atoms. Clearly, without the shutter a more heavily-faulted layer resulted because under similar biasing and growth temperature conditions, an epitaxial layer grown with a shutter between the target and substrate was free from dislocation loops and stacking-fault tetrahedra and contained a much smaller number of stacking faults and only loop-type dislocations.

4.1.4. Growth model

There were two possible mechanisms which could affect the epitaxial process for sputtered Si layers. Epitaxy could be inhibited either by oxygen on the Si surface or by the formation of surface disorder at the surface produced by ion bombardment.

4.1.4.1. Influence of oxygen

The usual partial pressure of oxygen during a deposition was 5×10^{-7} torr (see SECTION 3.7.) and, according to Lander and Morrison (1962), a previously-clean Si surface would become oxidised at temperatures less than 800 °C. The epitaxial temperature was between 700 and 730 °C for layers grown at ion source potential and between 650 and 850 °C for layers grown at earth potential. Even though the temperature necessary to initiate oxide growth appeared to agree quite well with the epitaxial temperature limits for both substrate biasing conditions, it was probable that oxygen was not affecting the growth because the defects observed in epitaxial layers and their characteristics were not consistent with those nucleated by oxygen impurity. For evaporated Si layers, where the epitaxial temperature limit was extremely sensitive to oxygen partial pressure (eg. Unvala 1963(a), Censlive 1971), the prominent defects in epitaxial layers were stacking faults and their number was correlated

directly with the partial pressure of oxygen. The only defects observed in sputtered epitaxial layers of Si grown at ion source potential were dislocations if the substrate temperature was greater than about 860°C. The absence of stacking faults in these layers grown in a partial pressure of oxygen of about $5x10^{-7}$ torr suggested that oxygen played no part in the epitaxial process. However, the role of oxygen in the epitaxial process of sputtered Si layers might be affected by other factors. It is known that the nucleation process for triode sputtered layers is influenced by the "extra" energy of sputtered atoms and also by ion bombardment conditions (Bovey 1969). These two factors might possibly explain why the homo-epitaxial temperature for Si layers grown by sputtering (approximately 700°C at 0.02µ/min) was less than the corresponding vacuum evaporation value (approximately 1100°C at 0.1µ/min in oxygen partial pressure of about 10^{-7} torr; Unvala 1963(a)), but the fact that stacking faults in epitaxial layers were only introduced when the rate of ion dose to the substrate was increased suggested that some other mechanism might be more applicable. If the presence of oxygen impurity was important, the opposite effect would have been expected because loosely-bonded oxygen impurity would be selectively sputtered decreasing the probability of nucleating stacking faults.

4.1.4.2. Ion bombardment model

The proposed ion bombardment model to explain the epitaxial process of sputtered Si layers involved the creation of surface disorder at the surface of the growing layer induced by bombarding ions. As the layer proceeded due to deposition the surface disorder moved as well so that material previously disordered was capable of reordering if the so-called "growth" temperature was sufficiently high. The history of the ion bombardment of any region and the "growth" temperature then determined the quality of the resulting sputtered Si layer.

The following points substantiated the validity of the ion bombardment model in the epitaxial process of

sputtered Si layers;

(a) during deposition, the substrate was bombarded with high energy (up to 12keV) secondary ions which could create small spherical damaged regions in the substrate lattice.

(b) surface disorder in epitaxial layers has been established from RHEED patterns (SECTION 4.1.2.2.) and TED patterns in very thin regions (SECTION 4.1.2.3.). The depth of disorder was estimated to be about 100 Å (SECTION 4.1.2.3.), which in the case of 10keV Xe^+ ions corresponds approximately to the average penetration depth of ions in (111) Si (Davies et al 1964).

(c) The necessary post-bombardment annealing temperature for complete surface disorder in Si single crystals created by low energy (10keV) Kr^+ ions was about 720 ± 70°C (Jech and Kelly 1969). This value of reordering temperature appeared to agree quite well with the epitaxial temperature of sputtered Si layers grown for the two different substrate biasing conditions. With substrates at ion source potential the epitaxial temperature was between 700 and 730°C and at earth potential it was between 650 and 850° C. Presumably, if the deposition temperature was less than the minimum reordering temperature to initiate single crystal growth (720 ± 70°C) then re-ordering could not be initiated and a completely polycrystalline or amorphous layer resulted.

(d) The final point in favour of the ion bombardment model was that defects remaining in epitaxial layers and their characteristics (SECTION 4.1.3.) were consistent with annealed ion bombarded specimens.

4.1.4.3. Nucleation and initial stages of growth

To study the initial stages of growth in sputtered epitaxial layers of Si, the region on the substrate differentiating the substrate from the layer was examined by scanning electron microscopy. Typical micrographs

depicting the growth sequence for the two different substrate biasing conditions are shown in FIG. 4.8. These micrographs were of different areas across the masked step on the substrate and effectively represented successive stages of growth. For the layer grown at ion source potential, arriving Si atoms seemed to migrate to large triangular nucleii on the substrate surface which, as the growth proceeded, coalesced to form a "worm-like" structure. Just before the layer became continuous numerous small holes were present in the layer. A similar growth sequence has been reported by Censlive (1971) for evaporated epitaxial Si layers grown in poor vacuum. However, it has been shown in SECTION 4.1.4.2. that the ion bombardment model controlled the epitaxial process of sputtered Si layers and epitaxial layers resulted from reordering of surface disorder created by ion bombardment. The presence of the growth sequence depicted in FIG. 4.8. could then only be explained if surface disorder was discontinuous. In SECTION 4.1.2.3. the thickness of surface disorder in epitaxial layers has been estimated to be about 100 Å and, since the diameter of individual spherically damaged regions is between 50 and 100 Å (Mazey et al 1966, 1968, and Large and Bicknell 1967), it would appear that surface disorder in epitaxial layers could well be discontinuous. The growth sequence for the layer grown at earth potential was similar to that for the layer grown at ion source potential. The only anomaly observed was that individual nucleii appeared to be more irregular in shape. This effect may be due to a more continuous region of surface disorder.

4.1.5. Electrical measurements

The resistivity of all epitaxial layers grown at ion source potential was between 20 and 150 ohm-cm and higher growth temperatures appeared to result in the lower resistivity layers. The conductivity type of all epitaxial layers was established to be N-type since diode characteristics could only be obtained from mesa sections if a P-type substrate was used. A typical diode characteristic with a reverse breakdown of 50 volts is shown in FIG. 4.9. Reverse breakdown voltages usually varied between 30 and

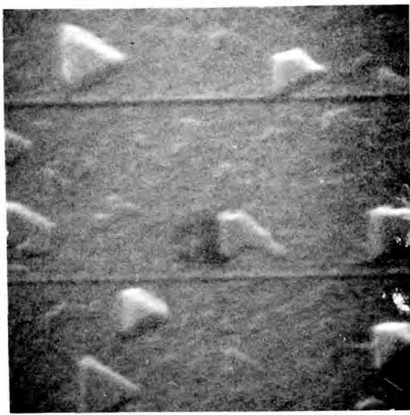

0·5μ

substrate side; individual nucleii

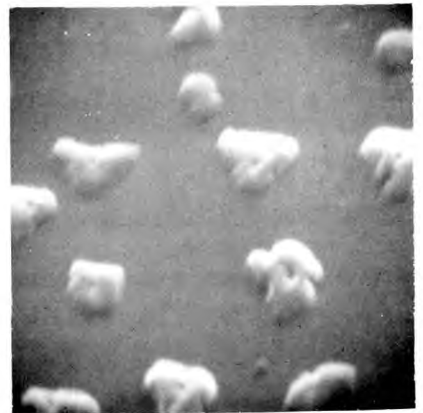

0·5μ

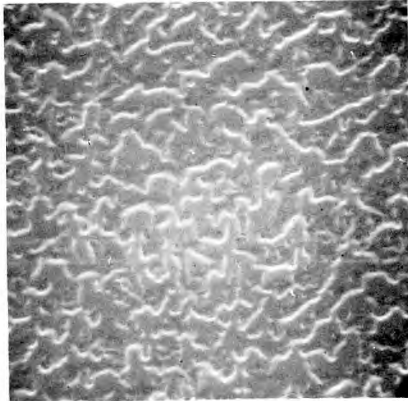

1·0μ

coalescence of nucleii to form "worm-like" structure

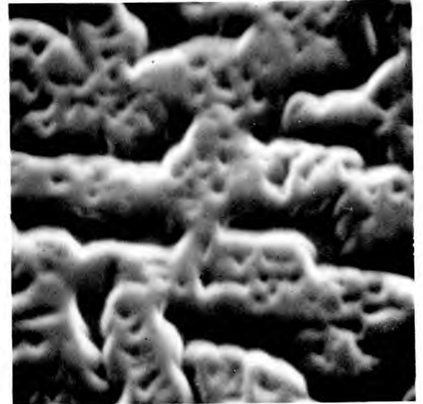

0·5μ

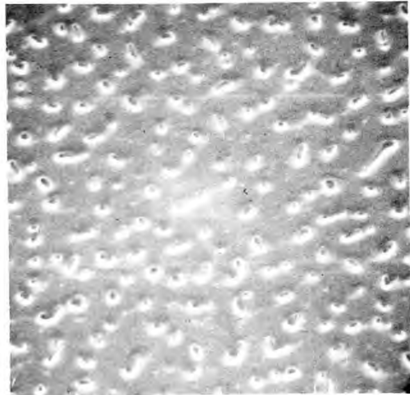

1·0μ

layer almost continuous but with holes

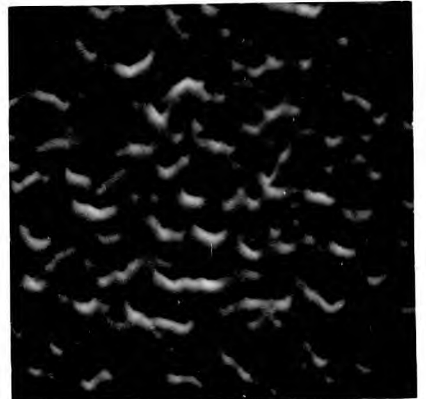

0·5μ

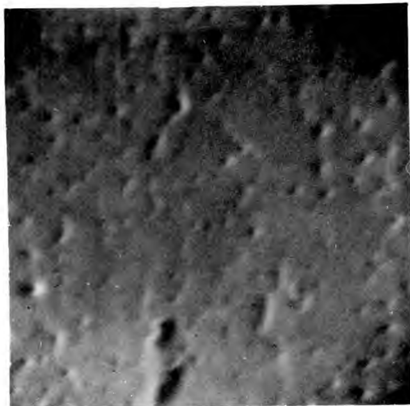

1·0μ

almost continuous layer

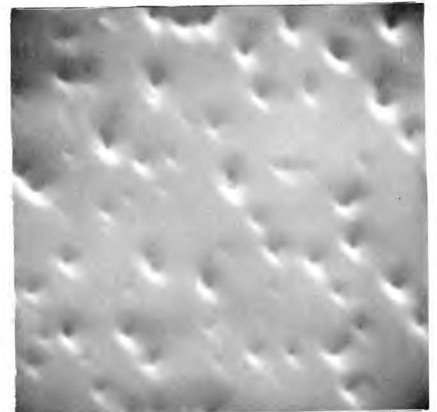

0·5μ

almost continuous layer

Layer grown with substrate at ion source potential; temperature about 860°C

Layer grown with substrate at earth potential; temperature about 920°C

FIG. 4.8. GROWTH SEQUENCE FOR DIFFERENT SUBSTRATE BIASING CONDITIONS

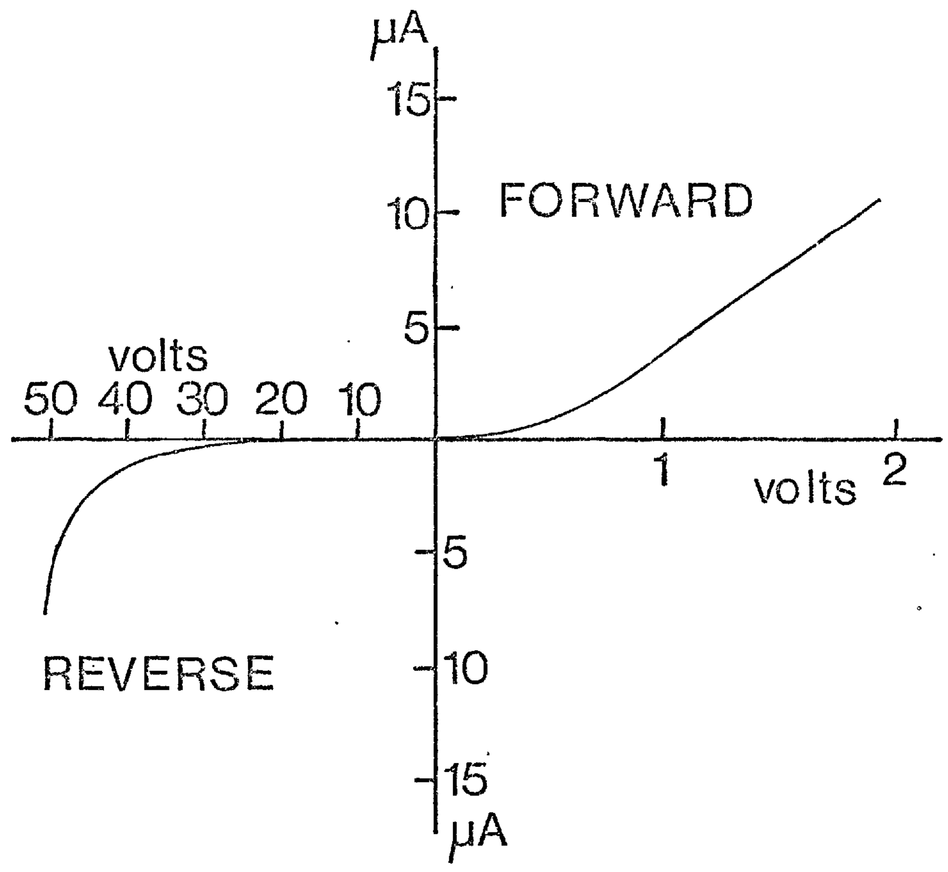

FIG. 4.9. DIODE CHARACTERISTICS (TYPICAL)
FROM 1mm. MESA OF N-TYPE Si LAYER
ON P-TYPE Si SUBSTRATE.

150 volts.

The total lack of reproducibility of target conductivity-type and resistivity in layers and the persistence of high resistivity N-type layers could be due to ion bombardment of layers during growth. Ohl (1952) and Ferber (1963) found that ion bombardment of P-type Si with 100eV to 1MeV H_2, He, N_2, O_2, Ne, A, Xe, P or B ions produced conversion to N-type usually of high resistivity. Ferber (1963) established for H_2, N_2, O_2, Ne and Xe bombardments at a rate of dose of $6x10^{12}$ ion sec^{-1} cm^{-2} that the type conversion could be attributed to ion bombardment damage produced donor sites and not to implanted donor atoms. Only for P and B bombardments was there any evidence of chemical doping effects. The possibility of donor damage sites introduced into the growing layer by ion bombardment thus producing N-type layers seemed quite likely for sputtered epitaxial layers because an ion bombardment model has at least been shown to control the growth of layers (SECTION 4.1.4.2.).

4.2. SPUTTERING YIELD AND TOPOGRAPHY OF TARGET SURFACES AFTER BOMBARDMENT

4.2.1. Sputtering yield

FIG. 4.10. shows apparent sputtering yield values plotted against target current (rate of ion dose) for Si targets bombarded at 60°, for different values of ion energy, for A^+ and Xe^+ ion beams, and for single crystal and polycrystalline Si. In FIG. 4.11. the values of apparent sputtering yield for 6keV and 12keV A^+ ion bombardment of Si(111) surfaces are plotted against total ion dose.

It would appear that the apparent sputtering yield for Si(111) crystals increased when either rate of A^+ ion dose or total A^+ ion dose was increased. From the atom ejection studies (SECTION 4.3.4.), an increase in either of these parameters resulted in a more complete disordered surface. The sputtering yield of a disordered Si surface was, therefore, higher than that of the true (111) surface bombarded at 60°. The transparency model predicted that the surface with the highest sputtering yield was disordered or amorphous. Confirmation that the damaged (111) Si surface gave an apparent sputtering yield close to that expected for a fully disordered surface was provided by comparing the results for 12keV Xe^+ bombardment of a Si(111) single crystal and a Si polycrystal in FIG. 4.10. Within the 7% measurement accuracy, the sputtering yield for the two surfaces was the same and about 2.4 ± 0.6 times that for a Si(111) surface bombarded with a 12keV A^+ ion beam. On the basis of a momentum increase process the change from A^+ to Xe^+ ions would have resulted in an increase of the sputtering yield by a factor of 1.8.

In FIG. 4.10 is also shown a single result for the apparent sputtering yield of a GaAs (111) single crystal target bombarded with a 12keV A^+ ion beam. The sputtering yield was clearly larger than the corresponding value for the Si(111) surface. A similar result was found at low ion energy (eg. 600eV A^+ ions) where the sputtering yield of a damaged (110) GaAs target (Comas and Cooper 1966)

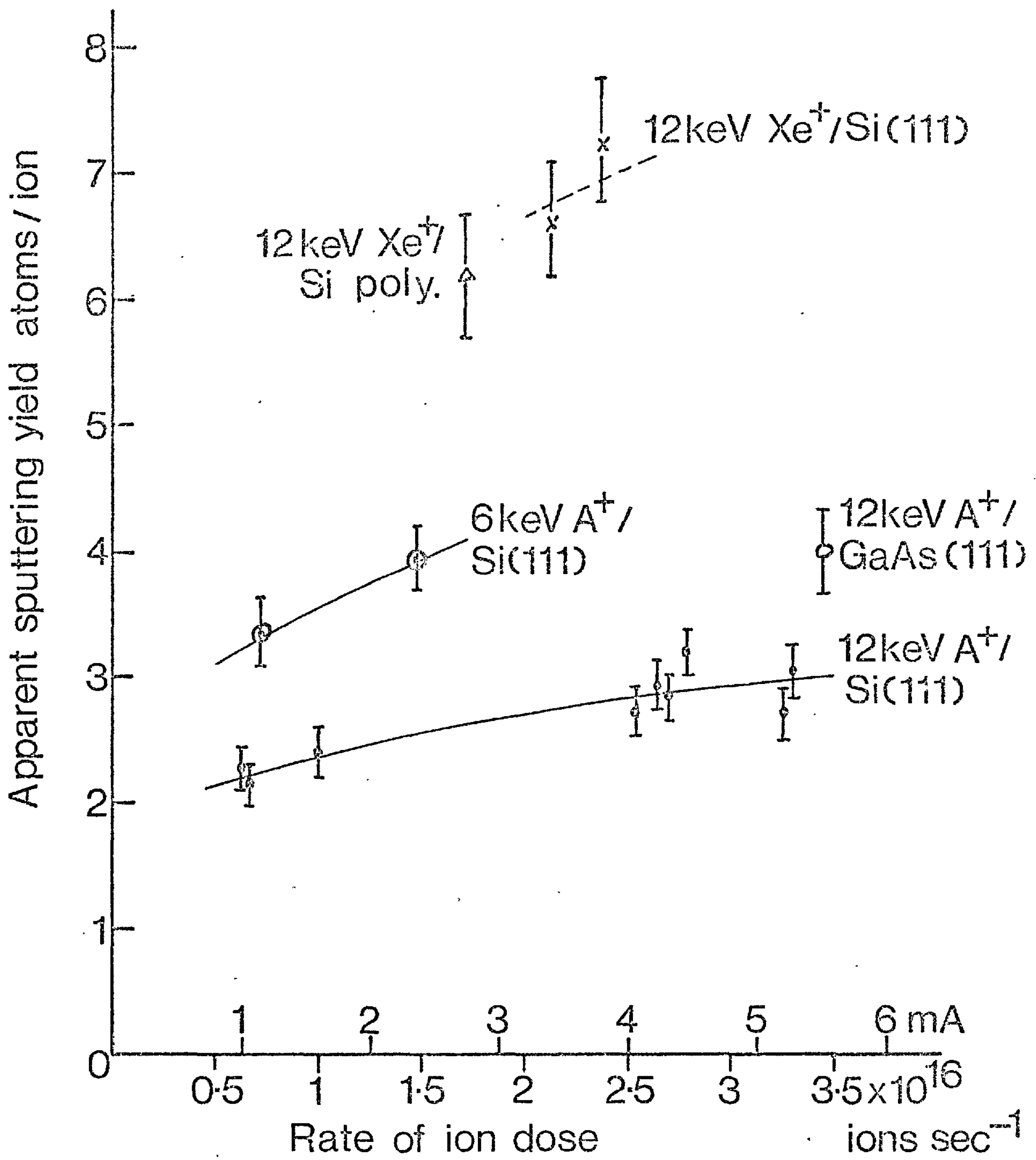

FIG. 4.10. VARIATION OF SPUTTERING YIELD WITH RATE OF ION DOSE FOR TARGETS BOMBARDED AT 60° INCIDENCE.

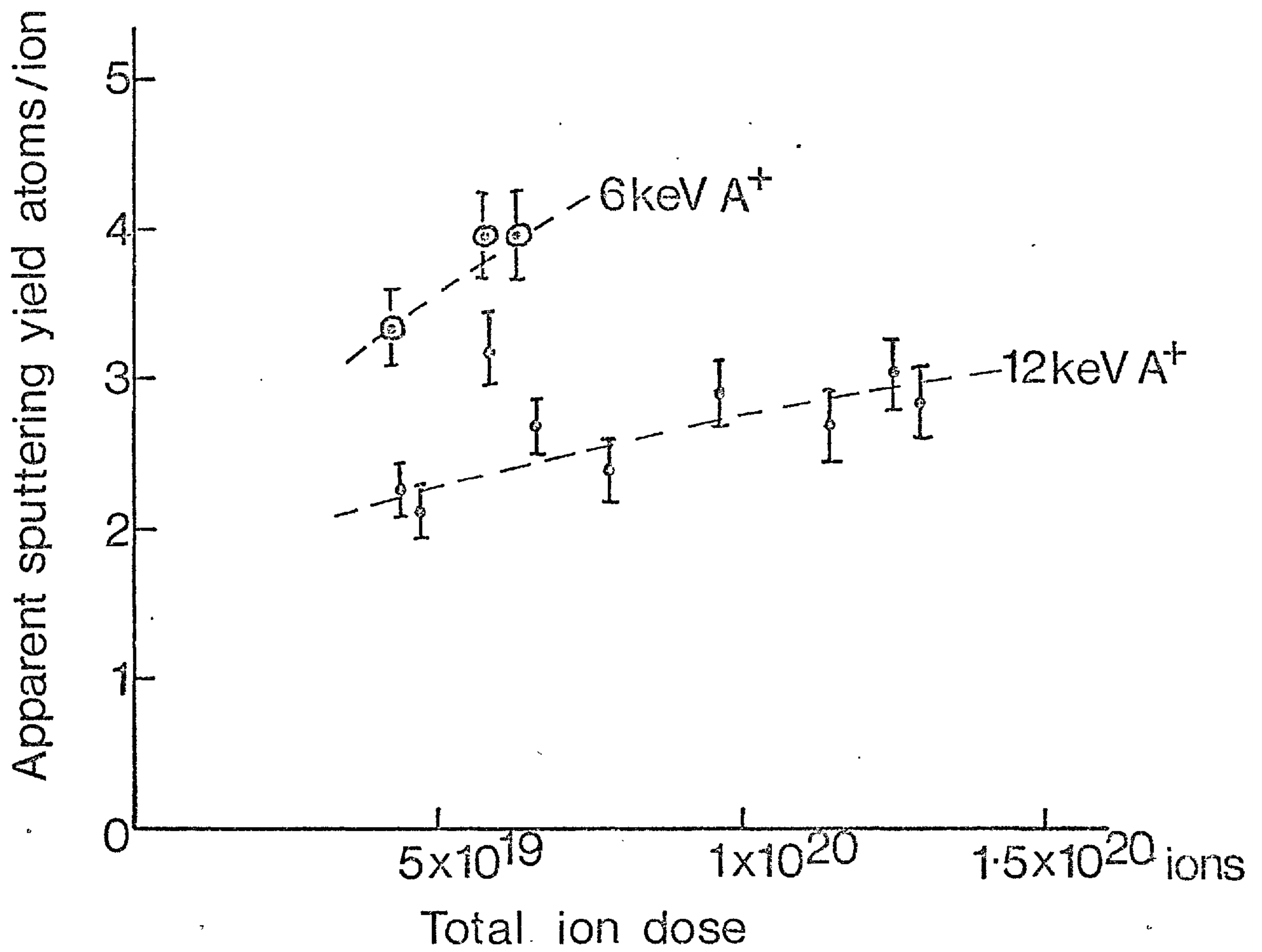

FIG. 4.11. VARIATION OF SPUTTERING YIELD WITH TOTAL ION DOSE FOR Si(111) TARGETS BOMBARDED AT 60° INCIDENCE.

was greater than that of polycrystalline Si (Laegrid and Wehner 1961).

A further observation to be made from both FIG. 4.10 and FIG. 4.11. was that 6keV A^+ ions produced a higher sputtering yield for the Si "(111)" surface than 12keV A^+ ions. The higher energy ions were expected to produce more damage and a more complete disordered surface giving higher sputtering yields but this was not the case. The most likely explanation for the contradiction was that higher energy ions penetrated the target further and energy transfer to the surface was more difficult causing a reduction in the sputtering yield. Southern et al (1963) found that the optimum value of A^+ ion energy for normal incidence bombardment of "(111)" Si was 5keV before the sputtering yield was reduced due to increased ion penetration. With ion incidence away from the target normal a higher optimum ion energy was possible because, even though ion penetration path lengths were longer, the length of the collision sequence needed to transmit a disturbance back to the surface could be the same. For the experiments described here where ion attack was at an angle of 60° to the target normal the optimum A^+ ion energy was less than 12keV.

Finally, the peak value of sputtering yield of 1.4 atoms/ion quoted by Southern et al (1963) for normal incidence 5 to 6keV A^+ ion bombardment of a Si "(111)" surface was a factor of about 2.65 ± 0.45 less than the value presented here for 6keV A^+ ion bombardment at 60° incidence (average of 2 readings in FIG. 4.10 gave sputtering yield of about 3.7 ± 0.6 atoms/ion). The increase in sputtering yield for ion attack away from the target normal was expected because momentum reversal was made easier and the length of the necessary collision sequence was shorter.

4.2.2. Macrotopography of targets after bombardment

FIG. 4.12 shows a typical profile determined by the Talysurf of a Si(111) slice initially 250 microns thick after bombardment. The upper trace (FIG. 4.12(i)) clearly shows that the sputtering process was governed by the

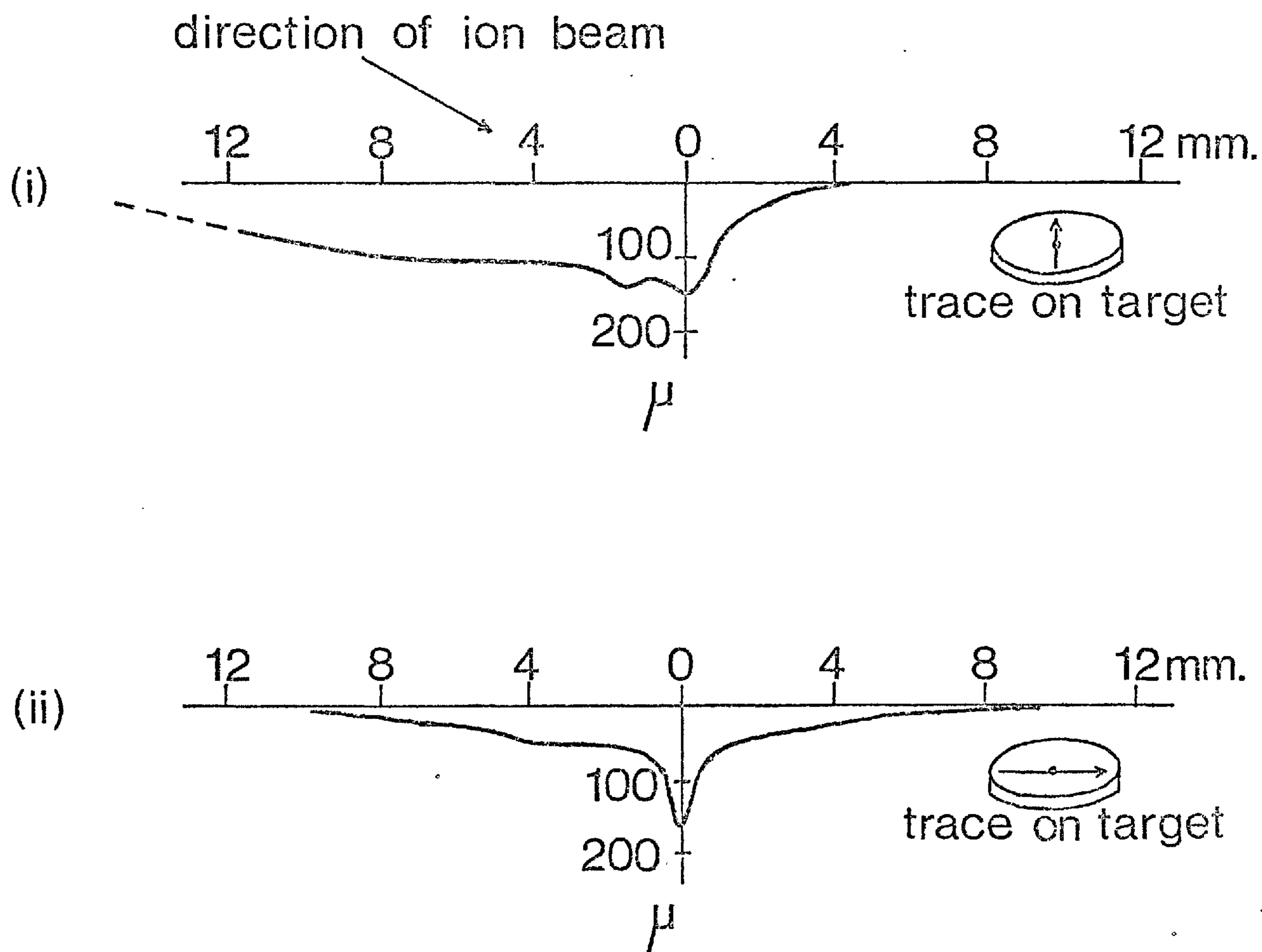

FIG. 4.12. PROFILE OF Si(111) TARGET AFTER BOMBARDMENT. 12keV A^+ ion beam of 4.35mA inclined at 60° to the target normal for 60 mins. Talysurf traces (rescaled) across the target in two directions. The traces on the target are shown with ion beam normal to the plane of the paper.

transfer of momentum (vectorial process) from the bombarding A^+ ions to the Si target and not simply by the transfer of energy. Similar visual evidence was presented by Cunningham et al (1960) for the bombardment of (100) Al by 8keV A^+ ions at 80° to the target normal.

The lower trace (FIG. 4.12(ii)) shows the cross-section of the ion beam which was obviously non-uniform although symmetrical. An estimate of two extremes of current density (mA cm^{-2}) was made by assuming that the amount of material removed was directly proportional to the ion current. On this basis 34% of the current was concentrated in the 2 mm. diameter central region of high current density. The remainder of the current was concentrated in the region 16 mm. in diameter. The corresponding values of current density were then 47mA cm^{-2} and 1.4mA cm^{-2} respectively. The equivalent values of bombardment ratio (N_i/N_g) of ions to reactive background gases were 1000 and 40 respectively under typical operating conditions where the partial pressure of oxygen was $5x10^{-7}$ torr (SECTION 3.7.). Therefore, on the basis of the work on semiconductors by Southern et al (1963), Honig (1958) and Wolsky and Zdanuk (1961) (SECTION 2.1.10.), sputtering yield measurements in this investigation were independent of background pressure.

4.2.3. Microtopography of targets after bombardment

Examination of ion beam bombarded Si "(111)" target surfaces with the scanning electron microscope revealed that the bombardment produced uniform removal of material with no sign of the gross etch pit production characteristic of single crystals reported by Wehner (1956), (1957) and (1958). The absence of etch pits was further evidence of a change in the surface structure of the single crystal to a disordered state. Dillon and Oman (1960) interpreted the absence of etch pits in their low energy studies in a similar manner. However, all surfaces examined exhibited conical protrusions formed with their axes along the direction of ion incidence (60° to surface normal). A typical cone is shown in the photograph in FIG. 4.13(i). Hillocks on sputtered semiconductor targets have also

⊢ 30μ ⊣

(i) Ion beam 12keV 2.6mA Xe^+ for 100 mins.

⊢ 30μ ⊣

(ii) Ion beam 12keV 2.5mA A^+ for 70 mins.

⊢ 30μ ⊣

(iii) Ion beam 12keV 4.35 mA A^+ for 60 mins.

FIG. 4.13. CONICAL PROTRUSIONS FORMED ON "(111)" Si SURFACES BY ION BOMBARDMENT

been observed by Meckel and Swalin (1959), Dillon and Oman (1960), Honig (1958), Meckel (1966) and Stewart and Thompson (1969) and attributed to various sources. The most common interpretation for the formation of hillocks was that impurity particles at or on the surface of the target shielded minute parts of the bombarded surface and delayed sputtering of those regions (Honig 1958, Meckel 1966, Stewart and Thompson 1969). This would seem to be the most likely explanation here also because the existence of surface disorder excluded single crystal effects proposed by Meckel and Swalin (1959).

Further examination of surfaces has shown that the size and magnitude of the cones appeared to depend on the rate at which material was removed from the surface.

The cone shown in FIG. 4.13(i) was on the surface of a Si(111) target bombarded with a 12keV 2.6mA Xe^+ beam for 100 minutes. Slightly larger cones were observed on a Si(111) surface bombarded with a 12keV 2.5mA A^+ beam for only 70 minutes (FIG. 4.13(ii)). Therefore, it would appear that smaller cones were consistent with a higher sputtering yield (the sputtering yield of Si with Xe^+ ions was about 2.4 ± 0.6 times that for A^+ ions, SECTION 4.2.1.) On a Si(111) surface bombarded with a 12keV 4.35mA A^+ beam for 60 minutes substantially smaller cones were observed. (FIG. 4.13(iii)). This same target was used for estimating the variation of current density in the ion beam, the results of which are depicted in FIG. 4.12. The cones depicted in FIG. 4.13(iii) were observed in a region about 2 mm. from the centre of the target. At the centre of the target, where the current density was greatest (up to 50mA cm^{-2}) no cones were observed. Therefore, it would appear that for either higher currents or higher current densities even smaller or no cones at all were formed.

Conical protrusions formed by ion bombardment were not exclusive to single crystal surfaces alone. Similar cones to those observed on Si(111) surfaces have been observed on the surface of a Si polycrystal and appeared more numerous at grain boundaries where the presence of foreign inclusions in the specimen was greatest

(FIG. 4.14(i)). With the polycrystalline target of Si, grain boundaries were more easily attacked and appeared as grooves. Furthermore, differently oriented grains were attacked at different rates and appeared at different elevations. These features are clearly illustrated in the photograph in FIG. 4.14(ii). Similar features, but without conical protrusions, were observed at low ion energies by Wehner (1956), (1957), and (1958) and could be reproduced by standard chemical etchants. FIG. 4.15 shows a typical micrograph of the surface of an unbombarded polycrystalline Si target which had undergone the standard 3-15-5 etch for a few minutes. The initial stages of groove formation were quite evident.

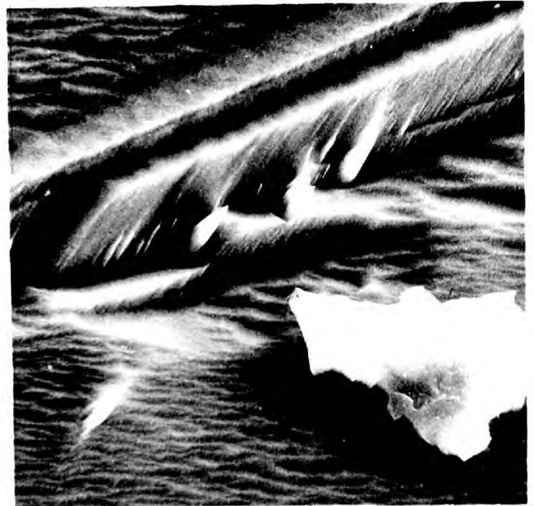

(i) Conical protrusions

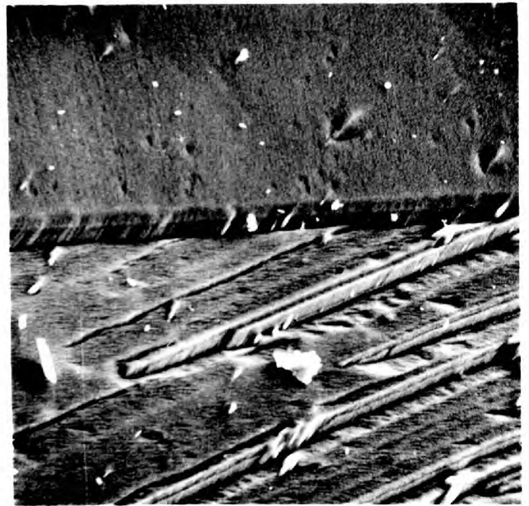

(ii) Grain boundaries appear as grooves. Differently oriented grains appear at different elevations

FIG. 4.14. POLYCRYSTALLINE Si TARGET AFTER ION BOMBARDMENT

FIG. 4.15. POLYCRYSTALLINE Si TARGET AFTER CHEMICALLY ETCHING FOR FEW MINUTES ONLY

4.3. THE ANGULAR DISTRIBUTION OF SPUTTERED ATOMS

4.3.1. Polar distributions of sputtered Si

Typical polar distributions for Si(111) targets bombarded with 12keV A^+ and Xe^+ ion beams are shown in FIG. 4.16. The most significant observation from these curves was the absence of strong ejection maxima along certain preferred crystallographic directions. In fact there was a striking similarity in the polar distribution curves to those for a polycrystalline Si target (FIG. 4.17) where only a single symmetrical deposit was observed. In the plane parallel to the ion beam the distribution peaks were approximately 80 to 100° away from the ion beam illustrating again the importance of momentum transfer in the sputtering process. Perfect specular reflection would have occurred at $\Theta_1 \sim 120°$. In the plane perpendicular to the ion beam the distribution for the polycrystalline Si was "under-cosine" after the curve was corrected by the inverse square law (see FIG. 4.17).

The most probable explanation for the similarity in polar distribution curves for single crystal and polycrystalline targets was that a change in the surface structure of the single crystal to a disordered state was induced by the ion bombardment. It has been reported that the threshold dose for damage in Si is about 10^{13} ions cm^{-2} and the dose necessary for the formation of a continuous disordered surface layer in Si is about 10^{14} ions cm^{-2} (see TABLE 2.C). It would therefore be surprising if the single crystal surface in these investigations was not severely disordered because typical ion doses were between 6 and 9×10^{19} ions.

Confirmation of a change in the surface structure of the single crystal target was made by glancing-angle reflection high-energy electron diffraction (RHEED) which probed only the top few atomic layers of the surface. A typical diffraction pattern is shown in FIG. 4.18. which clearly illustrates a single crystal spot pattern with strong superimposed rings characteristic of polycrystalline material.

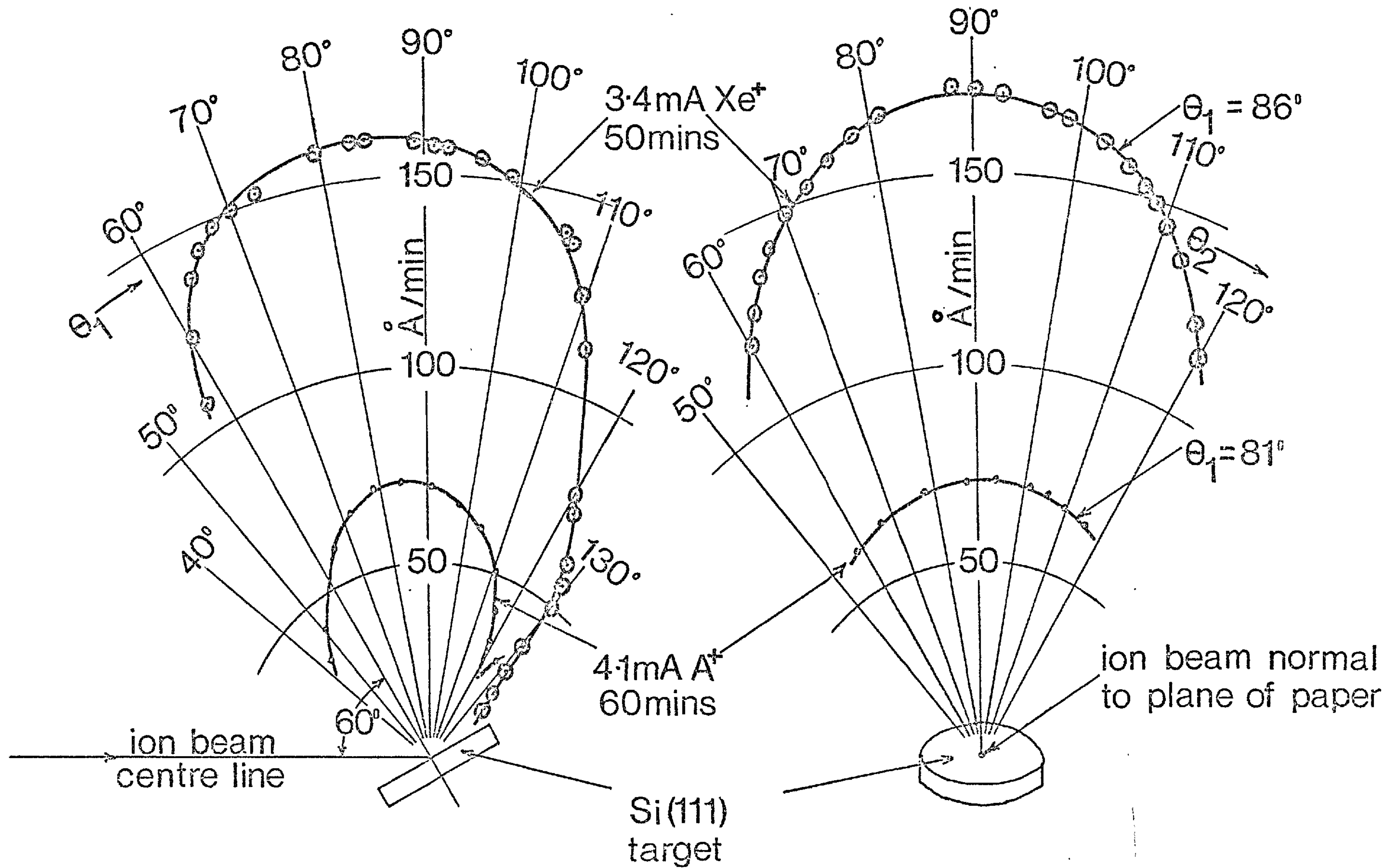

FIG. 4.16. POLAR DISTRIBUTION OF SILICON SPUTTERED FROM (111) SINGLE CRYSTAL TARGETS BY 12keV A^+ AND Xe^+ ION BEAMS
Plane of deposit $2\frac{3}{8}$ in. from ion beam centre line.

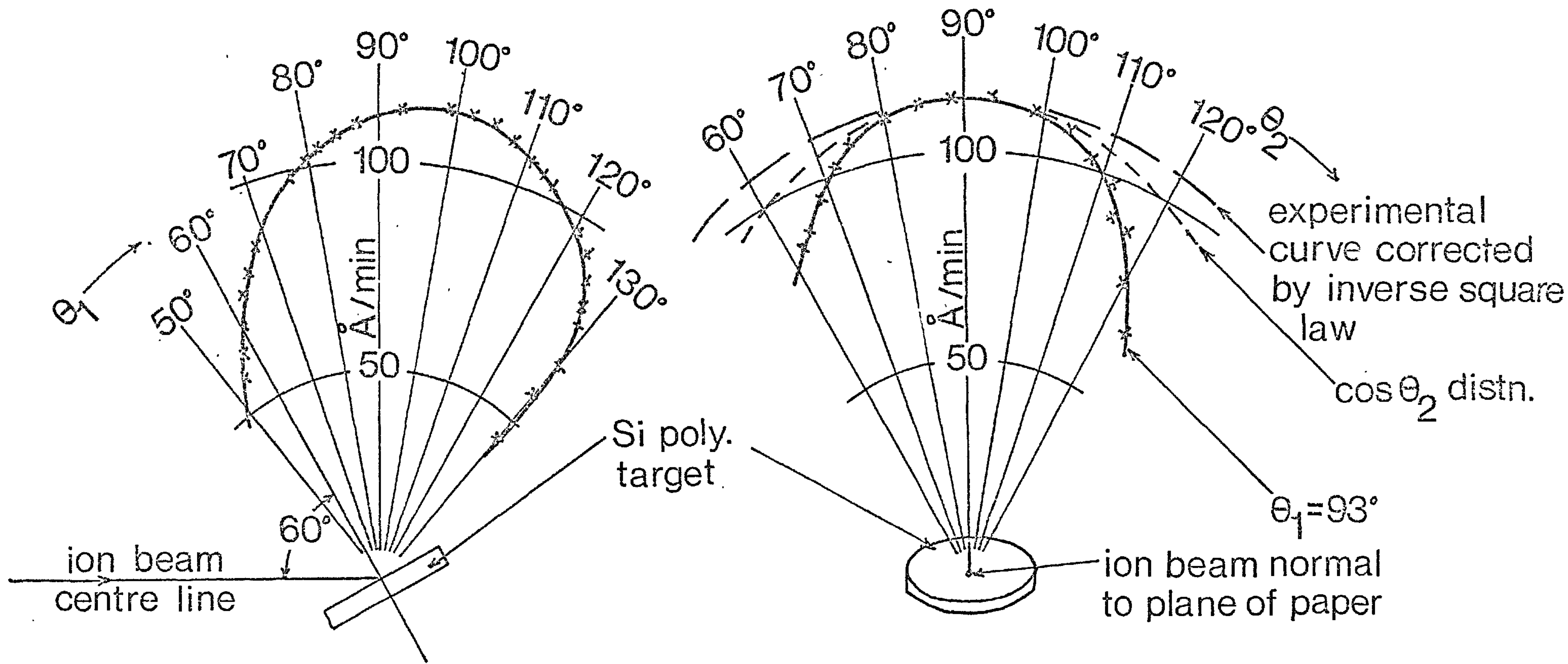

FIG. 4.17. POLAR DISTRIBUTION OF SILICON SPUTTERED FROM A POLYCRYSTALLINE TARGET BY A 12keV 2.7mA Xe^+ ION BEAM FOR 60 MINS. Plane of deposit 2⅜ in. from ion beam centre line.

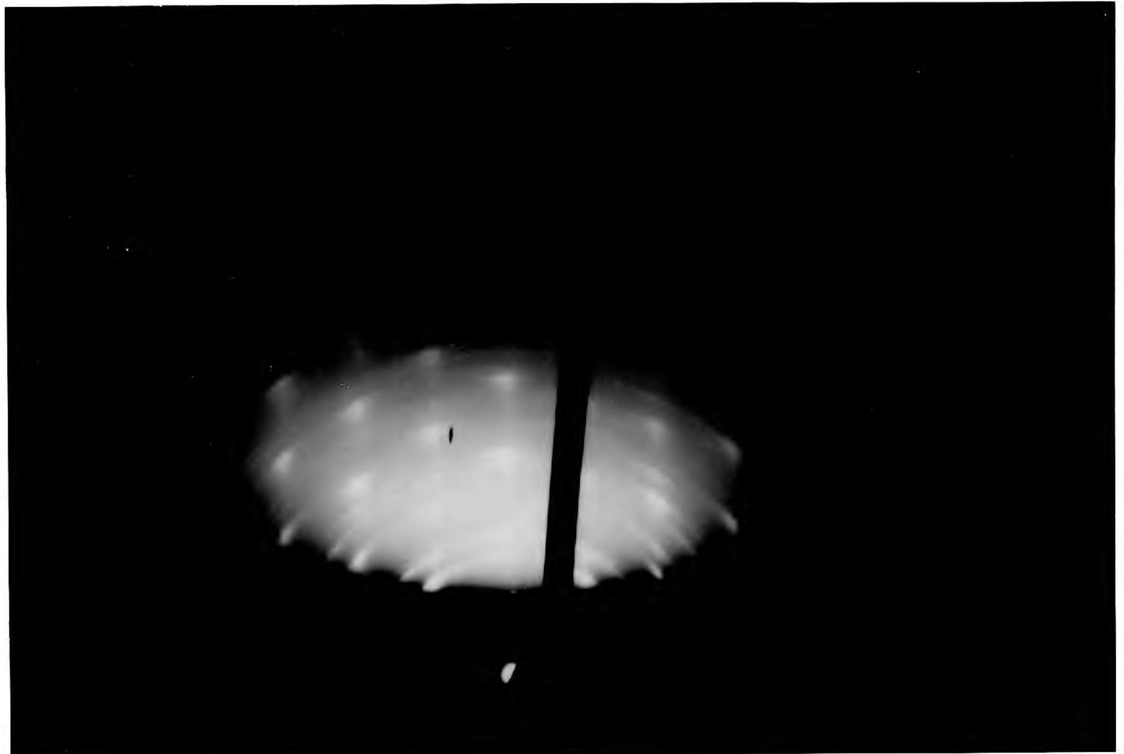

FIG. 4.18. RHEED PATTERN OF Si(111) SURFACE AFTER BOMBARDMENT BY 12keV A^+ ION BEAM AT A RATE OF DOSE $3x10^{16}$ ions sec^{-1} TO A TOTAL DOSE 10^{20} ions

4.3.2. Contour map distributions of sputtered Si

Complete distribution curves in the form of deposition rate contour maps showed that limited single crystal properties remained for Si(111) targets, indicating perhaps that the surface disorder was not complete. An example is shown in FIG. 4.19. where the rate of ion dose was 3.2×10^{16} ions sec^{-1} and the total dose 4.8×10^{19} ions. The central maximum appeared in a direction in between the [111] direction and that corresponding to a complete disordered surface. The two elongated deposits, which tended to thicker deposits in $\langle 100\rangle$ directions, represented the degree of single crystal properties which remained. Colombie et al (1966) similarly found for 80keV A^+ ion bombardment of (111) Ge that a nearly isotropic deposit was formed when the rate of ion dose and total dose were $2\frac{1}{2}\times10^{16}$ ions sec^{-1} cm^{-2} and 2×10^{19} ions cm^{-2} respectively. In this case of very high energy bombardment a channelling mechanism of ejection was dominant because the order of effectiveness of ejection directions was $\langle 110\rangle$, $\langle 112\rangle$. The observation of $\langle 100\rangle$ ejection directions for Si in this study at lower energies (12keV) was consistent with the results of Yurasova and Sirotenko (1962) in the same energy range. Presumably ejection in $\langle 100\rangle$ directions corresponded to collisions with least energy loss. Specific $\langle 110\rangle$ and $\langle 111\rangle$ ejection, reported by Yurasova and Sirotenko (1962) and Yurasova et al (1964) for low keV ion energies, could not be resolved because of the magnitude of the main deposit.

4.3.3. Deposition rate of sputtered Si onto self substrates

The deposition rate contour map of sputtered Si atoms (FIG. 4.19), determined with the glass microscope slides in a plane $2\frac{3}{8}$ in. (60 mm.) above the target, was useful in giving an estimate of the deposition rate and thickness variation across sputtered Si layers on single-crystal Si slices. For the experiments where homo-epitaxy was attempted, the Si slices were 1 in. above the target and the unmasked area of each slice covered the area shown in FIG. 4.19. The difference in deposition rate and thickness of a layer at the step to the centre was between 13 and 33%, the central region of the slice having a thicker deposit.

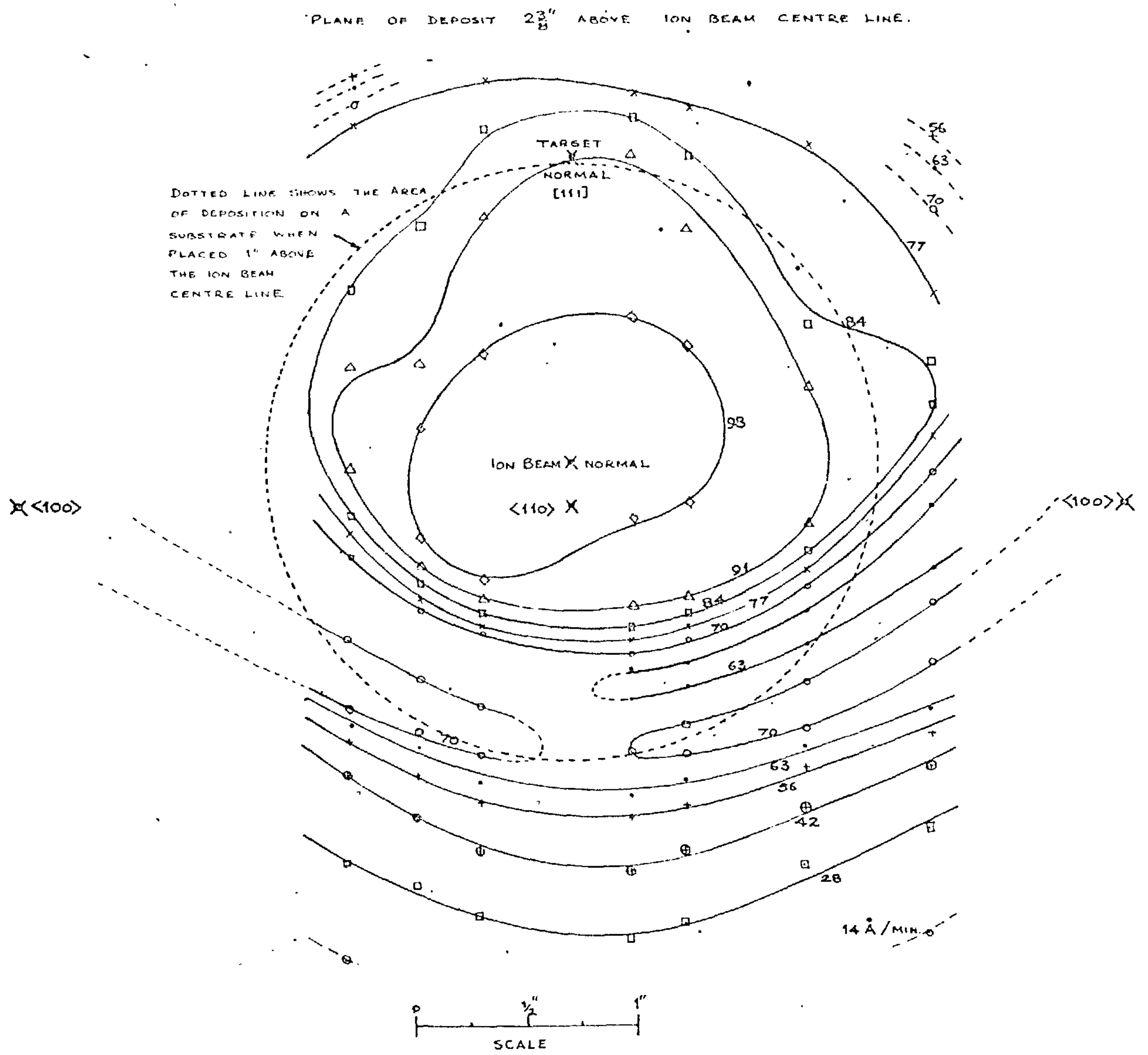

FIG. 4.19 DEPOSITION RATE CONTOUR MAP OF SILICON SPUTTERED FROM A (111) SURFACE BY A 12 KeV, 5·2 mA ARGON ION BEAM FOR 25 MINUTES

Therefore all measured values of deposition rate and thickness with the Talysurf at the step on the Si substrate were up to 33% below maximum values.

With 8mA A^+ ion beams, the measured deposition rate of sputtered Si onto self substrates was about 400 Å/min decreasing to between 150 and 250 Å/min for 3 to 5mA A^+ ion beams.

4.3.4. <u>Effect of rate of ion dose and total dose on contour map distributions</u>

A typical deposition rate contour map was shown in FIG. 4.19. and explained in SECTION 4.3.2.

A series of experiments (RUN numbers 1 to 3 to Table 4.A.) showed that as the ion current (rate of ion dose) was increased then the angle of the main peak increased from the [111] direction and approached that corresponding to a complete disordered surface (98° for Xe^+ beam; RUN number 5 in Table 4.A). A comparison between RUN numbers 4 for Xe^+ and 1 and 2 for A^+ in Table 4.A. showed the angle for the main peak was larger for a Xe^+ beam because of the greater momentum and damaging power of Xe^+ ions. Furthermore, as the total ion dose was increased then the intensity ratio of a deposit approaching a ⟨100⟩ direction to the main deposit decreased (RUN numbers 1 to 3 in Table 4.A.) Comparison between RUN numbers 4 for Xe^+ and 2 and 3 for A^+ in Table 4.A. indicated that Xe^+ ions did more damage for the same total dose because a lower intensity ratio was recorded. The polycrystalline Si target (RUN number 5 in Table 4.A) exhibited no single crystal properties and so the intensity ratio was zero.

The tendency to a more complete disordered surface when rate of ion dose or ion mass was increased was consistent with the results of Anderson, Wehner, Evdokimov, Mashkova, Molchanov and Abroyan, discussed in SECTIONS 2.3.1.6(a) to 2.3.1.6(d), who found that increasing either or both of these parameters necessitated a higher value of T_a, the critical annealing temperature. A more complete disordered surface due to increased total ion dose was consistent with the results of Nelson and Mazey (1968), Irving (1969) and Colombie et al (1966).

RUN No.	TARGET	BOMBARD-ING ION	CURRENT (mA)	(RATE OF ION DOSE) (ion sec^{-1})	BOMBARD-MENT TIME (minutes)	TOTAL DOSE (ions)	ANGLE FOR MAIN PEAK (degrees)	INTENSITY RATIO OF A $\langle 100 \rangle$ DEPOSIT TO MAIN DEPOSIT (see text)
1.	Si(111) SLICE	A^+	1.6	1.0×10^{16}	120	7.2×10^{19}	$77\frac{1}{2}$	0.64
2.	Si(111) SLICE	A^+	4.05	2.5×10^{16}	60	9.0×10^{19}	$81\frac{1}{2}$	0.46
3.	Si(111) SLICE	A^+	5.2	3.2×10^{16}	25	4.8×10^{19}	$85\frac{1}{2}$	0.72
4.	Si(111) SLICE	Xe^+	3.4	2.1×10^{16}	50	6.3×10^{19}	90	0.38
5.	Si POLYCRYST	Xe^+	2.7	1.7×10^{16}	60	6.1×10^{19}	98	0
6.	GaAs POLYCRYST	Xe^+	4.3	2.7×10^{16}	62	1.0×10^{20}	101	0
7.	GaAs (111)	A^+	5.5	3.4×10^{16}	64	1.3×10^{20}	95	1.08

ION ENERGY FIXED AT 12keV

TABLE 4.A.

4.3.5. Effect of temperature on contour map distributions

In the case of RUN 4 in Table 4.A. where a Si(111) slice was bombarded with a 12keV Xe^+ ion beam at a rate of dose of $2x10^{16}$ ions sec^{-1} to a total dose of $6x10^{19}$ ions the temperature of the central region of the Si slice was estimated to be 790°C using a near-focussing optical pyrometer. This temperature was not sufficient to prevent the formation of a nearly isotropic deposit and indicated that for the bombardment conditions used the critical annealing temperature T_a, was in excess of 790°C. For studies where the total dose did not exceed $6x10^{16}$ ions cm^{-2}, temperatures in the range 300 to 600°C were sufficient to prevent the formation of a disordered surface in Si (see SECTIONS 2.3.1.6(a) to 2.3.1.6(e)). No information is available in the literature for values of T_a for Si bombarded with ions to a higher total dose. However, extrapolation of the threshold ion dose for damage curve obtained by Nelson and Mazey (1968) and depicted in FIG. 2.18. indicated that at a temperature of about 790°C the dose of 30keV Ne^+ ions necessary to produce visible surface disorder was only approximately $2x10^{17}$ ions cm^{-2}. Visible surface disorder (ie. milky appearance of the bombarded surface) has been identified for most targets bombarded in this investigation but generally the discolouration was non-uniform perhaps because both temperature and rate of ion dose across the target were also non-uniform.

4.3.6. Contour map distribution of sputtered GaAs

A contour map for the distribution of sputtered atoms from a GaAs (111) target is shown in FIG. 4.20. This experiment with a 12keV A^+ ion beam is tabulated as RUN number 7 in Table 4.A. The results for the GaAs (111) target were similar to those presented for the Si (111) targets in that the distribution showed, firstly, a central maximum at 95° between the [111] direction and the angle corresponding to a complete disordered surface (101° for

PLANE OF DEPOSIT $2\frac{3}{8}''$ ABOVE ION BEAM CENTRE LINE.

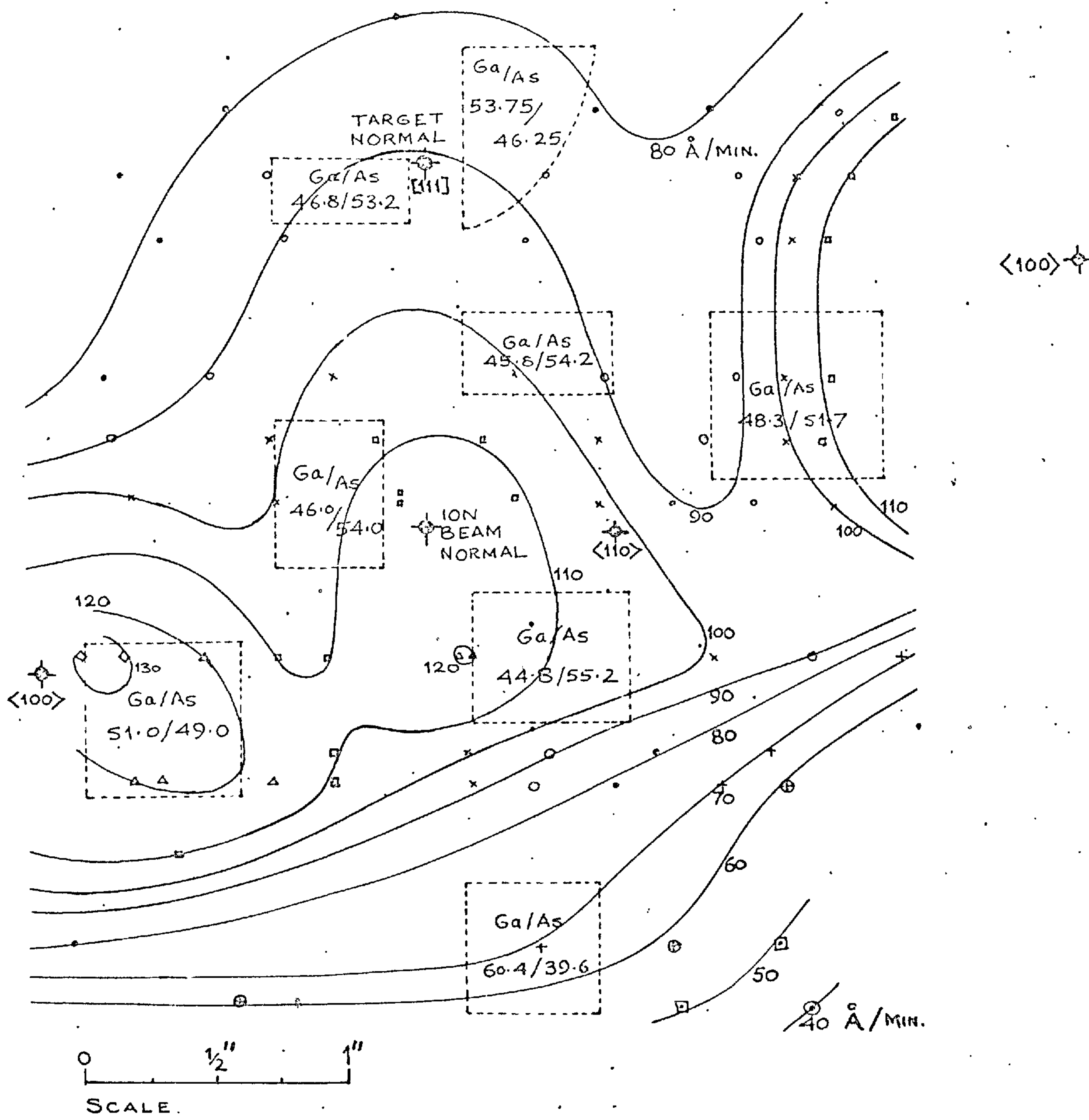

FIG. 4.20 DEPOSITION RATE CONTOUR MAP OF GaAs SPUTTERED FROM A (111) SURFACE BY A 12 KeV, 5.5 mA ARGON ION BEAM FOR 64 MINUTES.
(ATOMIC PERCENTAGE RATIOS OF GA:AS SHOWN IN DOTTED ENCLOSURES).

Xe^+ beam; RUN number 6 in Table 4.A.), and, secondly, enhanced sputtering along approximate $\langle 100 \rangle$ directions. Specific $\langle 110 \rangle$ ejection again could not be detected, if present, due to the overriding prominence of the main deposit. However, in this case sputtered deposits in $\langle 100 \rangle$ directions were more clearly defined, the intensity ratio was 1.08, which was greater than that obtained for RUN number 2 for a Si(111) target under similar bombardment conditions, indicating that the GaAs (111) target was less severely damaged. These observations were directly connected to the fact that under indentical bombardment conditions the corresponding value of T_a for GaAs is less than that for Si (Anderson and Wehner 1964, and Anderson 1966(b)).

4.3.7. Chemical composition of sputtered deposits from GaAs targets

The contour map of the sputtered atom distribution from the GaAs (111) target (FIG. 4.20) also shows values of the ratio of the atomic percentage of Ga to As in dotted enclosures which represent the areas where the chemical analysis was made. The two $\langle 100 \rangle$ spots tended to be stoichiometric. The deposit in the [111] target normal direction would also seem to be stoichiometric because on one side the area investigated was Ga rich and on the other side As rich. Three samples in the central maximum region appeared to be As rich whereas in a region close to a $\langle 111 \rangle$ direction $70\frac{1}{2}°$ from the [111] target normal the composition was extremely Ga rich. A wide disparity in chemical composition therefore resulted for different parts of the sputtered deposit from the GaAs (111) target bombarded with a 12keV A^+ ion beam. At lower ion energies Wolsky et al (1964), Anderson and Wehner (1964), Anderson (1966(b)), Comas and Cooper (1968), and Yurasova et al (1964) also reported large deviations from stoichiometry for deposits resulting from single crystal targets.

On the other hand, measurements from 6 selected samples of the sputtered deposit from a polycrystalline GaAs target bombarded with a 12keV Xe^+ ion beam showed that for each sample the deviation from stoichiometry was less than 0.4 atomic percentage, the accuracy of the measurement. At

low ion energies, Moulton (1962) also reported that stoichiometric deposits could be obtained from polycrystalline compound semiconductors.

CHAPTER 5

CONCLUSIONS AND RECOMMENDATIONS FOR FURTHER WORK

5.1. CONCLUSIONS

The work described in the preceding chapters has shown that using the ion beam sputtering technique developed it was possible to produce homo-epitaxial Si layers for the first time by any sputtering technique.

Considerable modification to the initial ion beam source design and mode of operation of Hill and Nelson (1965) was necessary before the source was suitable for semiconductor thin film application. The modified ion beam source was then capable of giving the purity needed for the production of semiconductor layers without mass analysis of the ion beam. Si was chosen as the initial semiconductor material to verify the purity of the source because of its known sensitivity to contamination and also because there was previously no published account of good quality epitaxial Si layers grown by any sputtering method.

Typically, a 12keV 4mA beam of A^+ ions struck a Si target at 60° incidence and ejected sputtered atoms were deposited at a rate of 200 Å/min on a heated Si(111) substrate placed just above the target. Epitaxial layers were grown at temperatures above about 700°C and, under the best conditions, these layers contained only dislocation defects and were of N-type conductivity of high resistivity. For a layer grown at 900°C the density of dislocation defects was about 8×10^9 cm^{-2}.

The structural quality, epitaxial temperature and electrical behaviour of epitaxial Si layers has been correlated with ion bombardment conditions of the growing layer. Contamination did not appear to affect the epitaxial process indicating that high purity was probably achieved with the modified ion beam source. An ion bombardment model has been developed to explain the mode of growth of layers and, in each case, the bombardment conditions were severe enough to continually transform a

thin 100 Å thick surface region of the newly-deposited sputtered layer to a disordered state. The subsequent reordering characteristics of this disordered surface controlled the quality of layers.

The sputtering properties of Si and GaAs have also been investigated using intense beams of high energy ions.

The similarity in results for single crystal targets to those for polycrystalline targets was again attributed to surface disorder in single crystal targets created by ion bombardment. The individual points suggesting the presence of surface disorder in single crystal targets were:

(i) sputtering yield data,
(ii) the absence of etch pits,
(iii) sputtered atom distributions,
and (iv) discolouration of target surfaces by ion bombardment.

Moreover, sputtering yield data and sputtered atom distributions indicated that more complete surface disorder was obtained if rate of ion dose, total dose and ion mass were all increased.

Experiments have also confirmed that the ejection of sputtered atoms was controlled by a momentum transfer mechanism. The observations supporting this statement were:

(i) sputtering yields did not depend solely on ion energy but also on ion mass. Heavier noble gas ions produced correspondingly higher sputtering yields
(ii) 12keV ions produced a lower sputtering yield than 6keV ions because the more energetic ions penetrated deeper beneath the surface.
(iii) for ions incident away from the target normal, increased sputtering yield was obtained because the length of the necessary collision sequence to transmit a disturbance back to the surface was correspondingly shorter.
(iv) the shape of the profile of the target after bombardment and sputtered atom distribution

curves indicated that atoms were ejected at an angle near to that expected for specular reflection of the ion beam.

and (v) atoms were ejected from partially disordered single crystals along preferred crystallographic directions.

Finally, stoichiometric layers of GaAs could only be obtained from polycrystalline targets.

5.2. RECOMMENDATIONS FOR FURTHER WORK

The first stage of future work should be allocated to developing an ion beam sputtering method which prevents entirely bombardment of the substrate with secondary positive or negative ions from the target. Only then can one assess the full potential of homo-epitaxial layers of Si by ion beam sputtering before attempting to grow epitaxial layers of GaAs and other compounds not readily possible by conventional evaporation methods. By the total elimination of ion bombardment of the substrate during deposition it should then be possible to grow better quality Si layers at lower temperatures. There are also indications that the conductivity- type and resistivity of targets will be reproduced in layers grown under ion bombardment-free conditions because, in the case of polycrystalline GaAs targets, each element is sputtered equally.

The proposed ion beam sputtering equipment to prevent entirely bombardment of the substrate with positive or negative ions is shown in FIG. 5.1. In this equipment the ion beam would be extracted from the ion beam source by a Si extraction electrode which would act as target at earth potential. The beam, on entering the region of magnetic field produced between the pole pieces of an electromagnet, would be deflected so as to strike the inside wall of the Si electrode. The usual particles would be emitted ie. neutral Si atoms, electrons and secondary positive and negative ions. On emerging from the Si extraction electrode, the paths of the charged particles would be governed by the magnetic field created and these particles would be deflected to pass the substrate, whereas the path of neutral sputtered Si atoms would be unaffected.

Estimates for the strength of the magnetic field, the length of cylindrical Si extraction electrode and bombardment angle for the proposed arrangement have been made in APPENDIX A.3.

Before constructing the proposed arrangement it

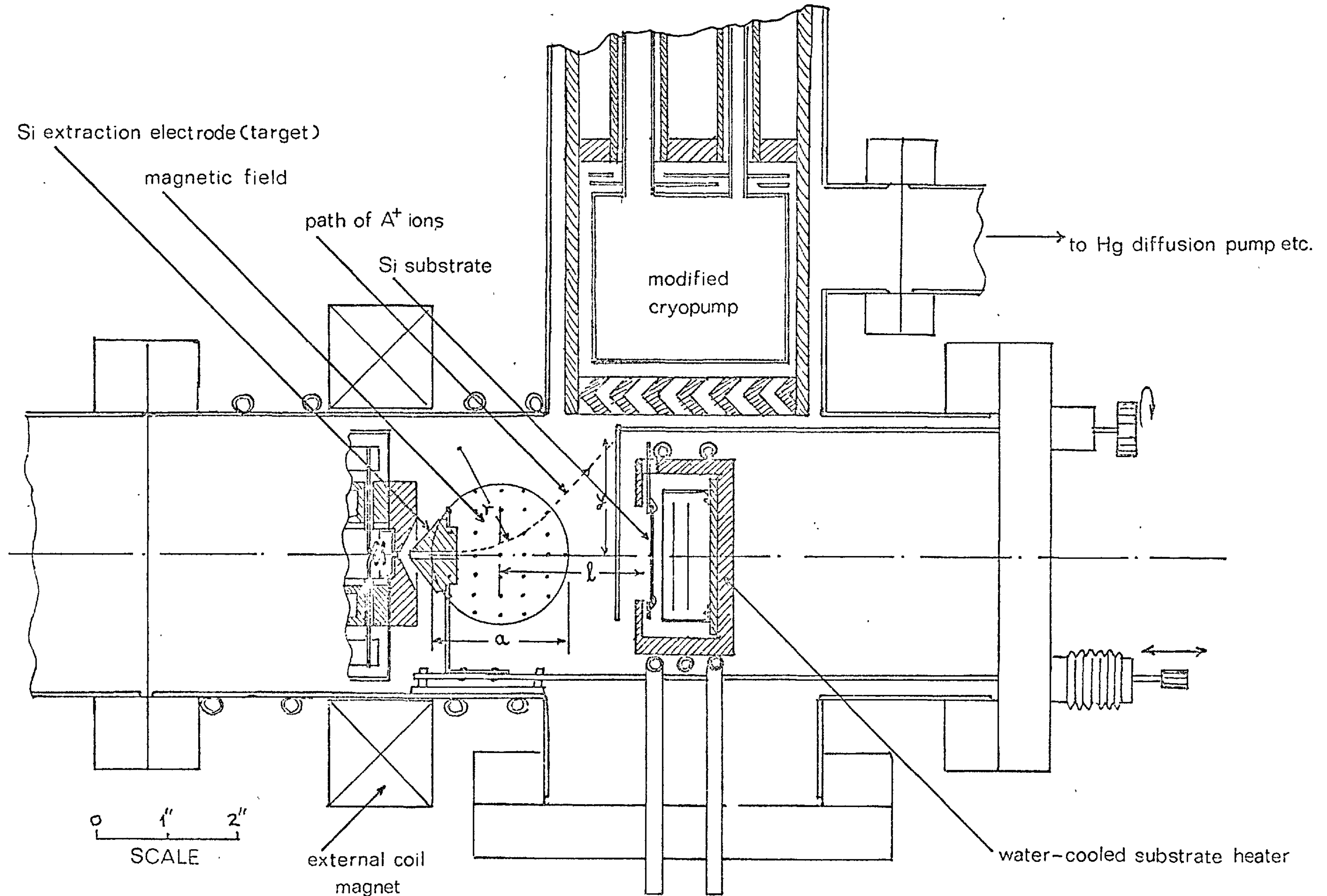

FIG. 5.1. PROPOSED ION BEAM SPUTTERING EQUIPMENT TO PREVENT ENTIRELY BOMBARDMENT OF THE SUBSTRATE WITH CHARGED PARTICLES

would be advisable first to ensure that an adequate deposition rate could be achieved. A simple experiment to test this would be to use a cylindrical Si extraction electrode and rely on beam spreading to make the beam deflect and give sputtering. The sputtered material could then be collected on a glass microscope slide placed in the same position as the substrate in the proposed arrangement.

As well as modifications to the sputtering method to prevent ion bombardment of the substrate during deposition, the following further improvements should also be made. Firstly, the vacuum system should be an all-metal system (see FIG. 5.1.) with no viton gaskets enabling baking to be carried out to at least 350°C. A lower ultimate pressure should then be possible. Secondly, the inert gas handling system should be improved. The flow of inert gas from glass cylinders to the ion beam source should be controlled by a bakeable all-metal leak valve. By baking the entire all-glass and metal gas handling system to 350°C it should be possible to improve on the present impurity level of $2x10^3$ vpm for O_2 and approach the manufacturer's level of lvpm. Thirdly, the liquid helium cryopump should be modified to realise its full pumping speed. In the present design (FIG. 3.3.), the pumping speed is limited to about 180 l/sec by the conductance of the tube supporting the chevron baffle. If the tube diameter could be extended to the full 3 in. diameter of the surrounding stainless steel tube, as shown in FIG. 5.1., the pumping speed might be increased up to as much as 400 l/sec. Fourthly, a water-cooled tungsten strip radiation heater of the type developed by Censlive (1971) should be used to heat the substrate as shown in FIG. 5.1. The advantage of this type of heater is that the Si "flashing" temperature of 1250°C can easily be reached. The disadvantage is that there must be some degree of contamination of the substrate originating from the tungsten strips. However, Censlive (1971) has shown that the degree of contamination with this form of heater must

be negligible because the electrical properties of layers are unaffected by its use. Fifthly, and finally, an external coil magnet should be placed around the ionisation chamber and electrodes of the ion beam source as shown in FIG. 5.1. to improve ionisation efficiency inside the source and help to constrain the extracted ion beam in the region between the 2 electrodes. Increased ion beam currents should then be possible together with greater purity because any sputtering of the Si extraction electrode will now be deliberate.

A P P E N D I X

A.1. BRAZING TO UHV STANDARDS

In the construction of both the liquid helium cryopump and the ion beam source, brazed joints were needed which would satisfy the following requirements:

(a) the braze material must flow smoothly into both surfaces to be joined giving a strong mechanical joint in which no gas bubbles are trapped

(b) For UHV work the braze used must have a low vapour pressure at elevated temperatures

These two requirements exclude the use of flux which tends to leave by-products of low vapour pressure and gas trapped in bubbles. Joints formed with the aid of flux are also usually rough in structure and mechanically weak.

The technique used for the construction of the cryopump (see FIG. 3.3.) was RF brazing in an atmosphere of forming gas (90% N_2, 10% H_2), which was particularly suitable for Cu to Cu joints. The braze used was a Ag-Cu eutectic 28.1wt (39.9 at) % Cu which melts at 780°C. The machined parts of the cryopump were put together, mounted in a 4 in. transparent silica tube and heated to 800°C in forming gas at atmospheric pressure by RF heating. The Ag-Cu eutectic jointing material in the form of a thin rod was then fed to the joints to be brazed through a small hole in a rubber bung on the gas outlet side of the silica tube. The braze was observed to run through the joints smoothly and fill in all the crevices. When all the Cu to Cu joints had been brazed, the assembly was allowed to cool slowly. The success of the brazing procedure was evident from the fact that thorough leak testing failed to show up any leaks.

The method of RF brazing just described was not suitable for the construction of the ionisation chamber cooling jacket in the ion beam source, where stainless steel was required to be joined to Cu, for reasons outlined by Lewin (1965). Firstly, stainless steel will oxidise in the slightest traces of oxygen or water vapour in the inert atmosphere used preventing proper "wetting" of the surface by the eutectic. Secondly, oxide-free

stainless steel is only "wetted" properly by the Ag-Cu eutectic when the temperature is over 1000°C at which temperature Ag evaporates noticeably. Because of these disadvantages and the much smaller size of components to be joined in this case, it was decided to do the brazing in vacuum. The arrangement for vacuum brazing of the ionisation chamber cooling jacket is shown in FIG. A.1. The brazing material used was pure Au wire placed between the components to be joined and the area around the join was heated by electron bombardment from a circular tungsten filament held at about -2kV with respect to earth. The electron current used was about 100mA for joint 1 and about 500mA for joint 2. Each joint was slowly taken up to the melting point of Au and, as soon as the Au was observed to melt and flow around the joint, the temperature was held for about 10 seconds and then reduced. For both joints the stainless steel surface smoothly blended with the Cu surface and the absence of leaks confirmed that successful joints had been achieved. In trial runs, prior to using Au wire as the jointing material, Ag-Cu eutectic was tried unsuccessfully, but Au, despite being very near to Cu in its melting point (Cu 1083°C; Au 1063°C), gave near perfect results each time tried.

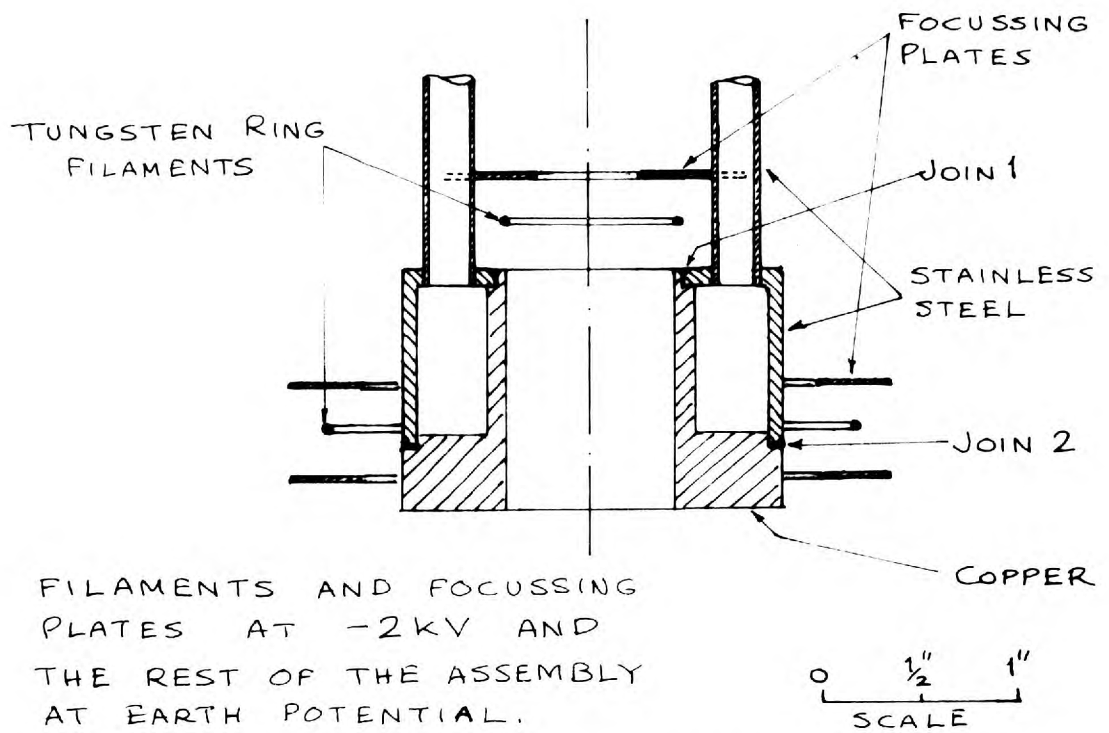

Brazing arrangement

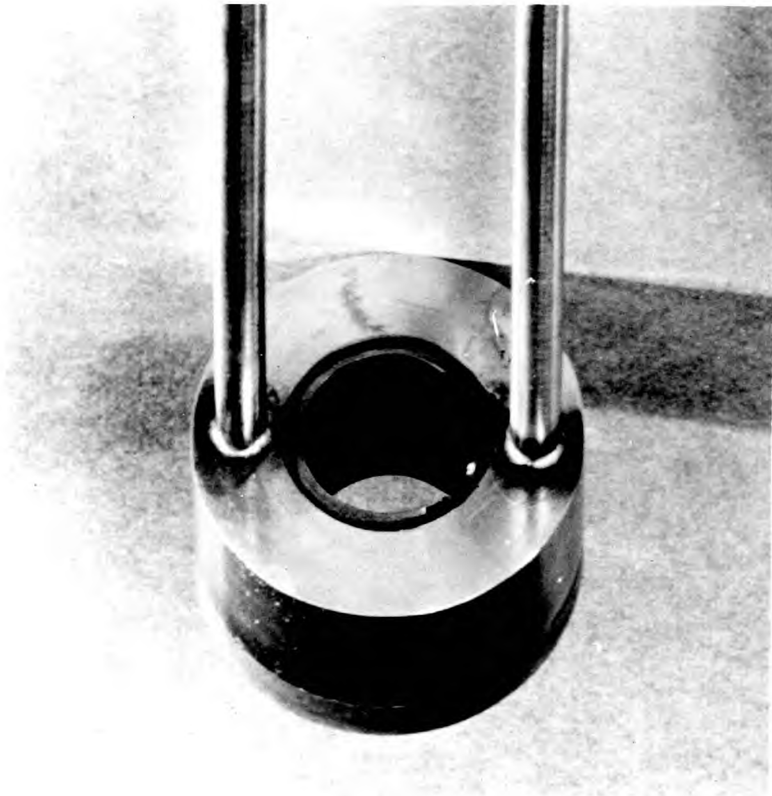

Completed assembly

FIG. A.1. VACUUM BRAZING OF IONISATION CHAMBER COOLING JACKET

A.2. ESTIMATE OF RATE OF ION DOSE TO SUBSTRATE DURING DEPOSITION

During deposition, Si substrates were maintained at (a) ion source potential when they were bombarded by high energy secondary negative ions and electrons, or (b) earth potential when they were bombarded with high energy secondary positive and negative ions and electrons. These secondary charged particles originated at the target due to the interaction of the ion beam with it (usual ion beam current 4mA which is equivalent to about $2\frac{1}{2} \times 10^{16}$ ions sec^{-1}) In SECTION 3.3.6. the secondary electron emission coefficient for a 12keV A^+ ion beam incident at 60° on a Si surface was estimated as being 0.3 ± 0.1. Since most of these electrons would be attracted to the substrate, the substrate electron current would then be about 1.2mA. To differentiate between ions and electrons reaching the substrate it was necessary to remove electron bombardment of the substrate during deposition. A 200 gauss magnet was placed between the target and substrate and the field strength was sufficient to deflect all electrons to pass the substrate holder. The passage of ions was hardly affected and so these reached the substrate if the biasing conditions were favourable.

With substrates at ion source potential the ion current to the substrate was less than the measurement accuracy (1μA) so the corresponding rate of ion dose due to secondary negative ions was less than 6×10^{12} ions sec^{-1}. The yield K_- of negatively-charged ion species was therefore less than 3×10^{-4} ion/ion if they were present. Comas and Cooper (1967) bombarded GaAs single crystals with 140eV A^+ ions and similarly concluded that if negative ion species characteristic of the target were present then the yield K_- of these ions was less than about 10^{-4} ion/ion. Typical values for perfectly clean and heated metal targets were between 10^{-6} and 10^{-5} ion/ion.

With substrates at earth potential the ion current to the substrate was about 150μA so the corresponding rate of ion dose primarily due to secondary positive ions

was about 10^{15} ions sec^{-1}. The secondary positive ions reaching the substrate were primary ions reflected by the target and ion species characteristic of the target. The probability of a secondary positive ion reaching the substrate was therefore about 4×10^{-2} ion/ion. Beske (1967) determined that the total yield K_+ of Si target ion species was about 1.5×10^{-2} ion/ion. The reflection coefficient R of primary ions was then about 2.5×10^{-2} ion/ion in the experiments described here where Si targets were bombarded at 60° incidence. A typical value of R for Cu at 60° incidence is about 5×10^{-2} ion/ion (see SECTION 2.2.2.1.).

A.3. PROPOSED SPUTTERING METHOD TO PREVENT ENTIRELY BOMBARDMENT OF THE SUBSTRATE WITH CHARGED PARTICLES

FIG. A.2. shows the path of secondary charged and uncharged particles through a region of magnetic field. These secondary particles originated from the interaction of 10keV A^+ ions in a narrow beam with the inside wall of the Si "target". The calculations which follow have been simplified by assuming that spreading of the ion beam was not significant.

A.3.1. Estimate of the strength of the magnetic field

The equations governing the passage of a parallel ion beam through a uniform magnetic field are:

$$y/l = Ba\sqrt{\frac{e^*}{2m^*V_o}} \quad \ldots\ldots. (1)$$

and

$$r^2 = \frac{2m^*V_o}{e^*B^2} \quad \ldots\ldots. (2)$$

where y, l, a and r are in metres,
B is the field strength in Weber m^{-2},
V_o is the accelerating potential in volts,
and e^*/m^* is the charge to mass ratio for individual charged particles in coulomb kg^{-1}.

For A^+ ions, $e^*/2m^* \sim 10^6$ coulomb kg^{-1}.
For 10kV A^+ ions, (1) becomes

$$y/l = 10\ Ba \quad \ldots\ldots. (3)$$

For reasonable deposition rates, the Si electrode and electromagnet pole pieces are required to be as close to the substrate as possible. Furthermore, if those primary 10keV A^+ ions which do not strike the wall of the Si electrode are to be deflected to pass the substrate then the value of y/l needs to be at least 1.
Substituting y/l = 1 into (3) gives

$$Ba = 10^{-1} \quad \ldots\ldots. (4)$$

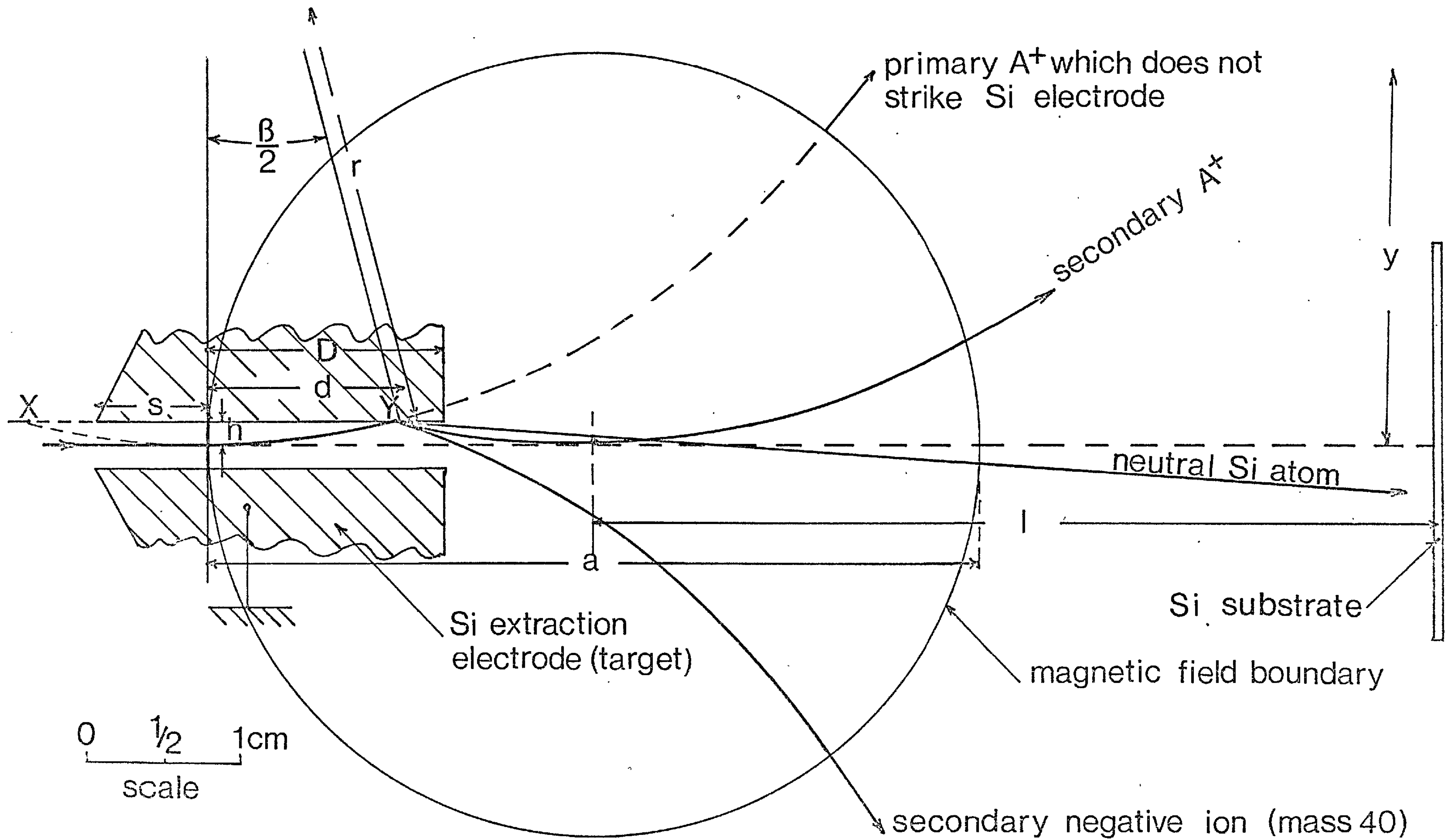

FIG. A.2. PROPOSED SPUTTERING ARRANGEMENT; Passage of 10keV A^+ ion beam through Si "target" and magnetic field with no beam spreading.

The normal type of electromagnet is limited to a value of B of about 2 Weber m^{-2} (20 k gauss).
Substituting B = 2 Weber m^{-2} into (4) gives

$$a = 5\ 10^{-2}m = 5\ cm.$$

and substituting the values of $e^*/2m^*$ and V_o for 10kV A^+ ions and B = 2 Weber m^{-2} into (2) gives

$$r = 5\ cm.$$

A.3.2. Estimate of the length of the Si extraction electrode

An estimate of the total length (s+D) of the Si electrode is now made assuming that in the region of length s outside the magnetic field the ion paths are not affected by the 2 Weber m^{-2} magnetic field. s should be about 0.75 cm. It is known from rules of geometry that,

$$\frac{\sin \beta}{\beta} = \frac{2d}{\text{chord XY}} \qquad \ldots\ldots\ (5)$$

$$\text{and} \quad (2r-h)h = d^2 \qquad \ldots\ldots\ (6)$$

h is fixed at 1.5 mm. since this is the radius of the extraction electrode aperture used at the moment.
Substituting h = 0.15 cm., and r = 5 cm. into (6) gives

$$d \sim 1.2\ cm.$$

Therefore, those 10kV A^+ ions which initially follow a parallel path should strike the wall of the Si electrode after travelling about 1.2 cm. in the magnetic field region. A suitable value of D would be 1.5 cm. to ensure that most A^+ ions strike the Si electrode before emerging from the electrode. The overall length (s+D) of the Si electrode would then be about 2.25 cm.

A.3.3. Estimate of the bombardment angle

The bombardment angle ($\beta/2$) can now be calculated.

chord XY = $r\beta$, where β is in radiaus

Substituting chord XY = $r\beta$, into (5) gives,

$$\sin \beta = \frac{2d}{r} \qquad \ldots\ldots\ (7)$$

Substituting d = 1.2 cm. and r = 5 cm. into (7) gives,

$$\beta \sim 29° \text{ and } \beta/2 \sim 14½°.$$

This value of $\beta/2 \sim 14½°$ is close to the value of $\beta/2 \sim 10°$ which according to Lindhard (1965) gives a maximum sputtering yield of Si for a 10keV A^+ ion beam.

REFERENCES

Abroyan I.A. and Titov A.I., 1969, Sov. Phys. Solid State, 10, 2716

Abroyan I.A., Belyakov V.S. and Tutov A.I., 1969, Sov. Phys. Solid State, 10, 2965

Allen F.G., Eisinger J., Hagstrum H.D. and Law J.T., 1959, J. Appl. Phys., 30, 1563

Almén O. and Bruce G., 1961(a), Nucl. Instr. and Meth., 11, 257

Almén O. and Bruce G., 1961(b), Nucl. Instr. and Meth., 11, 279

Anderson G.S. and Wehner G.K., 1960, J. Appl. Phys., 31, 2305

Anderson G.S., 1962, J. Appl. Phys., 33, 2017

Anderson G.S., Wehner G.K. and Olin H.J., 1963, J. Appl. Phys., 34, 3492

Anderson G.S. and Wehner G.K., 1964, Surf. Sci., 2, 367

Anderson G.S., 1966(a), J. Appl. Phys., 37, 2838

Anderson G.S., 1966(b), J. Appl. Phys., 37, 3455

Anderson G.S., 1967, J. Appl. Phys., 38, 1607

Ashby M.F. and Brown L.M., 1963, Phil. Mag., 8, 1649

Ayukhanov A.Kh. and Abdullaeva M.K., 1966, Bull. Acad. Sci. U.S.S.R. Phys. Ser., 30, 2083

Bacchilega A., Gondi P. and Missiroli G.F., 1965, Nuovo Cimento B, 40, 309

Beske H.E., 1967, Z. Natur., 22A, 459

Bicknell R.W., 1971 Private communication

Booker G.R. and Stickler R., 1962, Brit. J. Appl. Phys., 13, 446

Booker G.R. and Unvala B.A., 1963, Phil. Mag., 8, 1597

Booker G.R. and Unvala B.A., 1965, Phil Mag., 10, 10

Bovey P.E., 1969, Vacuum, 19, 497

Brown F. and Davies J.A., 1963, Canad. J. Phys., 41, 844

Carter G. and Colligon J.S., 1968, Ion Bombardment of Solids, American Elsevier

Censlive M., 1971, Ph.D. Thesis, London University

Clark A.H. and Alibozek R.G., 1968, J. Appl. Phys., 39, 2156

Colombie N., Fagot B. and Fert C., 1966, C.R. Acad. Sci. B., 263, 822

Comas J. and Cooper C.B., 1966, J. Appl. Phys., 37, 2820

Comas J. and Cooper C.B., 1967, J. Appl. Phys., 38, 2956

Comas J. and Cooper C.B., 1968, J. Appl. Phys., 39, 5736

Cunningham R.E., Haymann P., Lecomte C., Moore W.J. and Trillat J.J., 1960, J. Appl. Phys., 31, 839

Davies J.A., Ball G.C., Brown F. and Domeij B., 1964, Canad. J. Phys., 42, 1070

Dearnaley G., Kandiah K. and Nelson R.S., 1969, Phys. Bulletin, 20, May, 165

Dillon J.A. and Oman R.M., 1960, J. Appl. Phys., 31, 26

Evdokimov I.N., Mashkova E.S. and Molchanov V.A., 1967, Sov. Phys. Solid State, 9, 1434

Fagot B., Colombie N., Thiry R. and Fert C., 1966, C.R. Acad. Sci. B, 262, 173

Ferber R.R., 1963, Trans. I.E.E.E. Nucl. Sci., NS-10, 15

Gianola U.F., 1957, J. Appl. Phys., 28, 868

Hagstrum H.D., 1960, Phys. Rev., 119, 940

Haq K.E., 1965, J. Electrochem Soc., 112, 500

Harrison D.E. Jnr., Johnson J.P. and Levy N.S., 1966, Appl. Phys. Lett., 8, 33

Hasiguti R.R., Hanada R. and Yamaguchi S., 1963, J. Phys. Soc. Japan, 18, 164

Hennequin J.F., 1968, J. Physique, 29, 655

Hill K.J. and Nelson R.S., 1965, Nucl. Inst. and Methods, 38, 15

Hill K.J., Nelson R.S. and Francis R.J., 1968, Private communication

Hirsch P.B., Howie A., Nicholson R.B., Pashley D.W. and Whelan M.J., 1965, Electron Microscopy of Thin Crystals, Butterworths

Honig R.E., 1958, J. Appl. Phys., 29, 549

Honig R.E., 1964, Mass Spectrometric Methods, 193

Irving S.M., 1969, Semiconductor Silicon, Electrochem. Soc., New York, 433

Jacobson R.L. and Wehner G.K., 1965, J. Appl. Phys., 36, 2674

Jech C. and Kelly R., 1969, J. Phys. Chem. Solids, 30, 465

Kaminsky M., 1965, Atomic and Ionic Impact Phenomena on Metal Surfaces, Springer-Verlag

Krikorian E., 1964, Single-Crystal Films, Pergamon Press, 113

Krikorian E. and Sneed R.J., 1966, J. Appl. Phys., 37, 3665

Laegrid N. and Wehner G.K., 1961, J. Appl. Phys., 32, 365

Lander J.J. and Morrison J., 1962, J. Appl. Phys., 33, 2089

Large L.N. and Bicknell R.W., 1967, J. Mat. Sci., 2, 589

Layton C.K. and Cross K.B., 1967, Thin Solid Films, 1, 169

Lewin G., 1965, Fundamentals of Vacuum Science and Technology, McGraw-Hill, 208 and 209

Lindhard J. and Scharff M., 1961, Phys. Rev. 124, 128

Lindhard J., 1965, Matt. Fys. Medd., 34, 14

Loferski J.J. and Rappaport P., 1959, J. Appl. Phys., 30, 1296

Luby S., 1969, Thin Solid Films, 4, 81

MacDonald R.J. and Haneman D., 1966(a), J. Appl. Phys., 37, 1609

MacDonald R.J., and Haneman D., 1966(b), J. Appl. Phys., 37, 3048

Magnuson G.D. and Carlston C.E., 1963, J. Appl. Phys., 34, 3267

Mashkova E.S. and Molchanov V.A., 1968, Canad. J. Phys., 46, 713

Mayer J.W., Eriksson L., Picraux S.T. and Davies J.A., 1968, Canad. J. Phys., 46, 663

Mazey D.J., Barnes R.S. and Nelson R.S., 1966, Proc. 6th Internat. Congr. on Elec. Micy., Kyoto, 363

Mazey D.J., Nelson R.S. and Barnes R.S., 1968, Phil. Mag., 17, 1145

Mazur R.G. and Dickey D.H., 1966, J. Electrochem. Soc., 113, 255

Meckel B.B. and Swalin R.A., 1959, J. Appl. Phys., 30, 89

Meckel B.B., 1966, J. Appl. Phys., 37, 2516

Molchanov V.A., Tel'Kovskii V.G. and Chicherov V.M., 1961, Sov. Phys. Dokl., 6, 137

Molnar B., Flood J.J. and Francombe M.H., 1964, J. Appl. Phys., 35, 3554

Moulton C.W., 1962, Nature, 195, 793

Nelson R.S. and Thompson M.W., 1963, Phil. Mag., 8, 1677

Nelson R.S., Mazey D.J., Matthews M.D., and Holloway D.F., 1966, Phys. Lett., 23, 18

Nelson R.S. and Mazey D.J., 1968, Canad J. Phys., 46, 689

Nielson K.O., 1956, Electromagnetically Enriched Isotopes and Mass Spectrometry, Academic Press

Ogilvie G.J. and Ridge M.J., J. Phys. Chem. Solids, 10, 222

Ohl R.S., 1952, Bell Systems Tech. J., 31, 104

Parsons J.R., 1965, Phil. Mag., 12, 1159

Pearmain K. and Unvala B.A., 1971, 8th Annual Solid State Physics Conference, Manchester (To be published)

Pierce J.R., 1941, Proc. IRE., 29, 28

Pleshivtsev N.V., 1960, Sov. Phys. JETP., 10, 878

Ramer C.E., Narasimham M.A., Reynolds H.K. and Allred J.C., 1964, J. Appl. Phys, 35, 1673

Rol P.K., Fluit J.M. and Kistemaker J., 1960(a) Physica, 26, 1000

Rol P.K., Fluit J.M. and Kistemaker J., 1960(b) Physica, 26, 1009

Rosenburg D. and Wehner G.K., 1962, J. Appl. Phys. 33, 1842

Silsbee R.H., 1957, J. Appl. Phys., 28, 1246

Southern A.L., Willis W.R. and Robinson M.T., 1963, J. Appl. Phys., 34, 153

Stewart A.D.G. and Thompson M.W., 1969, J. Mat. Sci., 4, 56

Stuart R.V. and Wehner G.K., 1962, J. Appl. Phys., 33, 2345

Stuart R.V. and Wehner G.K., 1965, U.S. Govt. Res. Rpts., AD608946.

Thomas R.N. and Francombe M.H., 1967(a), Appl. Phys. Lett., 11, 108

Thomas R.N. and Francombe M.H., 1967(b), Appl. Phys. Lett., 11, 134

Unvala B.A., 1962, Nature, 194, 966

Unvala B.A., 1963(a), Le Vide, No. 104, 109

Unvala B.A., 1963(b), Thesis, St. John's College, Cambridge

Unvala B.A. and Booker G.R., 1964, Phil. Mag., 9, 691

Unvala B.A. and Pearmain K., 1970, J. Mat. Sci., 5, 1016

Vineyard G., Goland A., Milgram M. and Gibson J., 1960, Bull. Am. Phys. Soc., Ser. II, 5, 26

Wehner G.K., 1955, J. Appl. Phys., 26, 1056

Wehner G.K., 1956, Phys. Rev., 102, 690

Wehner G.K., 1957, Phys. Rev., 108, 35

Wehner G.K., 1958, J. Appl. Phys., 29, 217

Wehner G.K., 1959, J. Appl. Phys., 30, 1762

Wehner G.K., 1960, General Mills Rpt., 2136

Wehner G.K. and Rosenburg D., 1960, J. Appl. Phys., 31, 177

Weisberg L.R., 1967, J. Appl. Phys., 38, 4537

Wolsky S.P. and Zdanuk E.J., 1961, J. Appl. Phys., 32, 782

Wolsky S.P., Zdanuk E.J. and Shooter D., 1964, Surf. Sci., 1, 10

Wolsky S.P., Piwkowsi T.R. and Wallis G.,1965, J. Vac. Sci and Tech., 2, 97

Yonts O.C., Harrison D.E. and Normand C.E., 1960, J. Appl. Phys., 31, 447

Yurasova V.E., Pleshivtsev N.V. and Orfanov I.V., 1960, Sov. Phys. JETP, 10, 689

Yurasova V.E. and Sirotenko I.G., 1962, Sov. Phys. JETP, 14, 968

Yurasova V.E. Levykina L.N. and Brzhezinskii V.A., 1964, Bull. Acad. Sci. U.S.S.R. Phys. Ser., 28, 1337

Zdanuk E.J. and Wolsky S.P., 1965, J. Appl. Phys., 36, 1683

ACKNOWLEDGEMENTS

The author is grateful to Dr. B.A. Unvala, who supervised this project, for his constant advice and interest during the course of this work; to Professor J.G. Ball for the provision of laboratory facilities; to the Science Research Council for financial support; to Mr. B.H. Barter for help in the construction of experimental equipment and to all his colleagues for useful discussions.

Finally the author would like to thank Miss Madeline Burr for the many hours of spare time which she devoted to the typing.